Title
Novel Routes to Ethylene Glycol Synthesis via Acid-Catalyzed Carbonylation of Formaldehyde and Dimethoxymethane

Author
Celik, Fuat Emin

Publication Date
2010

Peer reviewed|Thesis/dissertation

Novel Routes to Ethylene Glycol Synthesis via Acid-Catalyzed Carbonylation of Formaldehyde and Dimethoxymethane

by

Fuat Emin Celik

A dissertation submitted in partial satisfaction of the

requirements for the degree of

Doctor of Philosophy

in

Chemical Engineering

in the

Graduate Division

of the

University of California, Berkeley

Committee in charge:

Professor Alexis T. Bell, Chair
Professor Alexander Katz
Professor T. Don Tilley

Spring 2010

Novel Routes to Ethylene Glycol Synthesis via Acid-Catalyzed Carbonylation of Formaldehyde and Dimethoxymethane

by

Fuat Emin Celik

Abstract

Novel Routes to Ethylene Glycol Synthesis via Acid-Catalyzed Carbonylation of Formaldehyde and Dimethoxymethane

by

Fuat Emin Celik

Doctor of Philosophy in Chemical Engineering

University of California, Berkeley

Professor Alexis T. Bell, Chair

Carbon-carbon bond forming carbonylation reactions were investigated as candidates to replace ethene epoxidation as the major source of ethylene glycol production. This work was motivated by the potentially lower cost of carbon derived from synthesis gas as compared to ethylene. Synthesis gas can be produced from relatively abundant and cheap natural gas, coal, and biomass resources whereas ethylene is derived from increasingly scarce and expensive crude oil. From synthesis gas, a range of C_1 compounds containing no C-C bonds, such as methanol, formaldehyde and its closely related acetals such as dimethoxymethane (DMM), can be readily obtained.

Formaldehyde carbonylation was once used commercially to produce precursors to ethylene glycol. Previous investigations of this reaction were carried out in the liquid phase, and required high carbon monoxide pressures (tens to hundreds of atmospheres) to overcome the low solubility of carbon monoxide. At lower carbon monoxide pressures, the reaction of formaldehyde with itself, the Cannizzaro disproportionation reaction, becomes the dominant process. The focus of this work was to carry out the carbonylation of formaldehyde and DMM with high selectivity and activity towards ethylene glycol precursors without requiring harsh conditions.

Formaldehyde carbonylation was investigated in the liquid-phase using methyl formate (MF) as the source of CO using silicotungstic acid and other heteropoly acids as the catalyst. Methyl glycolate (MG) and methyl methoxyacetate (MMAc), both precursors to ethylene glycol, were formed along with DMM and dimethyl ether (DME), the primary byproducts. Using MF as the CO source avoided the need to pressurize the headspace with high pressures of CO gas. The effects of formaldehyde source, reaction temperature, reaction time, and catalyst were investigated. Methoxymethanol, paraformaldehyde, 1,3,5-trioxane, and DMM were examined as sources of formaldehyde. The highest yields of methyl glycolate and methyl methoxyacetate were obtained using 1,3,5-trioxane as the source of formaldehyde. Release of carbon monoxide from MF was found to be slow and limited the rate of carbonylation. Of the heteropoly acids investigated, silicotungstic acid produced the highest yields of MG and MMAc, whereas methanesulfonic acid did not produce these products at similar acid loading. The difference in the effectiveness of heteropoly acids and methanesulfonic acid is ascribed to

the role of the anion of the heteropoly acid, a soft base, in stabilizing the reactive intermediates involved in the carbonylation of formaldehyde.

While using MF as the CO source provided milder conditions, the selectivity to ethylene glycol precursors was still low. To achieve high selectivity under mild conditions, a novel vapor-phase process was developed. By carrying out the reaction in the vapor phase, the need for high pressure to dissolve CO in a liquid was avoided, and by using the dimethyl acetal of formaldehyde, DMM, the need for water or alcohol was avoided. Using an acid zeolite, Faujasite (FAU), as the catalyst it was possible to produce MMAc with a selectivity of up to 79% and a yield of up to 20% based on DMM at 3 atm of CO pressure. The disproportionation of DMM to produce DME and MF was the only competing process observed. The rate of disproportionation was minimized by operating at high CO to dimethoxymethane feed ratios.

By selecting zeolites of different frameworks and Si/Al ratios, the effects of pore size and connectivity and the proximity of acid sites on the carbonylation of dimethoxymethane to produce methyl methoxyacetate were revealed. FAU, ZSM-5 (MFI), Mordenite (MOR), and Beta (BEA) showed very similar activity for DMM carbonylation. However, FAU had the highest selectivity compared to the other zeolites because of its very low activity towards disproportionation. The higher rate of DMM disproportionation observed for MFI, MOR, and BEA is ascribed to the small pores of these zeolites, which facilitate the initial and critical step in the formation of dimethyl ether and methyl formate. Ferrierite showed very low activity for both carbonylation and disproportionation. Increasing the Si/Al ratio for both FAU and MFI led to an increase in the turnover frequency for DMM carbonylation. The low rate of MMAc formation found at low Si/Al ratios was proposed to be due to repulsive interactions occurring between adsorbed species located within the same supercage of FAU or channel intersection of MFI.

Mechanisms were proposed for both DMM carbonylation and disproportionation reactions over acid zeolites and were evaluated using in situ infrared spectroscopy. Surface intermediates for both carbonylation and disproportionation reactions were observed spectroscopically, and their responses to changes in reaction conditions were consistent with steady-state kinetic experiments and the predictions of density functional theory (DFT) calculations. For DMM carbonylation, the solvation of the carbocationic transition state of the CO insertion step was observed when gaseous nucleophiles promoted the formation of the CO insertion product, a methoxyacetyl surface species. The surface concentration of the methoxyacetyl species at steady state, as measured by infrared spectroscopy, was 10 times smaller on zeolite FAU than on MFI, despite the higher rate of DMM carbonylation on FAU. This was supported by DFT calculations, which predicted a very small barrier for the reaction of the methoxyacetyl species over FAU, but a substantial barrier over MFI, leading respectively to smaller and larger concentrations of this species. The rate expression derived from the proposed mechanisms was used in a plug-flow reactor model to predict the rates of carbonylation and disproportionation over FAU as functions of reaction temperature and DMM and CO partial pressures. The results showed good agreement with steady-state rate measurements.

To Laura

for showing me strength

To Emre

for showing me laughter

and to my family

for always showing me love

Table of Contents

List of Figures

List of Tables

List of Abbreviations and Symbols

A	Pre-exponential factor in Arrhenius expression, $k = Ae^{-E_a/RT}$
BEA	zeolite Beta or possessing the BEA framework type
C-C bond	carbon-carbon bond
C_1, C_2, C_n compound	a compound containing 1, 2, or n carbon-carbon bonds
DFT	density function theory
DME	dimethyl ether, CH_3OCH_3
DMM	dimethoxymethane, $CH_3OCH_2OCH_3$
E_a	Activation energy in Arrhenius expression, $k = Ae^{-E_a/RT}$
FA	formic acid,
FAU	zeolite Faujasite or possessing the FAU framework type
FER	zeolite Ferrierite or possessing the FER framework type
F_i	molar flow rate of species i
GA	glycolic acid, $HOCH_2COOH$
HPA	heteropoly acid, HCOOH
k, k_i	reaction rate constant (for reaction i)
MEG	monoethylene glycol, $HOCH_2CH_2OH$
MF	methyl formate, $HCOOCH_3$
MFI	zeolite ZSM-5, pentasil, or possessing the MFI framework type
MG	methyl glycolate, $HOCH_2COOCH_3$
MMAc	methyl methoxyacetate, $CH_3OCH_2COOCH_3$
MOR	zeolite Mordenite or possessing the MOR framework type
P_i	partial pressure of formation component i
PMo_{12}	phosphomolybdic acid, $H_3PMo_{12}O_{40}$
PW_{12}	phosphotungstic acid, $H_3PW_{12}O_{40}$
P_i	partial pressure of species i
Q	gas volumetric flow rate
R	molar gas constant
r_i	rate of formation or consumption of component i
$SiMo_{12}$	silicomolybdic acid, $H_4SiMo_{12}O_{40}$
SiW_{12}	silicotungstic acid, $H_4SiW_{12}O_{40}$
S_{MMAc}	selectivity to MMAc from DMM
T	reaction temperature
t	time
W	moles of Al
$\Delta G°$	Gibb's free energy change of reaction at 1 bar and 25 °C
θ_i	surface coverage of surface species i, as fraction of total sites
τ	space time, volumetric flow rate divided by number of Al atoms

Acknowledgements

It takes a village to raise a child goes the proverb. I can now say firsthand that this is very nearly true. I add to this wisdom that it takes an academy to write a dissertation, and in what follows, I aim to acknowledge the contributions of many colleagues in realizing this dissertation.

First and foremost, I have carried out this research under the tutelage and guidance of the most agreeable and generous research adviser I could have asked for. I feel that I have always had Professor Alexis Bell's support and trust, allowing me great freedom in my research and great intellectual reward. I think we share a great rapport that I will surely miss.

Taejin Kim has been a fantastic coworker and coauthor. Our work together has been incredibly productive, but more importantly TJ has supported my career and given me invaluable advice.

My survival in graduate school depended on the support of the D-team, especially Anthony Goodrow and Dan Briggs. Paul Cordeiro should be an honorary member, because he's been right there in the trenches with us. We carried each other from early coursework to dissertation writing, and I will miss these guys.

Several members of the Bell group helped me out a lot when I was first getting my feet wet in the lab and navigating graduate school and the field of catalysis. I need to thank Jason Bronkema, Mark Zerella, Kostya Pokrovski, and Beata Kilos. Outside of the Bell group, Aditya Bhan asked the hard questions and inspired me to investigate zeolites.

I have had the privilege of working with many talented undergraduate researchers. Henry Lawrence established many of the research protocols that were later used in the liquid-phase work, and Arpen Shah and Andrew Pangestan collected tremendous amounts of data in tandem. Glenn Sebastian made a heroic effort to use zeolites in liquid-phase reactions which ultimately was never published, though interesting nonetheless. Anant Gill and Siddhartha Saha made valuable if not brief contributions to the research effort, and all of these students helped me develop as a teacher.

Recent years in the Bell group have yielded many scientific insights and distractions (intellectual and otherwise) with my fellow students Mike Zboray, William Vining, Andrew Behn, Bean Getsoian, Georges Siddiqi, Sean Dee, Shannon Klaus, Anton Mlinar, Joe Gomes, David Hanna, Amber Janda and Zheng Zhai. As post-docs, I have relied on Vlad Shapovalov, Pingping Sun, Chidam Mandan, Jennifer Strunk, and Arne Dinse for science and career advice, as well as the occasional laugh.

From day one, my research has been funded by the Methane Conversion Cooperative Funded by BP. I have had the fortune to interact with some outstanding people from Naperville, Sunbury, and Hull, Including Theo Fleisch, Mike Desmond, Ben Gracey, Sander Gaemers, and Glenn Sunley.

Laura, your contribution to this dissertation cannot be summarized with mere words. It's been a rollercoaster ride I would have never boarded without you, and together we've reached the end of the ride. I hope that you are proud of me and I am proud that will share life's next adventure with the E.

Chapter 1

Introduction

Producing fuel and chemical precursor molecules containing carbon-carbon bonds from synthesis gas is both appealing and challenging. The dwindling supply of crude oil has coincided with increases in the demand and therefore price of crude oil derivatives, leading many industrial and academic researchers to look for alternate carbon feedstocks that could produce the same range of fuel, polymer, and chemical products. A property that many of these products share with the crude oil from which they are currently derived is that they possess C-C bonds.

Natural gas, coal, and biomass are all possible candidate carbon feedstocks to replace crude oil. Biomass is of particular interest because it potentially can be produced renewably, although of these candidates it is currently the least technologically mature. All three of these carbon feedstocks can be used to generate synthesis gas (syngas), a reactive mixture of carbon monoxide and hydrogen. The challenge in using syngas as the starting point for the synthesis of C-C bond containing products is that, unlike crude oil, syngas possesses no C-C bonds. While many C_1 compounds, such as methanol, formaldehyde, methyl formate, and dimethoxymethane, which also lack C-C bonds, can be produced commercially from syngas today, there are few processes that can produce C_2 compounds containing one carbon-carbon bond, or higher C_n compounds with multiple C-C bonds.

One particular compound currently produced from a crude oil derivative is ethylene glycol (MEG). MEG is an important industrial chemical used in the manufacture of polyester resins and fibers and antifreeze. MEG synthesis begins with the epoxidation of ethene to form ethylene oxide, which is then hydrated to give mono-, di-, and triethylene glycol. Ethene itself is obtained from hydrocracking of crude oil hydrocarbons. Over the last decade, the demand for ethene has grown faster than the supply, driving up the price of MEG and other products. In addition, the demand for fiber-grade MEG has increased to supply raw materials for the production of polyesters such as polyethylene terephthalate, commonly found in disposable drink bottles among other uses. Fiber-grade MEG tolerates only very small concentrations of the higher glycol oligomers, while the conventional ethylene oxide hydrolysis route gives only 90% selectivity to MEG.

Direct synthesis of MEG from syngas is possible but requires pressures of 1300-7000 atm, temperatures above 200 °C, and gives very low yields [1-2]. Indirect syngas-based routes start with methanol or its C_1 derivatives, and show more promise. Of these, formaldehyde carbonylation was once practiced commercially, with coal as the carbon source [3-4]. Formaldehyde carbonylation is an acid-catalyzed reaction, which proceeds by the Koch mechanism with carbocationic reaction intermediates. The reaction of formaldehyde and carbon monoxide produces glycolic acid and its esters and ethers, which must then undergo hydrogenation along with esterification or hydrolysis to give MEG.

In a conventional formaldehyde carbonylation scheme, formaldehyde, a strong acid catalyst, and a solvent are mixed in the liquid-phase of a pressurized reactor along

with water or an alcohol. Either mineral acids or solid acids can be used. The headspace of the batch reactor is then pressurized with carbon monoxide up to a pressure between tens and hundreds of atmospheres. The need for such high pressures arises from the poor solubility of carbon monoxide in most solvents. Without the high CO pressures, the Cannizzaro self-disproportionation of formaldehyde becomes the dominant process, leading to low selectivities.

Prior to this work, improvements to formaldehyde carbonylation arose primarily by switching to solvents with higher CO solubilities and solid acid catalysts with higher selectivity to carbonylation. Even with these improvements, the pressure requirement was only reduced to a few hundred atmospheres of CO [5-6].

The objective of this dissertation has been to develop and investigate a reaction system capable of synthesizing MEG precursors with high selectivity at low pressure. Chapter 2 describes an investigation following up on recent interest in developing carbonylation chemistry without the use of gaseous CO [7]. Methyl formate (MF) was evaluated as an in situ source of CO using heteropoly acids to catalyze both the decomposition of MF and the carbonylation of formaldehyde. While the reaction was limited by the slow rate of MF decomposition, the effect of using different formaldehyde sources was observed. In particular, avoiding water and methanol in the reaction system improved the yield of MEG precursors. Dimethoxymethane (DMM), the dimethyl acetal of formaldehyde, was particularly effective at reacting with the CO generated from MF to form MEG precursors. The analogy between DMM carbonylation and formaldehyde carbonylation pathways to MEG can be seen in Figure 1.1.

Recently, other Koch carbonylation reactions were reported in vapor-phase continuous reactor systems using acidic zeolites, such as for methanol, producing acetic acid [8], *tert*-butanol, producing pivalic acid [9], and dimethyl ether, producing methyl acetate [10-12], with reasonable yields even at CO pressures below 10 atm. Chapter 3 describes the first example of vapor-phase DMM carbonylation, which was accomplished by using acidic zeolites as the catalyst. Using H-Faujasite (FAU), it was possible to achieve 79% selectivity to methyl methoxyacetate (MMAc), the carbonylation product, with 20% yield based on DMM at only 3 atm of pressure.

The discovery of a highly-selective and low-pressure route to MEG precursors from DMM was followed by detailed investigations of carbon-carbon bond formation in the zeolite-catalyzed vapor-phase system. Chapter 4 details the role of the zeolite framework structure and Si/Al ratio on the activity and selectivity of DMM carbonylation, and describes why FAU with high Si/Al ratios provide the most active and selective catalysts to-date. Chapter 5 focuses on mechanistic studies of DMM carbonylation and DMM disproportionation by using in situ infrared spectroscopy to probe the identity and concentrations of surface intermediates in the catalytic cycles for DMM carbonylation and disproportionation. Together with the kinetic evidence in Chapter 4, a rate expression and reactor model are developed in Chapter 5 to describe the kinetics of the reaction system and predict with reasonable quantitative accuracy the effects of reaction temperature and reactant partial pressures on the rates of MMAc and disproportionation product synthesis.

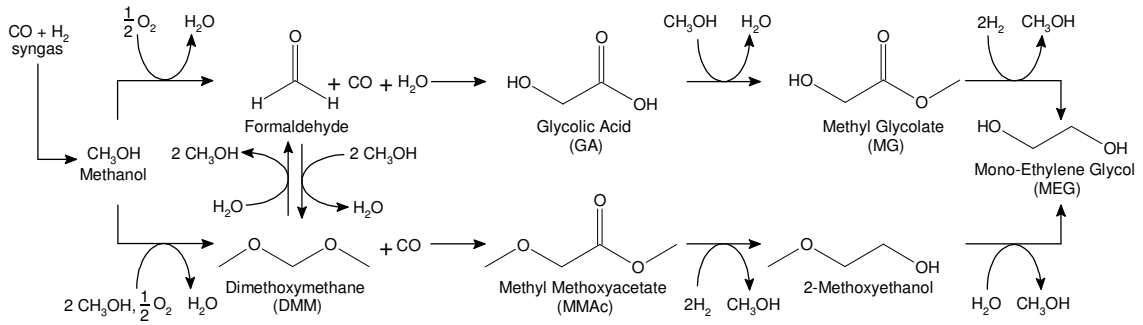

Figure 1.1 Scheme for producing MEG from syngas via formaldehyde or DMM carbonylation.

References

[1] R.L. Pruett, W.E. Walker, U.S. Patent 3 957 857 (1976), to Union Carbide Corporation.
[2] D.R. Fahey, J. Am. Chem. Soc. 103 (1981) 136.
[3] D.J. Loder, US Patent 2 152 852 (1939), to E. I. du Pont de Nemours & Co.
[4] A.T. Larson, U.S. Patent 2 153 064 (1939) to E. I. du Pont de Nemours & Co.
[5] S.Y. Lee, J.C. Kim, J.S. Lee, Y.G. Kim, Ind. Eng. Chem. Res. 32 (1993) 253.
[6] D.E. Hendriksen, Prepr. Pap.—Am. Chem. Soc., Div. Fuel Chem. 28 (1983) 176.
[7] T.Morimoto, K. Kakiuchi, Angew. Chem. Int. Ed. 43 (2004) 5580.
[8] B. Ellis, M. J. Howard, R. W. Joyner, K. N. Reddy, M. B. Padley, W. J. Smith, in 11th International Congress on Catalysis - 40th Anniversary, Pts A and B, Vol. 101, Elsevier Science Publ. B V, Amsterdam, (1996) 771-779.
[9] T. Li, N. Tsumori, Y. Souma, Q. Xu, Chem. Commun. (2003) 2070.
[10] P. Cheung, A. Bhan, G. J. Sunley, E. Iglesia, Angew. Chem. Int. Ed. 45 (2006) 1617.
[11] P. Cheung, A. Bhan, G. J. Sunley, D. J. Law, E. Iglesia, J. Catal. 245 (2007) 110.
[12] A. Bhan, A. D. Allian, G. J. Sunley, D. J. Law, E. Iglesia, J. Am. Chem. Soc. 129 (2007) 4919.

Chapter 2

Synthesis of Precursors to Ethylene Glycol from Formaldehyde and Methyl Formate Catalyzed by Heteropoly Acids

Abstract

The production of ethylene glycol from methanol and its derivatives, such as formaldehyde, is potentially attractive, since the carbon needed for such a process can be derived from synthesis gas, a cheaper carbon source than petroleum-derived ethylene. This study reports an investigation of formaldehyde carbonylation using methyl formate as the source of CO. Silicotungstic acid and other heteropoly acids were used as the catalyst. Methyl glycolate and methyl methoxyacetate, both precursors to ethylene glycol, were formed along with dimethoxymethane and dimethyl ether, the primary byproducts. The effects of formaldehyde source, reaction temperature, time, and catalyst were investigated. Methoxymethanol, paraformaldehyde, 1,3,5-trioxane, and dimethoxymethane were examined as sources of formaldehyde. The highest yields of methyl glycolate and methyl methoxyacetate were obtained using 1,3,5-trioxane as the source of formaldehyde. Release of carbon monoxide from methyl formate was found to be slow and limited the rate of carbonylation. Of the heteropoly acids investigated, silicotungstic acid produced the highest yields of methyl glycolate and methyl methoxyacetate, whereas methanesulfonic acid did not produce these products at similar acid loading. The difference in the effectiveness of heteropoly acids and methanesulfonic acid is ascribed to the role of the anion of the heteropoly acid, a soft base, in stabilizing the reactive intermediates involved in the carbonylation of formaldehyde.

2.1 Introduction

Ethylene glycol (monoethylene glycol - MEG) is an important industrial chemical used in the manufacture of polyester resins and fibers and antifreeze. While global antifreeze demand is stable, demand for polyester is increasing at roughly 10% per year, driven mainly by growth in China [1]. Demand for ethylene, the raw material used to make MEG, is outpacing supply, leading to price increases for MEG [2]. Replacing ethylene derived ultimately from crude oil, with syngas derived from natural gas, coal, or biomass could be economically competitive and increase MEG supply for the growing polyester market.

Direct synthesis of MEG from syngas is possible but requires pressures of 1300-7000 atm, temperatures above 200 °C, and gives very low yields [3,4]. MEG synthesis starting from methanol, formaldehyde, or other C_1 compounds that can be produced from syngas are referred to as indirect routes. Some examples include hydroformylation of formaldehyde [5,6], oxidative coupling of CO in methanol [7], and carbonylation of formaldehyde [8 , 9]. Of these, formaldehyde carbonylation has been practiced commercially by DuPont [8,10,11].

The acid-catalyzed carbonylation of formaldehyde occurs by the Koch mechanism, beginning with the protonation of the substrate to yield a carbocation, which undergoes CO addition to give a resonance-stabilized acyl carbocation in the carbon-carbon bond-forming step. Water addition and subsequent deprotonation yields glycolic acid (GA). Glycolic acid, as an intermediate to MEG, is esterified with methanol to methyl glycolate (MG), and then hydrogenated in the final step to yield MEG. The stoichiometric reactions involved in this process are shown below:

$$HCHO + CO + H_2O \rightarrow HOCH_2COOH \qquad \Delta G^\circ = -36.6 \text{ kJ/mol} \quad (1)$$
$$HOCH_2COOH + CH_3OH \rightarrow HOCH_2COOCH_3 + H_2O \qquad -34.2 \text{ kJ/mol} \quad (2)$$
$$HOCH_2COOCH_3 + 2H_2 \rightarrow HOCH_2CH_2OH + CH_3OH \qquad +9.2 \text{ kJ/mol} \quad (3)$$

The DuPont process for MEG synthesis via formaldehyde carbonylation achieved yields in excess of 96% using H_2SO_4 as the catalyst [3,4]. The reaction required 900 atm of CO pressure and temperatures between 150-200 °C. All reactants in the DuPont process were prepared from coal-derived syngas. Corrosive reaction conditions associated with using a mineral acid and high pressures of CO led to discontinuation of the technology in 1968 [8].

Renewed interest in formaldehyde carbonylation arose with the use of solid acids replacing sulfuric acid. Solid acids have a number of benefits over mineral acids, including ease of catalyst recovery, stronger acidity, and less corrosion. Hendriksen [6] has reported 48% yield of GA with CO pressure as low as 102 atm (1500 psi) using Nafion perfluorosulfonic acid resin at 150 °C, and 79% yield at 313 atm (4600 psi). Lee et al. [8] have investigated a number of acidic resins as well as two heteropoly acids (HPAs), $H_3PW_{12}O_{40}$ (PW_{12}), and $H_3PMo_{12}O_{40}$ (PMo_{12}). They achieved 36% yield of MG after esterification with 68 atm (1000 psi) of CO and 81% yield with 238 atm (3500 psi) using Amberlyst, a polystyrenesulfonic acid resin.

The high pressure requirement of formaldehyde carbonylation is due to low solubility of CO in the liquid phase. In the original DuPont process water was the only solvent, and at 150 °C and 60 atm of external CO pressure, the solubility of CO in water is only 0.054 mol/l [12]. Increasing the pressure to 900 atm increases the solubility to 0.81 mol/l. Hendriksen and Lee et al. used 1,4-dioxane as their solvent, for which the solubility is 0.56 mol/l at 150 °C and 60 atm CO pressure [13]. Much of the apparent decrease in required pressure can be attributed to the change in solvent. Despite the reduction, the pressure requirement is still considerable.

There has been recent interest in developing carbonylation chemistry without the use of gaseous CO [14]. Methyl formate (MF) has been suggested as a viable means for providing CO [15], since it can be decarbonylated catalytically to CO and methanol.

$$HCOOCH_3 \rightarrow CO + CH_3OH \qquad \Delta G^\circ = +0.4 \text{ kJ/mol} \quad (4)$$

Similarly, formic acid (FA) can be used to give CO and H_2O. Hendriksen [6] mentions that if MF is used, no additional CO pressure is required for the carbonylation of formaldehyde. In this reaction, MF acts as the sole CO source, and MG is produced directly instead of GA.

$$HCOOCH_3 + HCHO \rightarrow HOCH_2COOCH_3 \qquad -70.4 \text{ kJ/mol} \quad (5)$$

The release of methanol from Reaction 4 leads to methyl methoxyacetate (MMAc).

$$HCOOCH_3 + HCHO + CH_3OH \rightarrow CH_3OCH_2COOCH_3 + H_2O \qquad -96.4 \text{ kJ/mol} \quad (6)$$

MMAc can be hydrolyzed and then hydrogenated to give MEG, or hydrogenated directly to glycol ether, an important industrial solvent.

He et al. [16,17] have compared the activity of a number of mineral, organic, and solid acids, including PW_{12}, PMo_{12}, $H_4SiW_{12}O_{40}$ (SiW_{12}), and $H_4SiMo_{12}O_{40}$ ($SiMo_{12}$) for the carbonylation of formaldehyde with methyl formate. In their work, SiW_{12} and PW_{12} gave the best yields of MG and MMAc. Further study [18,19] showed that salts of SiW_{12} were less active than the parent acid, and that water was detrimental to product yield. A similar reaction between formaldehyde and formic acid in water to produce GA has also been shown using HCl as the catalyst [20].

The aim of the work presented here was to establish the effects of formaldehyde source, reaction temperature, and reaction time on the acid-catalyzed carbonylation of formaldehyde with methyl formate. Following the work of He et al. [18], HPAs were chosen as catalysts for this study, with particular interest in SiW_{12}. A reaction scheme describing the important chemistry was developed and used to explain the effects of reaction conditions on the distribution of observed products. The role of catalyst composition was also explored. This part of the investigation revealed the importance of the HPA anion composition in dictating the activity and selectivity of HPAs. In this paper, MG and MMAc are referred to as C_2 compounds as they contain only one carbon-carbon bond.

2.2 Experimental Methods

All reactions were carried out in a 25 ml Hastelloy C-276 autoclave (Parr Instruments), equipped with a temperature-programmed electric heating mantle, a magnetically driven Teflon coated stir bar, a Hastelloy C-276 thermowell containing an iron-constantan J-type thermocouple, and a gas pressure gauge. Hastelloy C-276 was chosen as the material of construction because of its broad corrosion resistance.

Paraformaldehyde (Aldrich) and 1,3,5-trioxane (Aldrich) were used as the sources of formaldehyde. In addition, formaldehyde methyl hemiacetal (hereafter referred to as methoxymethanol) was prepared by heating paraformaldehyde to 100 °C and bubbling the vapors through methanol at room temperature. A flow of 100 ml/min He was used to carry the vapors and the transfer tube was heated above 150 °C to prevent repolymerization of formaldehyde. A 39 wt% formaldehyde solution was prepared this way. Formaldehyde dimethyl acetal, (hereafter dimethoxymethane, DMM), obtained from Sigma-Aldrich was also used as a formaldehyde source in some experiments. Reagents were used without further purification.

Heteropoly acids SiW_{12}, PW_{12}, $SiMo_{12}$, and PMo_{12} were obtained from Sigma-Aldrich and Strem Chemicals. Prior to use, these materials were dehydrated in a 50 cm^3/min He flow for 3 h at 300 °C according to He et al. [18].

In a typical reaction, the autoclave was loaded with 2 g of paraformaldehyde, 4 g of methyl formate, and 0.25 g of an acid catalyst. Methanol (0.5 g) was added to stabilize formaldehyde. The autoclave was then sealed. Additional gases could be added to the reactor through a gas inlet valve. The contents of the reactor were stirred and heated to 150 °C. The reaction temperature was reached after approximately 25 min. After 3 h at 150 °C, the reactor was cooled in an ice bath for approximately 30 min.

Liquid phase products were analyzed by gas chromatography using an Agilent 6890n GC. MF, DMM, MG, and MMAc concentrations were quantified using an HP-PLOT Q bonded polystyrene-divinylbenzene capillary column and a flame ionization detector. H_2O, HCHO, and CH_3OH concentrations were determined using a HayeSep DB divinylbenzene packed column and a thermal conductivity detector. A known mass (3.5-3.9 mg) of cyclohexane was added to a known mass of reaction liquid (~1 g) as an internal standard. Gas phase CO was analyzed with a HayeSep DB column and GC TCD.

2.3 Results and Discussion

2.3.1 Reactions with methoxymethanol as formaldehyde source

Initial experiments were carried out using methoxymethanol, the methyl hemiacetal of formaldehyde, as a monomeric formaldehyde source. The methoxymethanol solution prepared contained 39 wt% equivalent formaldehyde, 1 wt% water, and balance methanol. Typically, 3 g of 39 wt% HCHO solution and 3 g of MF were used. Reaction temperature and duration were varied, with results shown in Figures 2.1 and 2.2.

During reaction, CO released by MF decomposition (Reaction 4) accumulated in the reactor headspace. CO release increased with temperature from 135 °C to 165 °C, as did the concentrations of MG and MMAc. The solutions produced in these reactions were colored, ranging from pale yellow to very dark brown/black, with darker solutions produced at higher temperatures. In some reactions, a black solid was collected from the bottom of the reactor. Hendriksen [6] has reported a similar observation for a slightly different reaction system, and attributed the color to the formation of formose sugars from formaldehyde, which subsequently underwent acid-catalyzed carbonization. Formose chemistry is well known in the presence of bases [21], but is not possible under acidic conditions. Thus, we propose that the color may be due to the formation of polymers of glycolic acid or the acid-catalyzed carbonization of other reaction components (see for example Reaction 7). Polymers of glycolic acid copolymerized with formaldehyde give rise to yellow liquids, and those without formaldehyde are brown solids [22].

$$n\ HCHO \rightarrow C_{n\ (s)} + n\ H_2O \qquad (7)$$

Because of the large excess of methanol, DMM was formed as the primary product, by Reaction 8. DMM concentration was stable between two and four hours. MMAc was produced at only low concentration, and MG was not observed below 165 °C, even after 4h.

$$CH_3OCH_2OH + CH_3OH \rightarrow CH_3OCH_2OCH_3 + H_2O \qquad \Delta G^\circ = -16.9\ kJ/mol \qquad (8)$$

Reaction 8 produces equal amounts of DMM and water, and at 150 °C, between 2 and 4 h, the concentrations of DMM and water were almost equal. At 135 °C, the concentrations of these products are even closer to each other. With increasing temperature, the concentrations of DMM and H_2O began to diverge, the DMM concentration decreasing and the water concentration increasing. Additional water production came from the dehydration of methanol to form dimethyl ether (DME). Water release from Reaction 6 was insignificant as the MMAc concentration was low. The remaining source of water is believed to be the carbonization of reactants and/or products as in Reaction 7. The reduction in DMM concentration at higher temperature coincided with an increase in MMAc concentration and the formation of MG as a reaction product.

2.3.2 Reactions with paraformaldehyde as formaldehyde source

To reduce the amount of methanol used, paraformaldehyde/methanol mixtures were substituted for methoxymethanol solutions. The first data set shown in Figure 2.3 was obtained using a methoxymethanol solution as the formaldehyde source. The second set, with the same molar composition, was obtained using paraformaldehyde and methanol, reproducing the results from the methoxymethanol experiments. Analysis of the reaction products showed that methoxymethanol had been formed in situ from the addition of methanol to the formaldehyde monomer released from paraformaldehyde. It is assumed that the rate of paraformaldehyde depolymerization was rapid enough so as not to influence the results.

Reduction of the methanol content in the starting mixtures from 38 mole% to 5% (Figure 2.3), favored the formation of C_2 products, MG and MMAc, and reduced the concentration of DMM formed. This suggests that formaldehyde participates in two competitive reaction paths, one leading to DMM and the other leading to C_2 products.

For the reactant composition given as the last data set in Figure 2.3, corresponding to 5 mole% methanol, some repolymerization of formaldehyde to polyoxymethylene occurred in reactor cold spots, especially in the reactor head assembly. As noted in Section 3.1, methanol stabilizes formaldehyde as the hemiacetal; therefore, when the methanol concentration was reduced too far, repolymerization occurred. Maintaining 10 mole% methanol in the starting mixture was sufficient to prevent repolymerization when working with paraformaldehyde in all cases.

When excess methanol was used with paraformaldehyde, the concentrations of water and DMM were nearly equal to each other, as was the case when methoxymethanol was used as the formaldehyde source. Thus, the primary source of the water for these conditions was Reaction 8. As the methanol loading was reduced, the DMM concentration decreased but the water concentration increased, indicating a shift from Reaction 8 to carbonization reactions, such as Reaction 7, as the source of water, with an increasing contribution also coming from Reaction 6. DME concentration remained nearly constant, despite the reduction in the initial concentration of methanol in the reactant mixture. This was due to the production of methanol from MF, as evidenced by the increasing CO pressure developed in the reactor. The color of the reaction solutions darkened as the methanol concentration was decreased, further indicating an increase in polymer formation and/or carbonization of reaction components.

The effects of varying reaction time and temperature are given in Figures 2.4 and 2.5. DMM formation occurred at lower temperatures and shorter times than C_2 product formation. In particular, the maximum DMM concentration was obtained when the reactor was heated to 150 °C and then immediately cooled down (a hold time of zero hours) indicating that DMM formation from paraformaldehyde is not only fast, but reaches equilibrium. If DMM had not equilibrated, an increase in hold time to 0.5 h or 1 h would be expected to increase the concentration of DMM.

As seen in Figure 2.4, CO pressure increased with time. The slow accumulation of gaseous CO in the reactor was due to the apparently slow decomposition of MF. Assuming equilibration between gaseous and dissolve CO, a small CO pressure indicated a low concentration of dissolved CO, and therefore a slower carbonylation rate. Thus, the C_2 product concentrations were small while CO pressure was low for times less than 2 h, and increased with increasing CO pressure up to 5 h. Beyond 5 h of reaction, the concentration of C_2 products did not change significantly despite an increase in CO pressure, possibly due to the consumption of formaldehyde – as evidenced by the disappearance of DMM – to form other byproducts.

Increasing the reaction temperature increased the concentrations of MG and MMAc (Figure 2.5). However, the color of the solutions darkened, indicating an increase in polymer or carbon formation, or both. Water concentration also increased with temperature, consistent with an increased level of carbonization. The increase in C_2 product concentrations at higher temperature is attributed to the higher CO pressure released from MF under these conditions.

To simulate a faster release of CO from MF, some of the initial MF was replaced by methanol and gas phase CO. 7.0 mmol and 13 mmol of MF were replaced by 7.0 mmol and 13 mmol of CO and CH_3OH in separate experiments. The effect is equivalent to converting 10% and 20% of the MF (as per Reaction 4) prior to loading the reactor, increasing the CO initially available in the reactor. The results, shown in Figure 2.6, reveal an increase in C_2 product concentration when CO is available at short times.

In a separate experiment, 11 mmol of CO were added to the gas phase of the reactor without changing the starting amounts of MF or CH_3OH. The added CO increased the C_2 concentration, even more than that achieved by replacing MF with CO + CH_3OH. Considering the total amount of CO as being that contained in MF and gaseous CO, this experiment demonstrated that increasing the starting quantity of CO by only 16% led to a 170% increase in C_2 concentration and a 60% decrease in DMM concentration, further suggesting that CO release from MF is a limiting factor in the reaction. The addition of gas phase CO benefited the formation of MMAc, which increased by 240%, more than it did the formation of MG, which increased by only 130%.

A further experiment attempted the reaction without methyl formate, adding only 13 mmol of CO as a gas to 67 mmol of formaldehyde and 83 mmol of methanol (replacing MF with methanol). Only small amounts of MG and MMAc were observed (Figure 2.6), as DMM was by far the majority product due to the large amount of methanol present. This experiment demonstrated that by using MF to release CO slowly, the release of methanol is also slow, thereby inhibiting DMM formation. Although no MF was added to the reaction, a final MF concentration of 1.3 M was observed, indicative of the Cannizzaro coupling of formaldehyde with itself. The MF formed in

this way also decomposed to release a net 2.0 atm of CO gas above the CO initially charged to the reactor.

High water concentrations at the end of some reactions starting with paraformaldehyde led to conversion of a small fraction of the esters in the reaction mixture to their carboxylic acid forms. Formic acid (from MF), glycolic acid (from MG), and methoxyacetic acid (from MMAc) were all detected by GC/MS. Trace quantities of glycol ethers, such as 2-methoxy ethanol, 1,2-dimethoxyethane, and 1,3-dioxolane, were also detected by GC/MS.

2.3.3 1,3,5-trioxane as formaldehyde source

When 1,3,5-trioxane was used as the formaldehyde source, no repolymerization of formaldehyde to polyoxymethylene was observed, and so experiments were carried out without adding methanol. Unlike paraformaldehyde, 1,3,5-trioxane is anhydrous, so that no water was introduced at the beginning of the reaction as well. By excluding methanol, (except that released from MF) DMM concentrations were lower and C_2 concentrations were higher (Figures 2.7 and 2.8) that those observed when paraformaldehyde was used as the formaldehyde source (Figures 2.4 and 2.5). CO release from MF was also greater, possibly due to the lack of solvent leveling of the acidity for short reaction times. The CO pressure released was nearly double that observed when paraformaldehyde was used as the formaldehyde source (compare Figures 2.7 and 2.4). Unlike paraformaldehyde, which favored MG over MMAc, 1,3,5-trioxane gave nearly equal concentrations of both C_2 compounds. Less water was produced and solutions were generally lighter in color and less solid was collected when 1,3,5-trioxane was used as compared to when paraformaldehyde was used as the formaldehyde source.

2.3.4 Dimethoxymethane as formaldehyde source

The possibility of DMM carbonylation was explored using both MF and gaseous CO as the source of CO (Figure 2.9). In the absence of water, DMM should form only a single product, MMAc (Reaction 9). To form MG, either the ether group of MMAc must be hydrolyzed, or methoxymethanol must be formed as an intermediate. Some water was always produced from the dehydration of methanol released from MF to form DME and from the carbonization reaction. This would explain why MG was always observed in the reaction products formed. Formation of C_2 products from DMM indicates that the carbonylation of DMM also occurs under conditions where DMM is produced via the reaction of formaldehyde (released from paraformaldehyde or 1,3,5-trioxane) with methanol.

Reactions starting with DMM showed a greater selectivity to MMAc than MG, the reverse of what was observed starting with paraformaldehyde. A comparison of the first and second data sets in Figure 2.7 shows that the MG concentration fell by 10% upon switching from paraformaldehyde to DMM, while the MMAc concentration increased by 240%. While the reaction starting with paraformaldehyde generated 13.6 atm of CO, starting with DMM only 9.8 atm of CO were generated.

$$CH_3OCH_2OCH_3 + CO \rightarrow CH_3OCH_2COOCH_3 \qquad \Delta G^\circ = -68.9 \text{ kJ/mol} \quad (9)$$

An experiment starting with only DMM and CO had an even more dramatic result (fourth data set in Figure 2.9). The MG concentration was 0.57 M and the MMAc concentration was 1.19 M, the highest of any experiment, accomplished with only 13 mmol of CO, as compared to 67 mmol of MF in most reactions, and 67 mmol of MF plus 13 mmol of CO in the third data set in Figure 2.9. The high concentration of C_2 products given the small amount of CO gas present indicates a faster carbonylation rate with DMM than with either paraformaldehyde or 1,3,5-trioxane.

Across a range of reaction times and temperatures (Figures 2.10 and 2.11), reaction solutions were clear and almost colorless, especially when compared to paraformaldehyde, though an appreciable amount of black solid formed in the reactor. Total C_2 product concentration was intermediate between paraformaldehyde and 1,3,5-trioxane (compare Figure 2.10 with Figures 2.4 and 2.7). Starting with DMM, MG concentrations were comparable to the lower MG concentrations produced from using paraformaldehyde, and MMAc concentrations were almost as high as the higher MMAc concentrations produced from using 1,3,5-trioxane. The CO pressure generated was nearly one-half of that produced when using paraformaldehyde as the formaldehyde source, and one quarter that produced when 1,3,5-trioxane was used. DMM was also observed to undergo Cannizzaro self-disproportionation as evidenced by the formation of MF as a reaction product when only DMM and CO were loaded into the reactor. The MF generated in this way decomposed to produce additional gaseous CO according to Reaction 4.

2.3.5 Summary of formaldehyde sources

Table 2.1 summarizes the effects of formaldehyde source on the conversion of formaldehyde to MG, MMAc, DMM, and carbon (measured as H_2O) for a fixed set of reaction conditions. (Water accounted for in this way excludes water produced from the formation of DMM, DME, and MMAc.) Since all four formaldehyde source systems generated different CO pressures, the conversion of the generated CO to C_2 products is also given. It is evident that the highest conversion of formaldehyde to C_2 products is achieved using 1,3,5-trioxane as the formaldehyde source and the lowest conversion to these products is achieved using methoxymethanol. This is attributed to the effect of solvent leveling when methanol and water are present at short reaction times, reducing the acidity of the system and thus limiting the amount of CO released from MF. When using 1,3,5-trioxane, no methanol was added, and the formaldehyde source was anhydrous (unlike paraformaldehyde), so no protic solvents were present at short reaction times, and the highest CO pressures were reached of all the formaldehyde sources used. Although DMM is also anhydrous, and no methanol was added, methanol was released by reaction with the acid catalyst. Another interesting observation is that the conversion to carbon is lower when excess methanol is present, e.g., when using methoxymethanol, though this may be because the concentration of formaldehyde is lower in this case.

2.3.6 Proposed reaction scheme

The reaction scheme in Figure 2.12 is proposed as a means of relating observable products to reactants. The first step when either paraformaldehyde or 1,3,5-trioxane is used as a reactant is the generation of formaldehyde in solution. In the next step, the substrate is protonated to generate a carbocation. Protonation of monomeric

formaldehyde yields a hydroxycarbocation, while protonation of DMM yields a methoxycarbocation via loss of methanol. Protonation of methoxymethanol produces either the hydroxycarbocation via loss of methanol or the methoxycarbocation via loss of water. If water and methanol are both present, interconversion of the two carbocations via methoxymethanol occurs readily. Since DMM formation from formaldehyde was observed to occur rapidly, formaldehyde, DMM, and methoxymethanol are assumed to reach equilibrium rapidly once heated to the reaction temperature. Therefore the concentration of water and methanol determines the distribution of these C_1 formaldehyde sources, as well as the relative abundance of the hydroxy- and methoxycarbocations. The reactions between formaldehyde sources and carbocation intermediates are rapid and, hence, are very likely to be at equilibrium. Therefore, for this reason all of the processes above the dotted line in Figure 2.12 and are considered equilibrated.

Reaction of the hydroxy- and methoxycarbocations with CO leads to two resonance-stabilized acyl carbocations. Addition of methanol to the carbonylation product of the hydroxycarbocation leads to MG. (Addition of water leads to a small amount of glycolic acid, not shown). The carbonylation of the methoxycarbocation leads to MMAc after methanol addition. (Addition of water would lead to methoxyacetic acid, not shown.) The selectivities to MG and MMAc of the formaldehyde sources studied here are thought to reflect the relative abundance of the hydroxy- and methoxycarbocations, which themselves depend on the concentrations of water and methanol.

Paraformaldehyde and 1,3,5-trioxane are shown as the sources of monomeric formaldehyde from which the hydroxy- and methoxycarbocation intermediates are formed. However, the scheme also shows how DMM and methoxymethanol can also generate the same carbocations, thereby undergoing carbonylation as well.

The scheme shows the decomposition of MF as the CO source. The slow release of CO from MF limits the carbonylation rate, and therefore the formation of C_2 compounds. However, as MF is also a source of methanol, slow methanol release also limits DMM formation, enabling C_2 product concentrations to rise to a greater level. The formation of byproduct polymers and carbonization are shown as being formed from monomeric formaldehyde, although the true mechanism for this process is not understood. The carbonylation step, CO release from MF, and polymer and carbon formation reactions are all represented below the dotted line in Figure 2.12, indicating that they are kinetically relevant, in contrast with the equilibrated steps above the dotted line.

From Figure 2.12, it is apparent that the rate of formation of C_2 products would be enhanced if CO release from MF and CO incorporation into products occurred at faster rates. However, the rate of CO release has been shown to be slow, especially with respect to DMM formation from formaldehyde. High CO pressures were found to lead to higher C_2 product concentrations, as would be predicted from the scheme. It can also be seen that high methanol concentrations would lead to increased DMM formation.

The product solutions obtained using paraformaldehyde as the source of formaldehyde were generally darker than those using 1,3,5-trioxane. It is also not apparent why solutions generated from DMM were almost colorless, yet resulted in larger amounts of solid collected. It is clear, however, that low concentrations of methanol contributed to both darker solutions and more solid being collected. This

suggests that keeping the formaldehyde concentration low by including a solvent such as methanol may help to reduce the rates of unwanted byproduct formation.

2.3.7 Role of the catalyst

In the preceding discussion, the catalyst was treated solely as a proton source, and the role of the heteropolyanion was ignored. To determine whether the composition of the anion affects the catalyst activity, several heteropoly acids were examined.

The performance of SiW_{12}, PW_{12}, $SiMo_{12}$, and PMo_{12} in the carbonylation of paraformaldehyde were compared (Figure 2.13), using 0.25 g of catalyst in each experiment. The molybdic acids gave low combined yields of MG and MMAc compared to the tungstic acids. This is attributed to the greater reducibility of the molybdic acids [17,23]. Since reduced HPAs are more basic [23], their effectiveness as acid catalysts is diminished. Reduction of the HPA during reaction was evidenced by the blue color of post-reaction solutions containing $SiMo_{12}$ and PMo_{12}, indicating the formation of reduced "heteropoly blues." The composition of the reducing agent is not known, but both methanol and formaldehyde could serve this purpose. The selectivity to MG and MMAc reversed for the tungstic and molybdic acids; both SiW_{12} and PW_{12} were more selective to MG, whereas $SiMo_{12}$ and PMo_{12} were more selective to MMAc.

The difference between SiW_{12} and PW_{12} acids may be partially explained by differing number of protons – four in $SiW_{12,}$ and three in PW_{12}. Starting with equivalent numbers of protons (Table 2.2), SiW_{12} still gave a higher concentration of MG and MMAc than PMo_{12}. In contrast to HPAs, methanesulfonic acid (CH_3SO_3H), a typical strong liquid acid, produced only DMM and no C_2 products.

The relative activity of SiW_{12} cannot be explained by acid strength alone. Common measures of acid strength in heteropoly acids place them in the order $PW_{12}>SiW_{12}\geq PMo_{12}>SiMo_{12}$ [23, 24], although depending on the method used, the differences between the last three can be quite small or none at all [24]. However, the superior acid strength of PW_{12} is reproduced in almost all cases. Both Figure 2.13 and Table 2.2 show that C_2 production was greater for SiW_{12} than for PW_{12}. Methanesulfonic acid is a weaker acid than either of the heteropoly acids, but not so much weaker as to explain the lack of any detectable C_2 compounds from the reaction.

He et al. [17] have attributed the difference in reactivity between SiW_{12} and PW_{12} to the softness of the soft heteropoly anion formed from deprotonation of the parent acid, stating that it helped form a carbanion by deprotonating MF. Formation of a carbanion under acidic conditions is not usually possible, though the softness of the heteropoly anion most likely plays an important role in the catalysis. Izumi et al. [25] have investigated the cleavage of ethers catalyzed by heteropoly acids. The authors noted that in some cases SiW_{12} exhibited higher reactivity than PW_{12}, and attributed this difference to stabilization of the intermediate carbocations by the soft heteropoly anion base. In their study, equilibrium constants for formation of silver salts of heteropoly anions were two orders of magnitude larger for SiW_{12} than for PW_{12}, which were in turn one order of magnitude larger than those of either PMo_{12} or $SiMo_{12}$. Increased stabilization of soft carbocation intermediates through soft acid-soft base interactions could explain why SiW_{12}, while a weaker acid than PW_{12}, was a more effective carbonylation catalyst as seen in this study. It could also explain why methanesulfonic acid, which produces the

hardest conjugate base amongst acids considered here, would produce no carbonylation products at equal molar proton loadings to the heteropoly acids.

If the interaction of the carbocation and the heteropoly anion is considered as a coordinative interaction, a reaction mechanism can be proposed similar to Figure 2.14. In the mechanism, formaldehyde is carbonylated to form a carbocation stabilized by its coordination to the heteropoly acid. Carbon monoxide addition then takes place, forming a stabilized acyl carbocation, followed by reaction with methanol, releasing the product MG and regenerating the acidic proton. The function of the catalyst is purely as a Brønsted acid/soft base. The heteropoly acids considered here do not possess any Lewis acidity [24]. As such, CO has no sites to coordinate to prior to reaction with protonated formaldehyde, and CO insertion occurs by an Eley-Rideal mechanism. This may limit the rate at which CO insertion occurs.

As formaldehyde is proposed to be in equilibrium with methoxymethanol, DMM, and the hydroxy- and methoxycarbocation intermediates shown in the reaction scheme (Figure 2.12), the stabilization of these carbocations is not likely to be important in explaining the difference in activity between SiW_{12} and PW_{12}. The stabilization of the acyl carbocations formed after CO addition is therefore proposed to be the distinguishing effect between the activity of SiW_{12} and PW_{12}.

2.4 Conclusions

The acid-catalyzed carbonylation of formaldehyde by methyl formate (MF) produces methyl glycolate (MG) and methyl methoxyacetate (MMAc). These products, referred to as C_2 compounds, are precursors to ethylene glycol. Dimethyl ether (DME), dimethoxymethane (DMM), and a carbonaceous solid are the main byproducts. The selectivity to C_2 compounds is strongly influenced by the source of formaldehyde and the concentration of methanol in the reaction system. Methoxymethanol in methanol solution gave the lowest yields of C_2 products due to the large excess of methanol, which reacted to form DME and DMM. Paraformaldehyde required only a small amount of methanol to prevent polyoxymethylene formation, and gave a greater yield of C_2 products. 1,3,5-trioxane required no additional methanol, resulting in the highest yield of C_2 products. C_2 yields from DMM were intermediate between those for paraformaldehyde and 1,3,5-trioxane. DMM was also found to undergo carbonylation by gas phase CO more readily than paraformaldehyde.

Slow release of CO from MF was identified as the primary factor limiting the rate of formaldehyde carbonylation. High concentrations of methanol decreased the rate of CO release from MF. Introduction of modest amounts of CO into the gas phase gave more than proportional increases in C_2 products by increasing the availability of CO at short reaction times.

A reaction scheme was proposed to illustrate the relationships between reactants, products, and possible reaction intermediates. Formaldehyde, methoxymethanol, and DMM are taken to be in equilibrium with each other and with hydroxy- and methoxycarbocations of formaldehyde. The relative abundance of these species depends on the concentrations of methanol and water. Carbonylation of the carbocation intermediates is thought to be the rate-limiting step in the formation of C_2 compounds, a process that is further limited by the release of CO from MF. The carbocation

intermediates can also participate in the formation of carbonaceous deposits; hence, high CO partial pressures are required to increase the yield of C_2 compounds and minimize the formation of carbon.

The activities of common heteropoly acids were compared with each other and with the activity of methanesulfonic acid for similar acid loadings. Methanesulfonic acid, a strong acid with a hard counter anion, yielded no C_2 compounds, whereas the heteropoly acids, which are strong acids with soft counter anions, produced C_2 compounds. It is proposed that soft anions are responsible for stabilizing the acyl carbocations formed after CO addition to the protonated formaldehyde. High activity was also found to correlate with resistance of the anion to reduction.

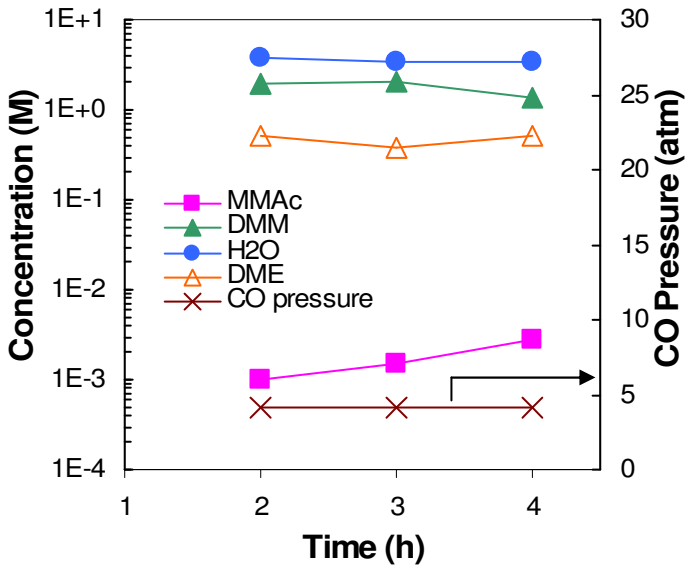

Figure 2.1 Effect of reaction time on product distribution using methoxymethanol as the formaldehyde source. T = 150 °C. SiW_{12} = 0.088 mmol, HCHO = 39 mmol as methoxymethanol solution, CH_3OH = 48 mmol, MF = 50 mmol.

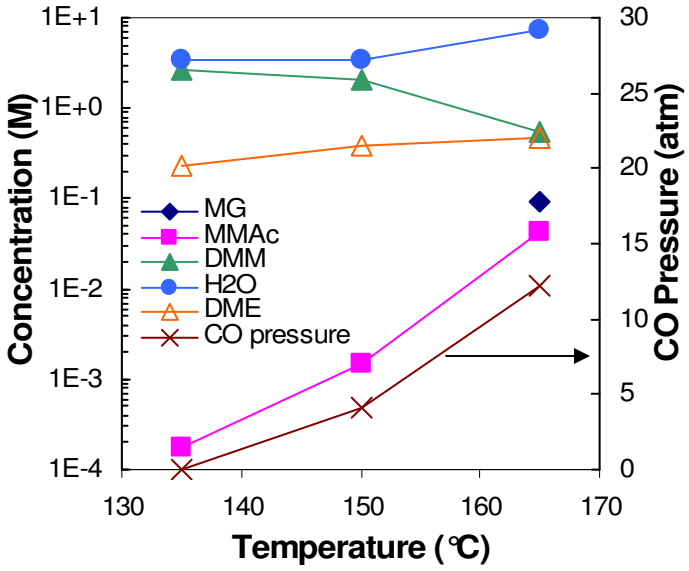

Figure 2.2 Effect of reaction temperature on product distribution using methoxymethanol as the formaldehyde source. time = 3 h. SiW_{12} = 0.088 mmol, HCHO = 39 mmol as methoxymethanol solution, CH_3OH = 48 mmol, MF = 50 mmol.

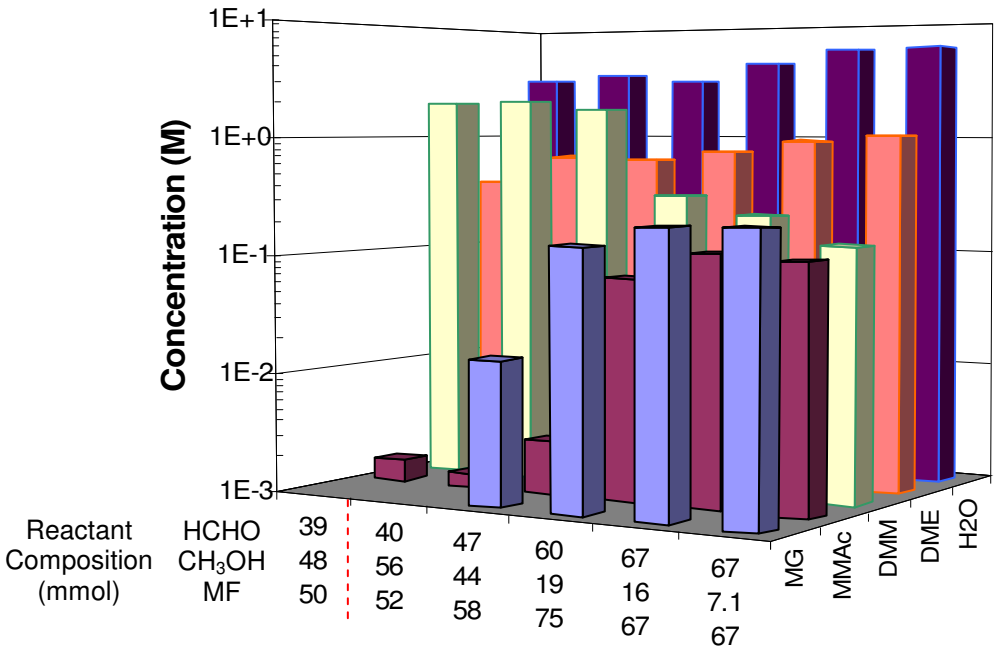

Figure 2.3 Effect of methanol content on product distribution using methoxymethanol and paraformaldehyde as the formaldehyde source. time = 3 h, T = 150 °C, SiW_{12} = 0.088 mmol. The first data set uses a 39 wt% HCHO solution in CH_3OH as the HCHO source. All others use paraformaldehyde.

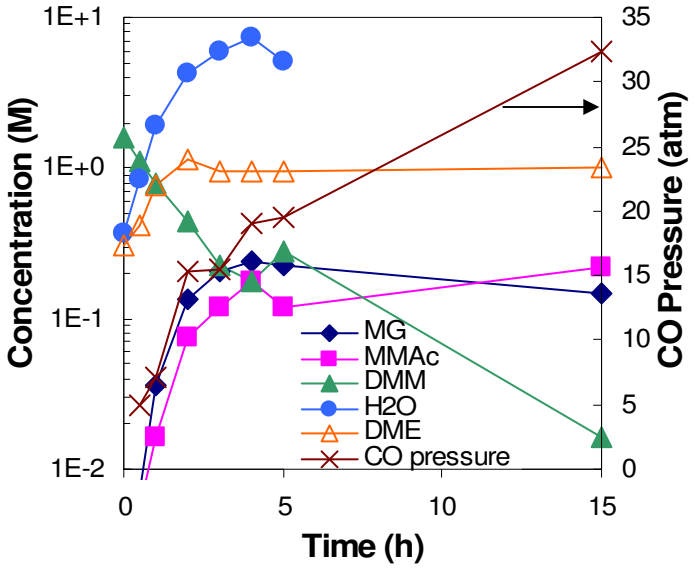

Figure 2.4 Effect of reaction time on product distribution using paraformaldehyde as the formaldehyde source. T = 150 °C, SiW_{12} = 0.088 mmol, HCHO = 67 mmol as paraformaldehyde, CH_3OH = 16 mmol, MF = 67 mmol. Reaction time of 0 h indicates heating to reaction temperature followed by immediate cooling. All other reaction times indicate hold period at reaction temperature.

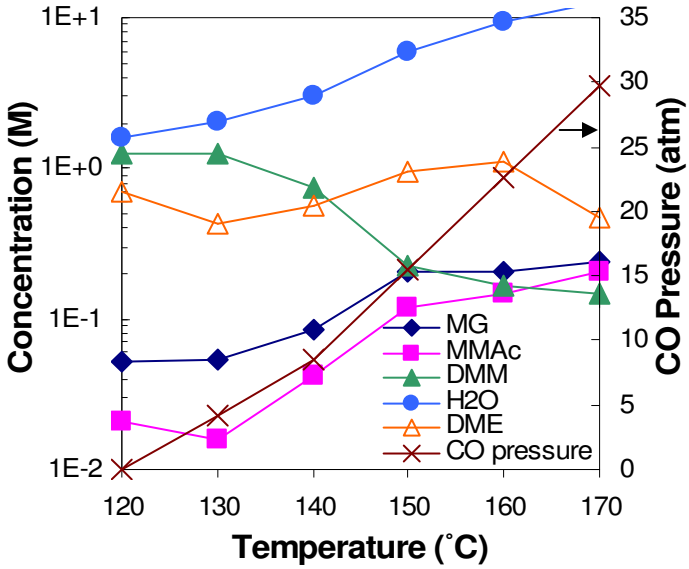

Figure 2.5 Effect of reaction temperature on product distribution using paraformaldehyde as the formaldehyde source. time = 3 h, SiW_{12} = 0.088 mmol, HCHO = 67 mmol as paraformaldehyde, CH_3OH = 16 mmol, MF = 67 mmol.

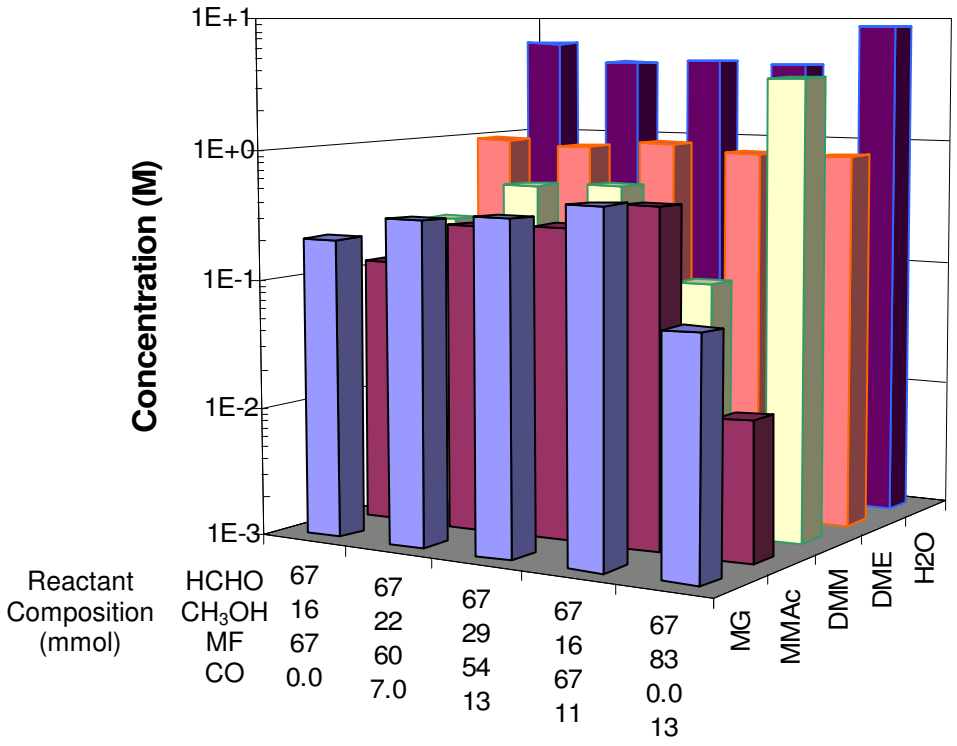

Figure 2.6 Effect of CO content on product distribution using paraformaldehyde as the formaldehyde source. time = 3 h, T = 150 °C, SiW_{12} = 0.088 mmol.

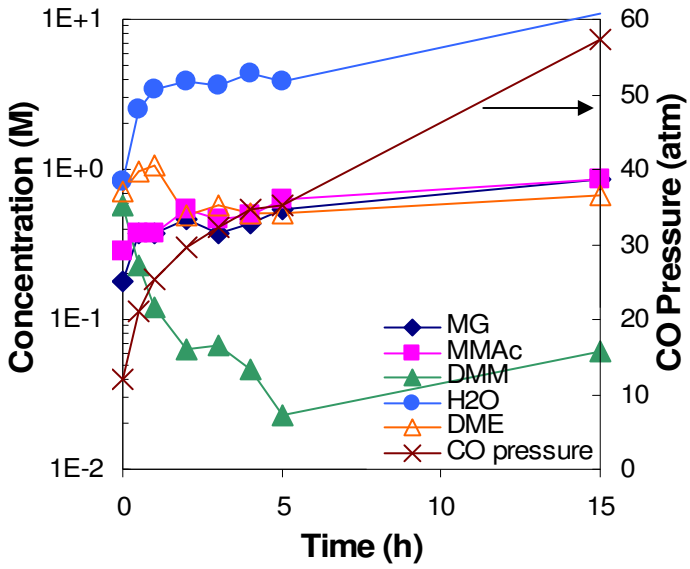

Figure 2.7 Effect of reaction time on product distribution using 1,3,5-trioxane as the formaldehyde source. T = 150 °C, SiW_{12} = 0.088 mmol, HCHO = 67 mmol as 1,3,5-trioxane, MF = 67 mmol. Reaction time of 0 h indicates heating to reaction temperature followed by immediate cooling. All other reaction times indicate hold period at reaction temperature.

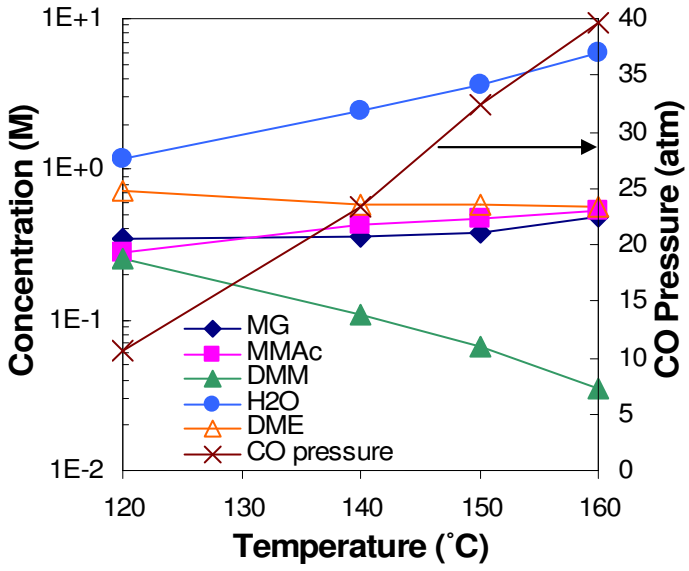

Figure 2.8 Effect of reaction temperature on product distribution using paraformaldehyde as the formaldehyde source. time = 3 h, SiW_{12} = 0.088 mmol, HCHO = 67 mmol as 1,3,5-trioxane, MF = 67 mmol.

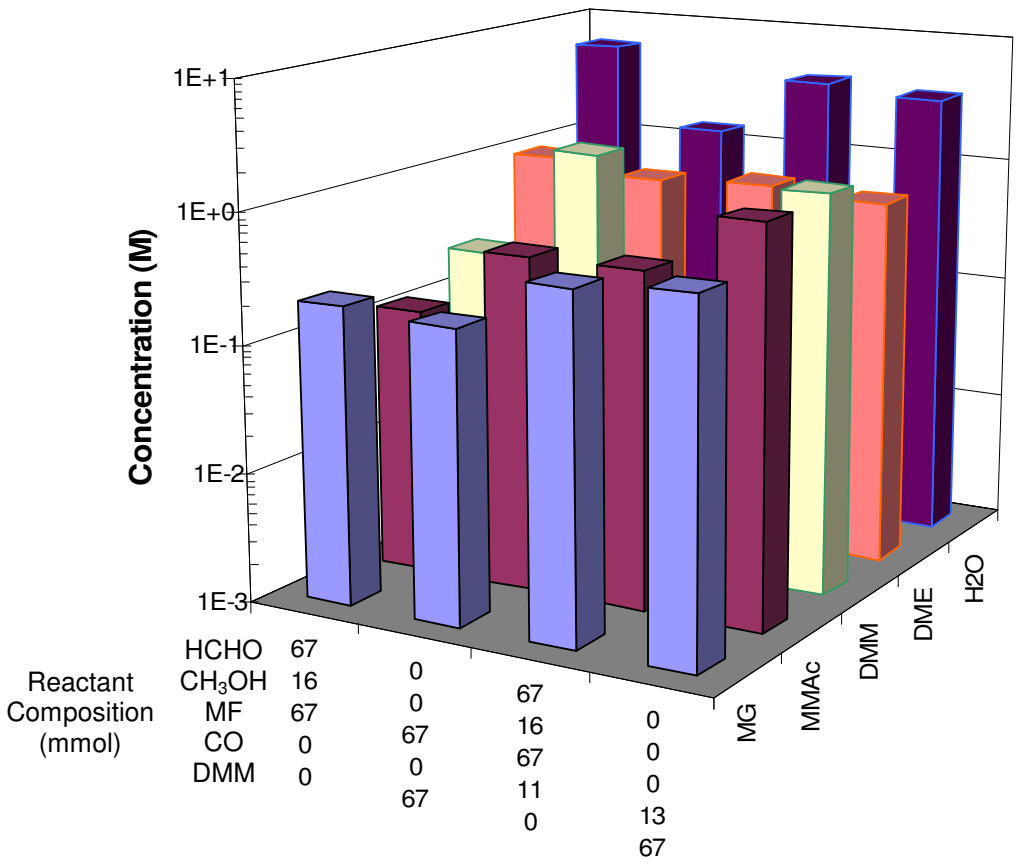

Figure 2.9 Effect of CO content on product distribution using paraformaldehyde and DMM as the formaldehyde source. time = 3 h, T = 150 °C, SiW12 = 0.088 mmol. Comparison of paraformaldehyde and DMM as formaldehyde sources for carbonylation by either MF or CO.

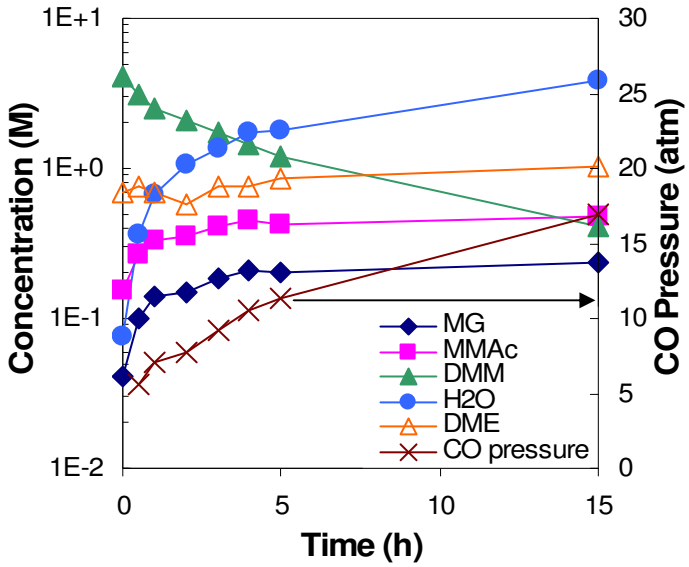

Figure 2.10 Effect of reaction time on product distribution using DMM as the formaldehyde source. T = 150 °C, SiW_{12} = 0.088 mmol, HCHO = 67 mmol as DMM, MF = 67 mmol. Reaction time of 0 h indicates heating to reaction temperature followed by immediate cooling. All other reaction times indicate hold period at reaction temperature.

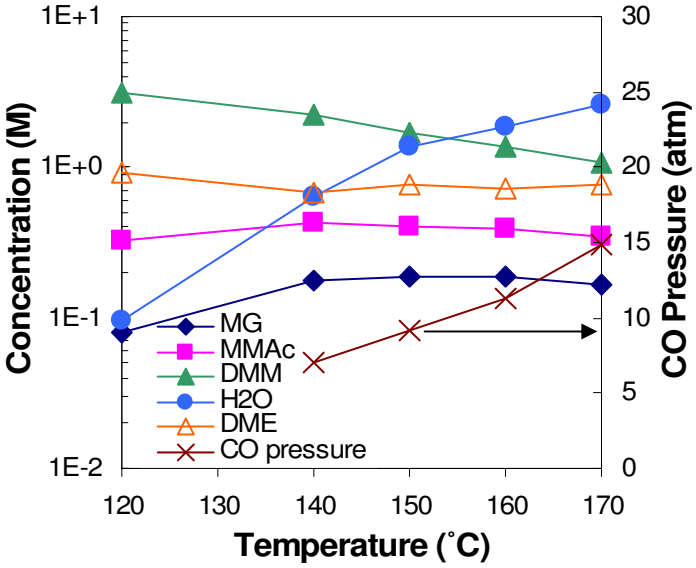

Figure 2.11 Effect of reaction temperature on product distribution using DMM as the formaldehyde source. time = 3 h, SiW_{12} = 0.088 mmol, HCHO = 67 mmol as DMM, MF = 67 mmol.

Table 2.1 Conversion of formaldehyde and CO to products. time = 3 h, T = 150 °C, SiW_{12} = 0.088 mmol.

Formaldehyde source	$X_{MG,HCHO}$ [a]	$X_{MMAc,HCHO}$ [a]	$X_{DMM,HCHO}$ [a]	$X_{C_{(s)},HCHO}$ [b]	$X_{C_2,CO}$ [c]
Methoxymethanol [d]	0.0%	0.01%	15%	7.2%	0.2%
Paraformaldehyde [e]	0.94%	0.55%	1.0%	13%	6.5%
1,3,5-trioxane [f]	3.1%	3.4%	0.28%	14%	15%
DMM [g]	1.5%	3.3%	5.3% [h]	12% [i]	41%

a) Conversion of formaldehyde to products as a molar percentage of starting formaldehyde; b) Conversion of formaldehyde to $C_{(s)}$ (measured as water less MMAc, DMM, and DME) c) C_2 products as a molar percentage of CO generated from MF; d) HCHO = 39 mmol as methoxymethanol solution, CH_3OH = 48 mmol, MF = 50 mmol; e) HCHO = 67 mmol as paraformaldehyde, CH_3OH = 16 mmol, MF = 67 mmol; f) HCHO = 67 mmol as 1,3,5-trioxane, MF = 67 mmol; g) HCHO = 67 mmol as DMM, MF = 67 mmol; h) Conversion of DMM to monomeric formaldehyde, i.e. $X_{HCHO,DMM}$; i) Conversion of DMM to $C_{(s)}$ (measured as water less DME plus MG and monomeric HCHO.

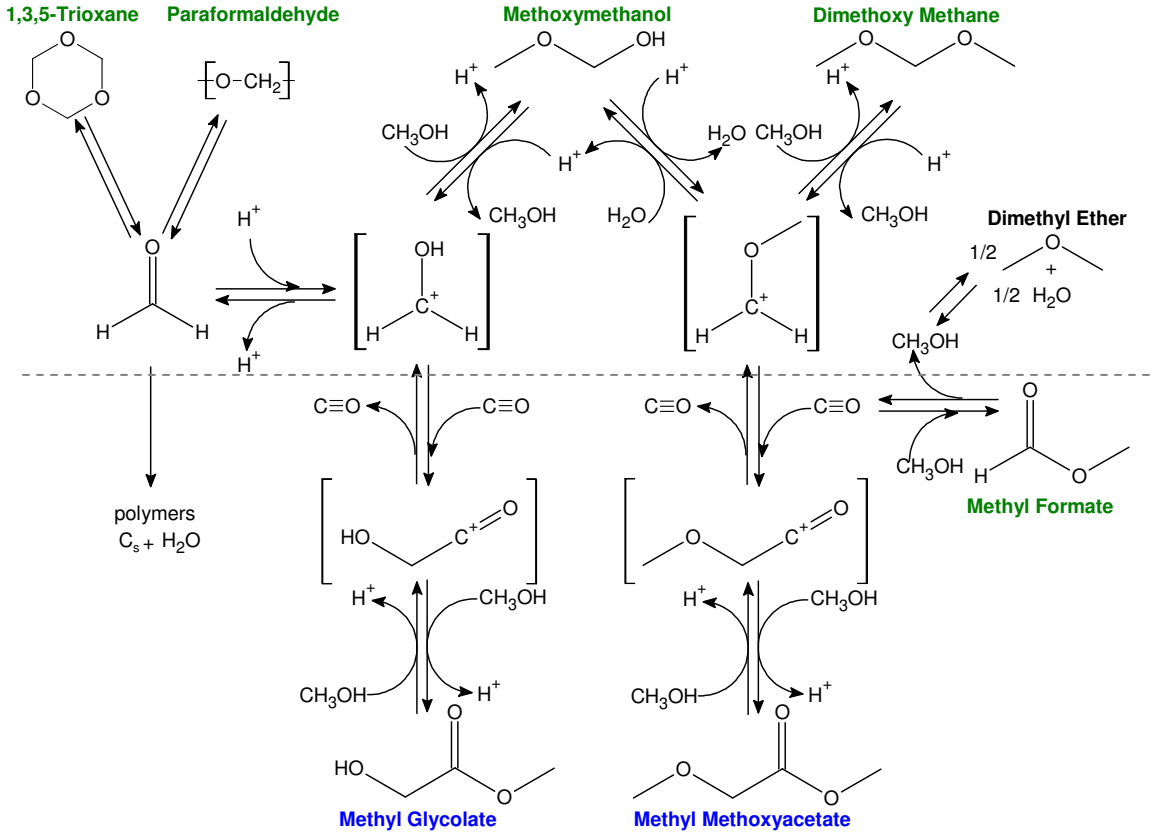

Figure 2.12 Proposed reaction scheme. Steps above the dotted line are considered to be in equilibrium, and the steps below the line are considered kinetically limited.

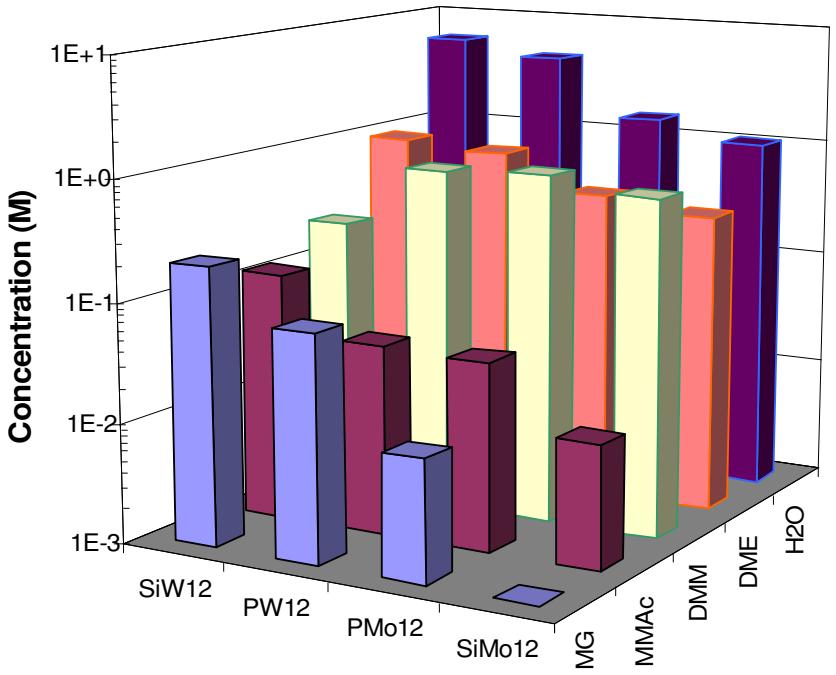

Figure 2.13 Comparison of heteropoly acids on an equal catalyst mass basis using paraformaldehyde as the formaldehyde source. time = 3 h, T = 150 °C, 0.25 g catalyst, HCHO = 67 mmol as paraformaldehyde, CH_3OH = 16 mmol, MF = 67 mmol.

Table 2.2 Comparison of SiW_{12}, PW_{12}, and methanesulfonic acid on an equimolar acid basis using paraformaldehyde as the formaldehyde source. time = 3 h, *T* = 150 °C, 0.35 mmol H^+, HCHO = 67 mmol as paraformaldehyde, CH_3OH = 16 mmol, MF = 67 mmol.

Concentration (M)	SiW_{12}	PW_{12}	CH_3SO_3H
MG	0.21	0.10	0.00
MMAc	0.12	0.06	0.00
DMM	0.94	0.49	1.2
H_2O	6.0	7.8	1.0

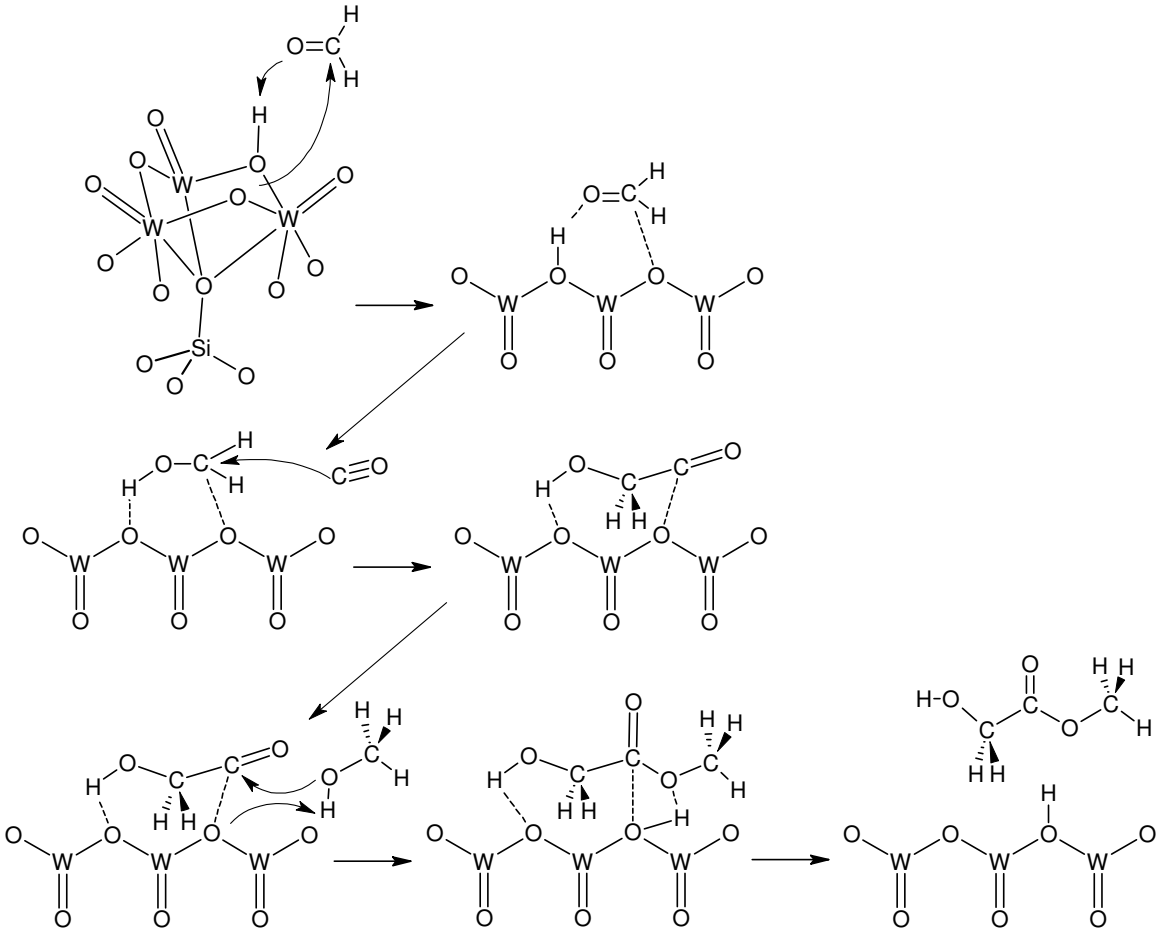

Figure 2.14 Proposed reaction mechanism for the carbonylation of free formaldehyde to methyl glycolate. The heteropoly acid Keggin unit has been simplified, first by considering one trimetallic cluster, and then representing that cluster linearly.

References

[1] MEGlobal press release, http://www.meglobal.biz/news_high_growth_year_04_05.shtml, April 4, 2005.
[2] Dow press release, http://www.dow.com/ethyleneglycol/news/20050405b.htm, April 5, 2005.
[3] R.L. Pruett, W.E. Walker, U.S. Patent 3 957 857 (1976), to Union Carbide Corporation.
[4] D.R. Fahey, J. Am. Chem. Soc. 103 (1981) 136.
[5] S.E. Jacobson, J. Mol. Catal. 41 (1987) 163.
[6] M. Marchionna, L. Garlaschelli, G. Longoni, J. Mol. Catal. 57 (1989) 221.
[7] A.M. Gaffney, J.J. Leonard, J.A. Sofranko, H.N. Sun, J. Catal. 90 (1984) 261.
[8] S.Y. Lee, J.C. Kim, J.S. Lee, Y.G. Kim, Ind. Eng. Chem. Res. 32 (1993) 253.
[9] D.E. Hendriksen, Prepr. Pap.—Am. Chem. Soc., Div. Fuel Chem. 28 (1983) 176.
[10] D.J. Loder, US Patent 2 152 852 (1939), to E. I. du Pont de Nemours & Co.
[11] A.T. Larson, U.S. Patent 2 153 064 (1939) to E. I. du Pont de Nemours & Co.
[12] S.B. Dake, V.C. Raghunath, J. Chem. Eng. Data 30 (1985) 400.
[13] E. Veleckis, D.S. Hacker, J. Chem. Eng. Data 29 (1984) 36.
[14] T. Morimoto, K. Kakiuchi, Angew. Chem. Int. Ed. 43 (2004) 5580.
[15] J.S. Lee, J.C. Kim, Y.G. Kim, Appl. Catal. 57 (1990) 1.
[16] D. He, W. Huang, J. Liu, M. Zhou, Q. Zhu, Korean J. Chem. Eng. 15 (1998) 556.
[17] D. He, W. Huang, J. Liu, Q. Zhu, Catal. Today 51 (1999) 127.
[18] D. He, W. Huang, J. Liu, Q. Zhu, J. Mol. Catal. A: Chem. 145 (1999) 335.
[19] W. Huang, D. He, J. Liu, Q. Zhu, Appl. Catal., A 199 (2000) 93.
[20] S. Morooka, C. Wakai, N. Matubayashi, M. Nakahara, J. Phys. Chem., A 109 (2005) 6610.
[21] J.F. Walker, Formaldehyde, American Chemical Society Monograph Series, Reinhold: London, 1964.
[22] M. Ragazzini, M. Modena, E. Gallinella, G. Cevidalli, J. Polymer Sci., A 2 (1964) 5203.
[23] I.V. Kozhevnikov, K.I. Matveev, Appl. Catal. 5 (1983) 135.
[24] M.N. Timofeeva, Appl. Catal., A 256 (2003) 19.
[25] Y. Izumi, K. Matsuo, K. Urabe, J. Mol. Catal. 18 (1983) 299.

Chapter 3

Vapor-Phase Carbonylation of Dimethoxymethane over H-Faujasite

Abstract

The usual liquid-phase, high-pressure process for carbonylating formaldehyde is avoided in a novel vapor-phase reaction. Using an acid zeolite (Faujasite) at near-atmospheric pressure dimethoxymethane (DMM; the dimethyl acetal of formaldehyde) is carbonylated to produce methyl methoxyacetate (MMAc). This approach provides a new route to ethylene glycol under mild conditions.

3.1 Introduction

The carbonylation of formaldehyde or formaldehyde derivatives has been investigated as a means for producing glycolic acid and its esters/ethers [1–8]. These products can be converted readily into ethylene glycol, an important industrial chemical used in polyester synthesis. Previous investigations of these reactions have been carried out in the liquid phase, and have required high carbon monoxide pressures (tens to hundreds of atmospheres) to overcome the low solubility of carbon monoxide. It has also been observed that at lower carbon monoxide pressures, the reaction of formaldehyde with itself, the Cannizzaro disproportionation reaction, becomes the dominant process.

We report herein the first example of the vapor-phase carbonylation of dimethoxymethane (DMM), the dimethyl acetal of formaldehyde. Using H-Faujasite (H-FAU; an acid zeolite) as the catalyst, it was possible to produce methyl methoxyacetate (MMAc) by the reaction in Equation (1) with a selectivity of up to 79% and a yield of up to 20% based on DMM. MMAc is an ether/ester of glycolic acid, and can be converted into glycolic acid and then ethylene glycol by hydrolysis and hydrogenation. Alternatively, MMAc can be reduced directly to 2-methoxyethanol, an industrial solvent. Disproportionation of DMM to produce dimethyl ether (DME) and methyl formate (MF), Equation (2), was the only competing process observed.

$$CH_3OCH_2OCH_3 + CO \rightarrow CH_3OCH_2COOCH_3 \quad (1)$$

$$2\ CH_3OCH_2OCH_3 \rightarrow 2\ CH_3OCH_3 + HCOOCH_3 \quad (2)$$

3.2 Experimental Methods

NH4-faujasite (Si/Al=30, Zeolyst), was heated for 3 h at 773 K (2 K min^{-1} ramp rate) in 100 cm^3 min^{-1} dry air to convert it into the H^+ form and remove water. Characterization by FT-IR using a Thermo Nicolet Nexus 6700 FTIR spectrometer showed no evidence for extra-framework aluminum formation following catalyst pretreatment (see 3.5 Supporting Information).

Reactions were carried out using 0.05 g of catalyst in a 6.35 mm outer diameter (OD) quartz reactor tube with an expansion in the middle (ca. 12.7 mm OD) packed with

quartz wool to hold the catalyst in place. A quartz-sheathed K-type thermocouple was placed in direct contact with the catalyst bed. The catalyst was pretreated for 3 h at 773 K in dry air (100 cm^3 min^{-1}) to remove residual moisture, and cooled to reaction temperature. CO (99.99% pure research grade, Praxair) was bubbled through a stainless steel saturator filled with DMM (99%, Sigma–Aldrich) and chilled to provide the desired vapor pressure. Additional CO or He was mixed with the saturator exit flow to set the desired CO/DMM ratio and the total gas volumetric flow rate. Reaction products were analyzed using an Agilent 6890n GC equipped with an HP-PLOT Q capillary column connected to a flame ionization detector. Experiments at elevated pressure were carried out by throttling a needle valve located downstream from the reactor.

Activity and selectivity data were collected as a function of temperature by increasing the reaction temperature at a fixed reactant composition and flow rate. Each temperature was held constant for 45 min.

The total gas flow rate in the reactor was maintained at 100 cm^3 min^{-1} at the reaction pressure, resulting in gas flow rates between 100 and 300 cm^3 min^{-1} at STP. The reactor space time, calculated on the basis of moles of aluminum in the zeolite framework, was held constant at 0.27 (mmol Al) min L^{-1} except where noted otherwise. When varied, changes in space time were accomplished by increasing the amount of catalyst used in the experiment.

Selectivities to MMAc from DMM are reported on the basis of moles of carbon using the following formula: 3(mole of MMAc formed)/[2(mole of DME formed)+2(mole of MF formed)+3(mole of MMAc formed)]. The selectivity to MMAc from CO was 100%.

3.3 Results and Discussion

The effects of temperature on the rate of DMM carbonylation to MMAc and the rate of DMM disproportionation to DME and MF are shown in Figure 3.1a. The products DME and MF were formed in a ratio DME:MF close to two, consistent with the stoichiometry of Equation (2). This observation and the absence of formaldehyde in the reaction products indicate that DMM decomposition to DME and formaldehyde did not occur. The rate of MMAc formation reached a maximum at 393 K, whereas the rate of DMM disproportionation increased monotonically with increasing temperature. As seen in Figure 3.1b, while the conversion of DMM increased with increasing temperature, the selectivity of DMM conversion into MMAc reached a maximum at 373 K.

The rate of DMM carbonylation and the selectivity of DMM conversion into MMAc increased with increasing carbon monoxide partial pressure (P_{CO}) while the DMM pressure was kept roughly constant (Figure 3.2a and b). The maximum rate and the MMAc selectivity shifted to lower temperatures as P_{CO} increased, with the selectivity maximum occurring 20–30 K lower than the rate maximum. A maximum selectivity of 79% was reached at 2.99 atm CO pressure and 373 K. Although the maximum rate increased nearly linearly with CO pressure, the maximum selectivity began to level off at CO pressures between 1.99 and 2.99 atm (see Supporting Information). DMM conversion increased with increasing P_{CO}, as the carbonylation rate increased, while the disproportionation rate stayed roughly constant.

Figure 3.3a shows that for a fixed CO pressure the rate of DMM disproportionation increased with increasing DMM partial pressure (P_{DMM}), while the rate of carbonylation went through a maximum. Figure 3.3b demonstrates that both DMM conversion and selectivity to MMAc decreased with increasing DMM pressure. These data indicate that higher DMM pressures favor disproportionation over carbonylation, as could be inferred from the stoichiometry of the reactions in Equations (1) and (2). For this reason, DMM pressure was kept low in all experiments, usually between 0.01 atm and 0.02 atm. Figure 3.3b suggests that even higher selectivities and conversions could have been achieved at DMM partial pressures below 0.01 atm.

Taken together the results presented in Figures 3.1–Figure 3.3 show that the selectivity of DMM conversion into MMAc increases with increasing P_{CO}/P_{DMM} ratio and that the overall rate of MMAc formation could be increased by increasing P_{CO} at a fixed P_{DMM}.

With increasing space time (number of Al centers within the catalyst sample divided by the total gas volumetric flow rate), the conversion of DMM increased but the MMAc selectivity remained nearly constant (see Supporting Information). While the rate of MMAc formation per mole of Al loaded into the reactor decreased with increasing space time, higher yields of MMAc could be achieved without sacrificing selectivity by operating at higher space times.

After an initial transient period of approximately 120 min, the catalyst showed stable steady-state activity and selectivity for at least 24 h. During the transient period, activity and selectivity to MMAc increased as a function of time until reaching their steady-state values.

The observed rate of DMM carbonylation is comparable to that reported for the carbonylation of DME over HMOR [9-11]. At 438 K, the turnover frequency for DME carbonylation to methyl acetate was approximately 0.2 h^{-1} at approximately 2 atm of CO and increased to approximately 1.1 h^{-1} at approximately 10 atm of CO with selectivity approaching 100%. By contrast, the turnover frequency for DMM carbonylation to MMAc over H-FAU reported herein was approximately 13 h^{-1} at approximately 1 atm of CO and 413 K with 35% selectivity, and increased to approximately 32 h^{-1} at approximately 3 atm of CO and 393 K with 69% selectivity. A MMAc selectivity of 79% from DMM was achieved with a turnover frequency of approximately 24 h^{-1} at approximately 3 atm of CO and 373 K. These observations are consistent with the higher reactivity of formaldehyde and its acetals relative to those of ethers.

The maximum MMAc selectivity of 79% achieved in the present study using a vapor-phase reaction is comparable to that reported previously for formaldehyde carbonylation using solid acids and carbon monoxide pressures of 314 atm (79%) [3] and 238 atm (81%) [5] in liquid-phase reactions with solid acid resin catalysts.

3.4 Conclusions

We have shown that high-selectivity, vapor phase, carbonylation of DMM to MMAc can be achieved at low pressure using H-FAU as the catalyst. DMM disproportionation to DME and MF can be minimized by keeping the ratio of P_{CO} to P_{DMM} high.

3.5 Supporting Information

As seen in Figure 3.4a, increasing the carbon monoxide partial pressure (P_{CO}) at a fixed temperature increased the rate of methyl methoxyacetate (MMAc) formation nearly linearly. The rate of the disproportionation reaction, producing DME and MF, remained roughly constant with P_{CO}. As a result, selectivity started to level off above P_{CO} = 1.99 atm while the conversion continued to increase (Figure 3.4b).

Following a brief increase at small space times, increasing the space time by adding more catalyst to the reactor had the effect of reducing the rates of formation of all the products per mole of aluminum (Figure 3.5a). However, the total conversion continued to increase almost monotonically throughout the space time range studied here (Figure 3.5b). This indicates that although the total product formation rates increased with space time, as the amount of catalyst was increasing, the aluminum content of the reactor increased faster, leading to the observed decrease in the rate per mole of aluminum. The formation rates per mole aluminum of all products fell with roughly the same slope, leading to the constant MMAc selectivity with space time in Figure 3.5b.

Figure 3.6 shows the FT-IR spectrum of the catalyst following pretreatment in air. The O-H stretching region is shown. The peak at 3744 cm^{-1} corresponds to external silanol groups of the zeolite, the peak at 3627 cm^{-1} corresponds to Brønsted acid sites inside the zeolite supercage, and the peak at 3564 cm^{-1} with a shoulder at 3552 cm^{-1} corresponds to Brønsted acid sites inside the sodalite cages and hexagonal prisms of the zeolite. The lack of peaks at between 3650 and 3700 cm^{-1} and between 3570 and 3610 cm^{-1} indicate that no Lewis-acidic extra-framework aluminum species were present. Peak assignments follow [12].

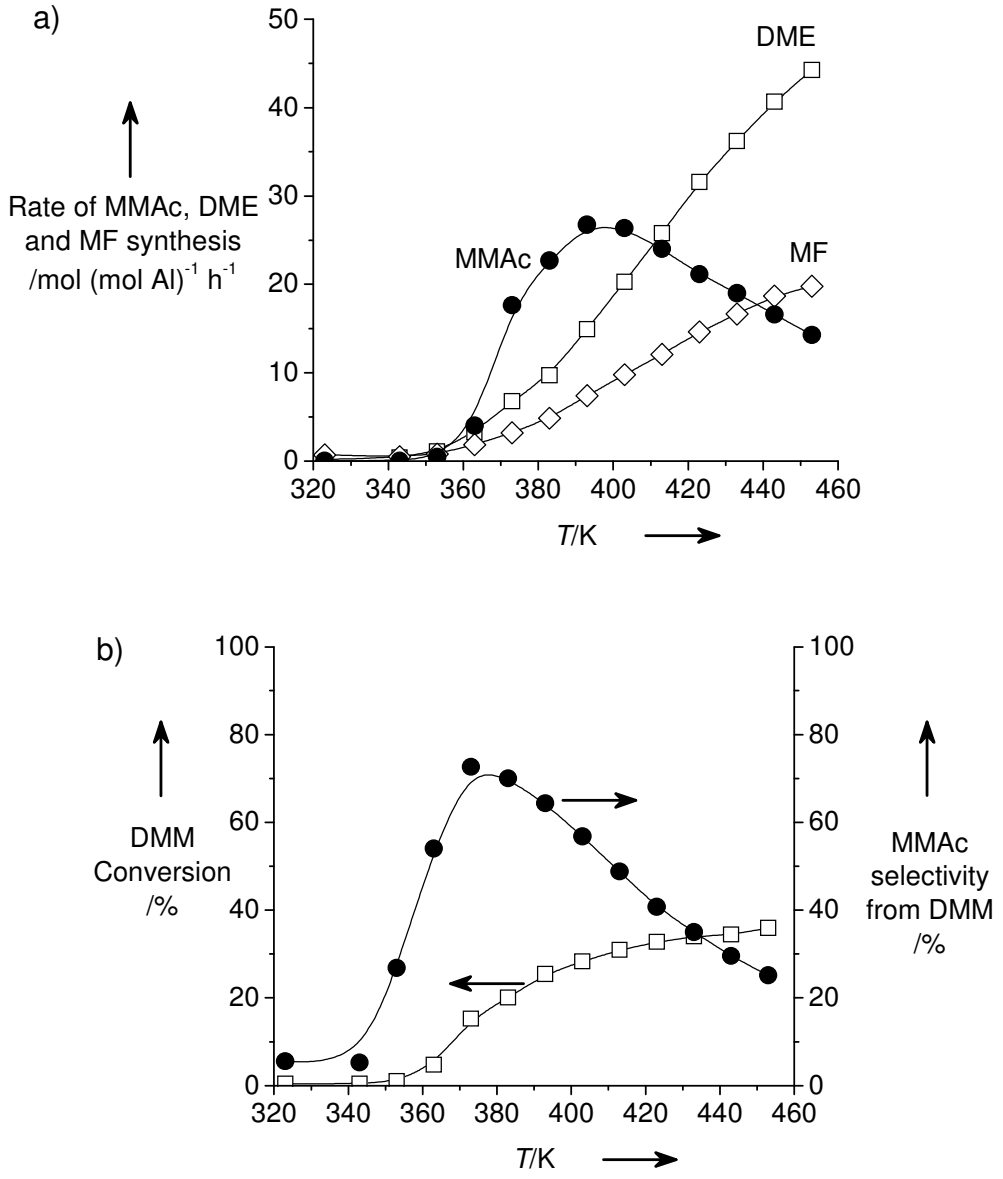

Figure 3.1 The effect of reaction temperature on a) the rates of MMAc, DME, and MF formation, and b) DMM conversion (left-hand axis), and selectivity to MMAc from DMM (right-hand axis). P_{CO} = 1.99 atm, P_{DMM} = 0.017 atm, total gas flow rate = 100 cm^3 min^{-1} at pressure, 200 cm^3 min^{-1} at STP.

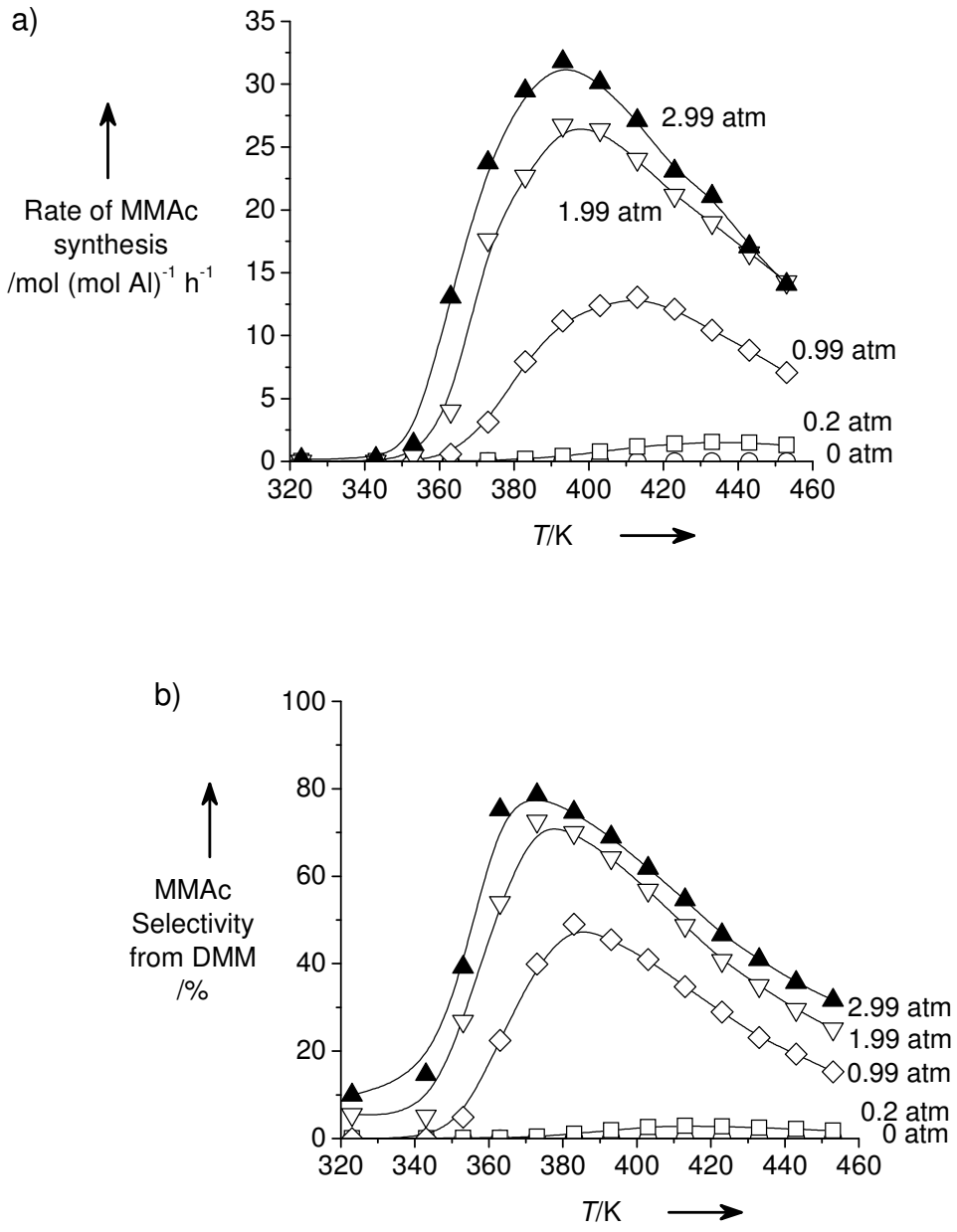

Figure 3.2 The effect of reaction temperature on a) the rate of MMAc formation at different CO pressures as labeled, and b) the selectivity to MMAc from DMM at different CO pressures as labeled. P_{DMM} = 0.013-0.019 atm, total gas flow rate = 100 cm^3 min^{-1} at pressure, 100-300 cm^3 min^{-1} at STP.

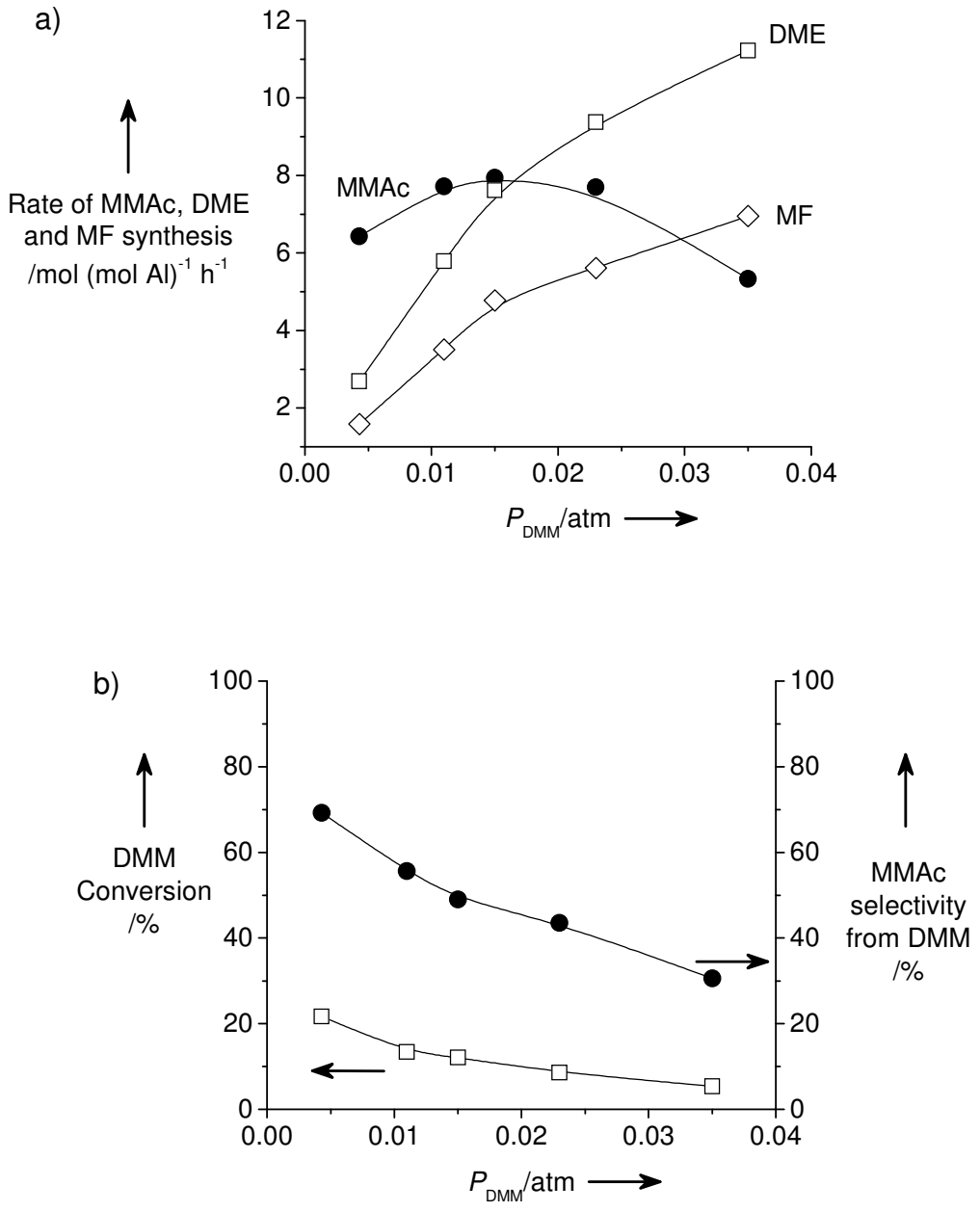

Figure 3.3 The effect of DMM partial pressure on a) the rates of MMAc, DME, and MF formation, and b) DMM conversion (left-hand axis), and selectivity to MMAc from DMM (right-hand axis). T = 383 K, P_{CO} = 1.0 atm, P = 2.0 atm (balance He), total gas flow rate = 100 cm_3 min^{-1} at pressure, 200 cm^3 min^{-1} at STP.

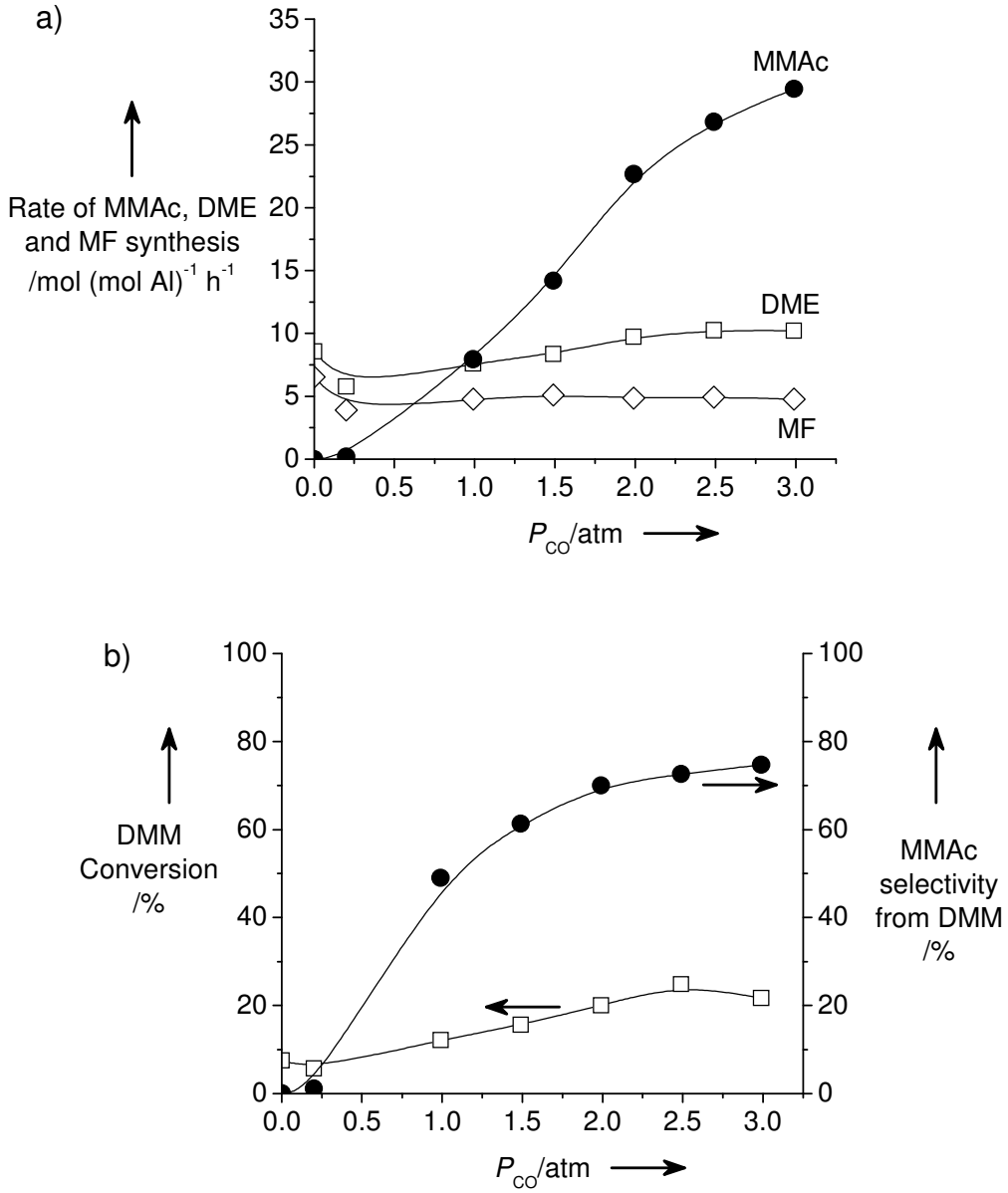

Figure 3.4 The effect of CO partial pressure on a) the rates of MMAc, DME, and MF formation, and b) DMM conversion (left-hand axis), and selectivity to MMAc from DMM (right-hand axis). T = 383 K, P_{DMM} = 0.013-0.019 atm, total gas flow rate = 100 cm^3 min^{-1} at pressure, 100-300 cm^3 min^{-1} at STP.

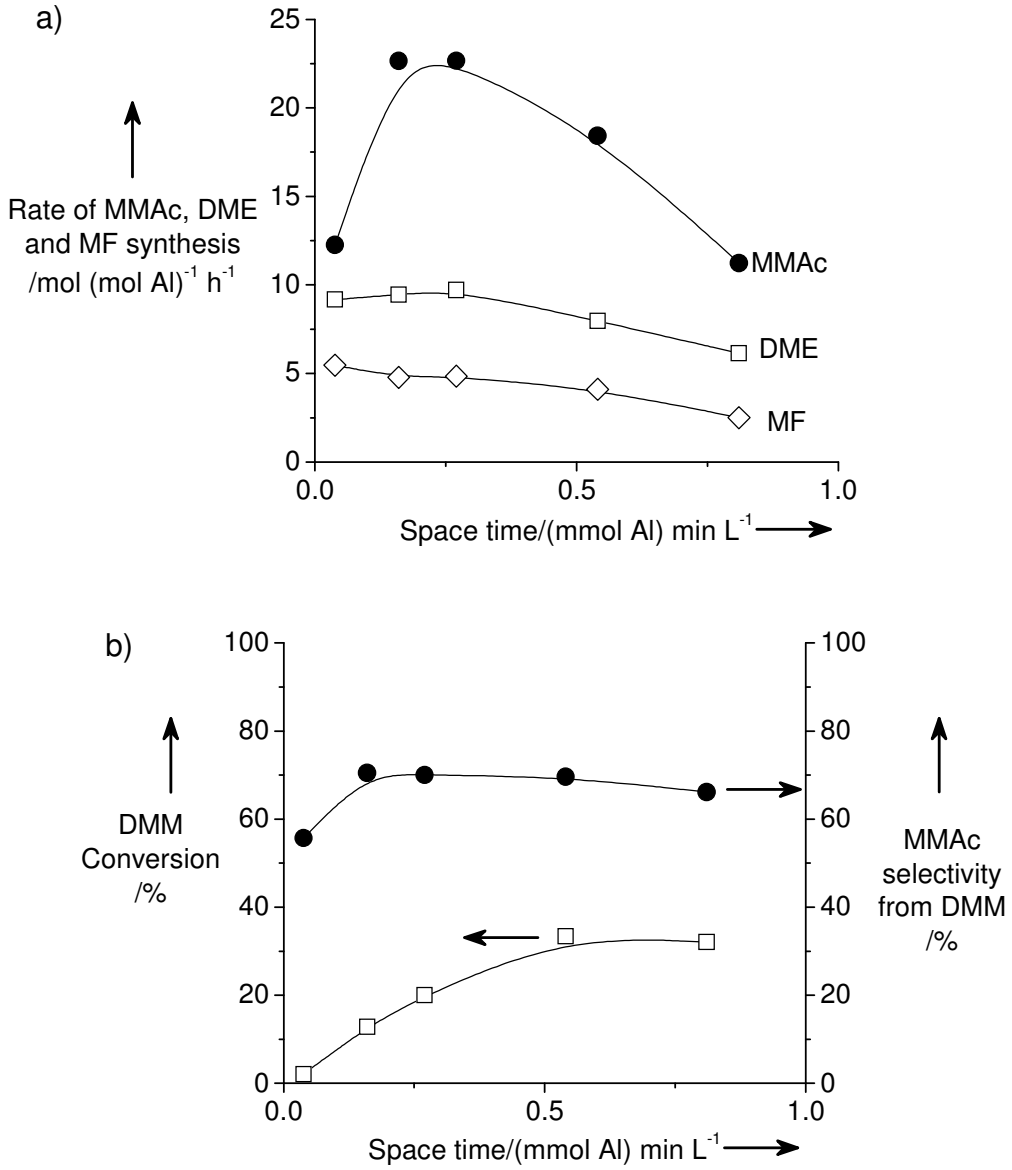

Figure 3.5 The effect of space time on a) the rates of MMAc, DME, and MF formation, and b) DMM conversion (left-hand axis), and selectivity to MMAc from DMM (right-hand axis). T = 383 K, P_{CO} = 1.99 atm P_{DMM} = 0.016-0.017 atm, total gas flow rate = 100 cm^3 min^{-1} at pressure, 100-300 cm^3 min^{-1} at STP.

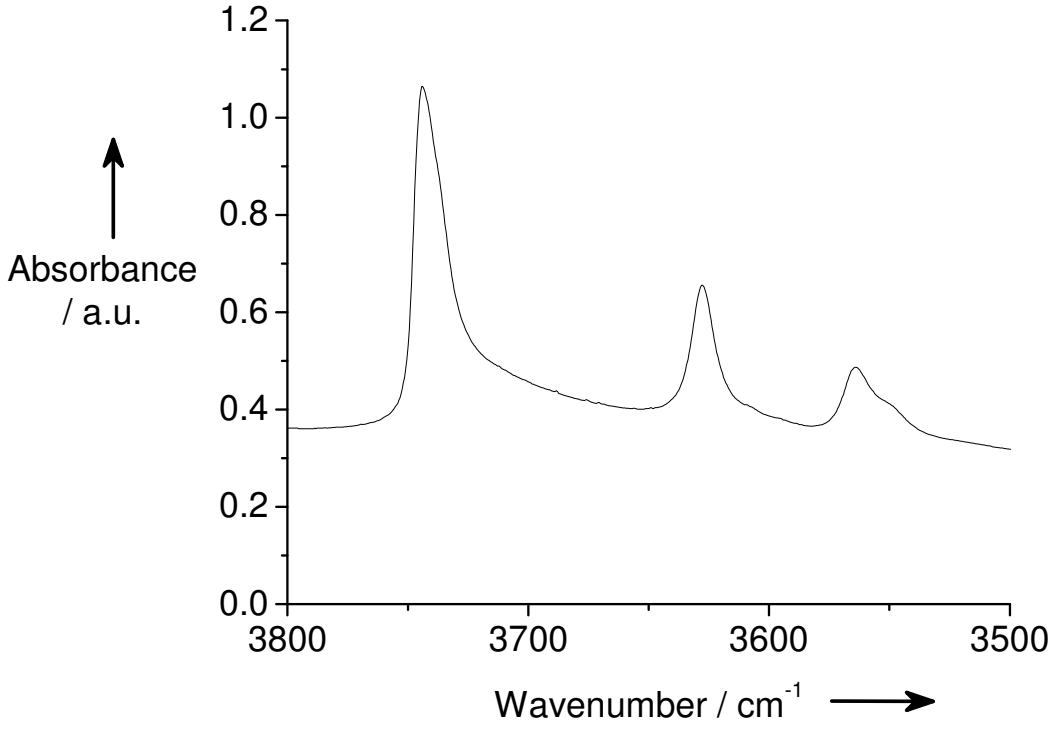

Figure 3.6 FT-IR spectrum of O-H stretching region in H-Faujasite (Si/Al ratio = 30) at 383 K.

References

[1] D.J. Loder, US Patent 2 152 852 (1939), to E. I. du Pont de Nemours & Co.
[2] H. Bahrmann, Koch Reactions, in: J. Falbe (Ed.), New Syntheses with Carbon Monoxide, Springer, Berlin, 1980, p. 372.
[3] D.E. Hendriksen, Prepr. Pap.—Am. Chem. Soc., Div. Fuel Chem. 28 (1983) 176.
[4] H.J. Schmidt, H.J. Arpe, US Patent 4 501 917 (1985), to Hoechst AG.
[5] S.Y. Lee, J.C. Kim, J.S. Lee, Y.G. Kim, Ind. Eng. Chem. Res. 32 (1993) 253.
[6] E. Drent, W.P. Mul, B.J. Ruisch, US Patent 6 376 723 (2002), to Shell Oil Company.
[7] T. Li, Y. Souma, Q. Xu, Catal. Today 111 (2006) 288.
[8] F.E. Celik, H. Lawrence, A.T. Bell, J. Mol. Catal. A: Chem. 288 (2008) 87.
[9] P. Cheung, A. Bhan, G. J. Sunley, E. Iglesia, Angew. Chem. Int. Ed. 45 (2006) 1617.
[10] P. Cheung, A. Bhan, G. J. Sunley, D. J. Law, E. Iglesia, J. Catal. 245 (2007) 110.
[11] A. Bhan, A. D. Allian, G. J. Sunley, D. J. Law, E. Iglesia, J. Am. Chem. Soc. 129 (2007) 4919.
[12] S.C.L. Dias, J.L. de Macedo, J.A. Dias, Phys. Chem. Chem. Phys. 5, 2003,5574.

Chapter 4

Effect of Zeolite Framework Type and Si/Al Ratio on Dimethoxymethane Carbonylation

Abstract

This work reports on the effects of zeolite framework type and Si/Al ratio on the carbonylation of dimethoxymethane (DMM) to produce methyl methoxyacetate (MMAc). Faujasite (FAU), ZSM-5 (MFI), Mordenite (MOR), and Beta (BEA) showed very similar activity for DMM carbonylation. However, FAU had a very high selectivity to MMAc compared to MFI, MOR, and BEA as a consequence of very low rates of dimethyl ether (DME) and methyl formate (MF) formation, by-products of the disproportionation of DMM. The high rate of DMM disproportionation observed for MFI, MOR, and BEA is ascribed to the small pores of these zeolites, which facilitate a critical initial step in the formation of DME and MF. FER showed very low activity for both carbonylation and disproportionation. Increasing the Si/Al ratio for both FAU and MFI led to an increase in the turnover frequency for DMM carbonylation. It is proposed that the low rate of MMAc formation found at low Si/Al ratios is due to repulsive interactions occurring between adsorbed species located within the same supercage (FAU) or channel intersection (MFI).

4.1 Introduction

Acid-catalyzed formaldehyde carbonylation has been investigated as a means for producing carbon–carbon bonds for seventy years [1–7]. The products of the reaction, consisting of glycolic acid and its esters and ethers, are desirable as precursors to monoethylene glycol (MEG). This approach to the synthesis of MEG is being pursued because formaldehyde can be produced from synthesis gas-derived methanol [8], a cheaper carbon source than ethene, the current starting material for the production of MEG [9]. Figure 4.1 shows schemes for synthesizing MEG from formaldehyde and dimethoxymethane (DMM) and demonstrates the equivalence of using formaldehyde and its acetal. Both formaldehyde and DMM are synthesized directly by partial oxidation of methanol [8,10]. The key step in each scheme is the formation of a carbon–carbon bond between formaldehyde/DMM and CO. Coupling carbon monoxide and formaldehyde leads to glycolic acid (GA), whereas the carbonylation of DMM leads to methyl methoxyacetate (MMAc), both of which are precursors to MEG.

Previous investigation of formaldehyde carbonylation has been carried out exclusively in the liquid phase, often requiring carbon monoxide pressures over 100 atm in order to achieve reasonable selectivities [1-6]. In a recent report, we demonstrated for the first time the gas-phase carbonylation of a formaldehyde dialkyl acetal, DMM, over H-Faujasite (H-FAU) [11]. At a CO pressure of 3 atm, 79% selectivity to MMAc could be achieved. Because acetals are often used as protecting groups for aldehydes, this reaction can be considered equivalent to formaldehyde carbonylation. In contrast to

liquid-phase carbonylation of formaldehyde, which produces a large number of by-products [2,4,7], the gas-phase carbonylation of DMM involves only two reactions – the carbonylation of DMM to form MMAc and the disproportionation of DMM to form dimethyl ether (DME) and methyl formate (MF).

$$CH_3OCH_2OCH_3 + CO \rightarrow CH_3OCH_2COOCH_3 \qquad \Delta G° = -69.0 \text{ kJ mol}^{-1} \quad [12]$$
$$2\ CH_3OCH_2OCH_3 \rightarrow 2\ CH_3OCH_3 + HCOOCH_3 \qquad \Delta G° = -72.3 \text{ kJ mol}^{-1}$$

The aim of the present investigation was to establish the effects of zeolite framework structure and Si/Al ratio on the gas-phase carbonylation of DMM to MMAc. Experiments were carried out to determine the effects of DMM and CO partial pressures and reaction temperature on the rate of MMAc formation as well. The observed effects of zeolite framework structure and Si/Al ratio are interpreted in the light of a proposed reaction mechanism.

4.2 Experimental Methods

4.2.1 Catalyst preparation

Zeolite samples were obtained commercially with different Si/Al ratios in either the NH_4^+ form (NH_4-FAU, Si/Al ≈ 2.6, Si/Al ≈ 6, Zeolyst; NH_4-MFI, Si/Al ≈ 13.5, Süd-Chemie, Si/Al ≈ 11.5, Si/Al ≈ 15, Si/Al ≈ 25, Si/Al ≈ 40, Si/Al ≈ 140, Zeolyst; NH_4-MOR, Si/Al ≈ 10, Zeolyst; NH_4-BEA, Si/Al ≈ 12.5, Zeolyst; NH_4-FER, Si/Al ≈ 10, Zeolyst) or the H^+ form (H-FAU, Si/Al ≈ 15, Si/Al ≈ 30, Si/Al ≈ 40, Zeolyst). As-received samples were heated to 773 K for 3 h at the rate of 2 K min^{-1} in 100 cm^3 min^{-1} flow of dry air (zero grade) to convert from the NH_4^+ form to the H^+ form and to drive off any adsorbed water. Dried samples were stored in a desiccator prior to use to minimize further adsorption of water.

One sample (Na-MFI, Si/Al ≈ 27.5, Süd-Chemie) was obtained in the Na^+ form, and was converted to the NH_4^+ form by aqueous exchange with 1 M NH_4NO_3 solution. 5 g of Na-MFI was exchanged with 0.1 L of solution for 12 h at 353 K three times, filtering and washing with 0.1 L deionized water each time. After the final exchange, the sample was filtered and rinsed again and dried at 383 K for 36 h. Conversion to the H^+ form was achieved by treatment in dry air for 3 h at 773 K as described earlier.

4.2.2 Steady-state catalytic data

Reactions were carried out in a 6.35 mm OD quartz tube reactor with an expanded section (~12.7 mm OD, ~20 mm length "bubble"). The reactor was packed with quartz wool above and below the catalyst bed to hold the catalyst powder in place. The reactor was placed inside a resistively heated ceramic furnace with external temperature control, and the catalyst bed temperature was measured with a K-type thermocouple sheathed in a quartz capillary placed in direct contact with the bed.

Residual moisture was removed from the catalyst by heating it to 773 K for 3 h at a rate of 2 K min^{-1} in 100 cm^3 min^{-1} flow of dry air. Samples were then cooled to the desired reaction temperature.

CO (99.99% pure research grade, Praxair) was bubbled through a stainless steel saturator filled with DMM (99%, Sigma-Aldrich) and chilled to provide the desired vapor

pressure. Additional CO or He (99.999% ultra-high purity, Praxair) was mixed with the saturator exit flow to set the desired CO/DMM ratio and the total gas volumetric flow rate. Reaction products were analyzed using an Agilent 6890n GC equipped with a bonded polystyrene-divinylbenzene (HP-PLOT Q) capillary column connected to a flame ionization detector. Experiments at elevated pressure were carried out by throttling a needle valve located downstream from the reactor.

The total gas flow rate in the reactor was maintained at 100 cm^3 min^{-1} at the reaction pressure, resulting in a gas flow rate between 100 and 300 cm^3 min^{-1} at STP. Since the active centers for carbonylation of DMM are Brønsted-acid sites and the concentration of these sites is proportional to the Al content in a given zeolite, reactor space time was calculated on the basis of the number of moles of Al contained in a given zeolite. Using this definition, space time was varied by choosing the weight of catalyst loaded.

Selectivities to MMAc from DMM are reported based on moles of carbon in MMAc that originated from DMM and were calculated as $S_{\mathrm{MMAc}} = \frac{3r_{\mathrm{MMAc}}}{2r_{\mathrm{DME}} + 2r_{\mathrm{MF}} + 3r_{\mathrm{MMAc}}}$, where r_i is the rate of formation of each product i in molar units. Note that only three atoms of carbon in MMAc are derived from DMM, and the fourth carbon atom is derived from CO.

4.3 Results

4.3.1 Effect of zeolite framework type

Figure 4.2 shows the effect of zeolite framework type on the steady-state rates of MMAc formation (Figure 4.2a), DME, and MF formation (Figure 4.2b), MMAc selectivity from DMM (Figure 4.2c), and DMM conversion (Figure 4.2d) as functions of reaction temperature. Zeolites of similar Si/Al ratios were chosen, and the space time was fixed based on moles of Al in the sample at ~0.8 mmol Al min L^{-1}. The partial pressures of CO and DMM in the feed gas were fixed at 1.98 atm and 0.02 atm respectively.

The dependence of the MMAc formation rate with temperature was complex and depended on zeolite framework type. The MMAc rate showed a maximum with temperature over each zeolite, but the temperature of the maximum rate depended on the zeolite structure. MOR and BEA possessed higher activity to MMAc than FAU and MFI at temperatures in the range of 363–393 K, whereas FAU and MFI possessed higher activity to MMAc than MOR and BEA at higher temperatures in the range of 393–433 K. FER was almost completely inactive but also showed increasing activity to MMAc formation at higher temperatures. The maximum MMAc formation rates observed for FAU, MFI, MOR, and BEA were roughly comparable, varying only by a factor of two from each other.

DME and MF formation rates also showed a dependence on zeolite framework type. The rates of both DME and MF formation increased monotonically with temperature, except for the MF formation rate over MOR as discussed in the following paragraphs. MOR and BEA showed very high disproportionation rates that increased almost linearly with temperature above 353 K. The rate of DMM disproportionation was low for MFI up to 393 K and then rose rapidly at higher temperatures such that DME and

MF formation rates exceeded those over MOR and BEA at 453 K. By contrast, FAU and FER showed very low, albeit increasing, disproportionation rates at all temperatures.

The ratio of DME to MF was approximately two in most cases, as expected from the stoichiometry of DMM disproportionation. The DME/MF ratio exceeded two at higher temperatures over all zeolite types tested here, except over FAU, where it remained near two, up to 453 K. The deviation from a DME/MF ratio of two was most apparent over MOR, where the deviation from two began at lower temperature (403 K) and reached a greater value (DME/MF = 3.6 at 453 K) than for the other zeolites. BEA, MFI, and FER showed a significant deviation from a DME/MF ratio of two only above 433 K. The deviation from DME/MF = 2 over MOR was so severe that the MF formation rate decreased with temperature above 433 K. The deviation in the DME/MF ratio from a value of two is attributed to methyl formate decomposition and subsequent dehydration of methanol, as shown below. Taken together, these two reactions could cause a significant increase in the DME/MF ratio.

$$HCOOCH_3 \rightarrow CO + CH_3OH \qquad \Delta G^\circ = +0.4 \text{ kJ mol}^{-1}$$
$$2\ CH_3OH \rightarrow CH_3OCH_3 + H_2O \qquad \Delta G^\circ = -16.6 \text{ kJ mol}^{-1}$$

At temperatures above 423 K, experiments carried out over MOR showed very small quantities of methyl acetate formation. Methyl acetate arises from the carbonylation of DME [13-15].

$$CH_3OCH_3 + CO \rightarrow CH_3COOCH_3 \qquad \Delta G^\circ = -77.0 \text{ kJ mol}^{-1}$$

Methyl acetate was not observed as a product over any of the other zeolites, consistent with observations that MOR catalyzes DME carbonylation more effectively than the other zeolites studied here.

MFI and BEA showed very similar trends in selectivity to MMAc from DMM (Figure 4.2c), reaching a maximum selectivity of 40–45% at 363 K. MOR did not show a maximum in selectivity to MMAc, but rather a monotonically declining selectivity with increasing temperature. The high selectivity of MOR at low temperature coincided with a very low MMAc synthesis rate. FAU showed significantly higher selectivity to MMAc than the other zeolites, up to 64% at 383 K, and the temperature range of high selectivity coincided with that for which the rate of MMAc formation was also high. The high selectivity of FAU relative to other zeolites was due partly to its higher MMAc rate, but even more important was its very low rate of DME and MF.

Because of its high selectivity to MMAc and low disproportionation rates at all temperatures, the conversion over FAU was lower than over BEA and MOR at all temperatures, and lower than that over MFI at temperatures above 403 K. The conversion over MFI showed a rapid increase at temperatures above 393 K, coinciding with the increase in the disproportionation rate.

The selectivity to MMAc from CO was 100% for all zeolites. In the few cases where DME carbonylation to methyl acetate occurred over MOR, methyl acetate formation had a negligibly small impact on the selectivity from CO.

Figure 4.3 shows the effect of zeolite framework type on the rate of MMAc formation (Figure 4.3a) and DME and MF formation (Figure 4.3b) as functions of time

on stream for FAU, MFI, and MOR at 383 K. Zeolites of similar Si/Al ratios were chosen, and the space time was fixed based on moles of Al in the sample at ~0.8 mmol Al min L^{-1}. The partial pressures of CO and DMM in the feed gas were fixed at 1.98 atm and 0.02 atm, respectively.

Over FAU and MFI, the rate of MMAc formation increased initially, reached a maximum value, and then declined slightly and stabilized at a steady value as a function of time on stream. Steady values were reached after about 150 min of exposure to the reaction mixture. Over MOR, the MMAc formation rate also increased for short times on stream, but continued to decrease up to at least 350 min. The DME and MF formation rates were initially high over all zeolites at short times on stream. As with MMAc, the DME and MF formation rates reached a steady state after 150 min over FAU and MFI, and continued to decrease up to at least 350 min over MOR. After 50 min, selectivity was constant over all three zeolites.

Discrepancies between the steady-state values shown in Figure 4.2 and the transient data shown in Figure 4.3 can be attributed to the slightly different partial pressures of DMM used in the two types of experiment. The effect of DMM partial pressure can be seen in Figure 4.7 and is discussed below.

4.3.2 Effect of Si/Al ratio over FAU and MFI

Figure 4.4 shows the effect of the Si/Al ratio of FAU on the rate of MMAc formation (Figure 4.4a) and MMAc selectivity from DMM (Figure 4.4b) at steady state for different reaction temperatures. FAU was selected because of the higher activity and selectivity toward MMAc seen for the Si/Al ≈ 15 sample shown in Figure 4.2. The partial pressures of CO and DMM in the feed gas were fixed at 1.98 atm and 0.02 atm, respectively. The space time was fixed based on moles of Al in the sample at ~0.27 mmol Al min L^{-1}.

Increasing the Si/Al ratio from 2.6 to 30 increased the MMAc formation rate at temperatures above 363 K. Increasing the Si/Al ratio from 30 to 40 did not increase the rate of MMAc formation any further. The temperature at which the maximum rate was observed shifted to lower values as the Si/Al ratio was increased.

The rate of DME and MF formation also increased with increasing Si/Al ratio up to 30, beyond which the rates did not increase any further upon increasing the Si/Al ratio to 40. The similarity of the effects of the Si/Al ratio on MMAc and disproportionation rates caused the selectivity to vary little over samples with different Si/Al ratios. The selectivities for a Si/Al ratio of 6 were only slightly lower than those for Si/Al ratios of 15, 30, and 40. The experiment using a Si/Al ratio 2.6 showed significantly lower selectivity than the other samples.

Increasing the Si/Al ratio of MFI also increased the rate of MMAc formation. Figure 4.5 compares the effect of Si/Al ratio on the rates of MMAc formation at 423 K over FAU and over MFI obtained from two different commercial suppliers, Süd-Chemie and Zeolyst. For similar Si/Al ratios, the activities of MFI samples from Süd-Chemie were higher than those obtained from Zeolyst. As with FAU, the MFI samples from Zeolyst showed that increasing the Si/Al ratio increased the MMAc formation rate up to a point, beyond which increasing the Si/Al ratio further showed little improvement. For FAU, this occurred at a Si/Al ratio ≈ 30, and for MFI the Si/Al ratio was ≈ 40.

4.3.3 Effect of reaction conditions over FAU and MFI

The effects of CO partial pressure (P_{CO}), DMM partial pressure (P_{DMM}), and space time (τ) on the reaction rates and selectivities were investigated for FAU (Si/Al ≈ 30) and MFI (Si/Al ≈ 27.5), at a fixed temperature of 383 K.

MFI was chosen for the comparison with FAU because like FAU, it showed a low DMM disproportionation rate at lower temperatures, but unlike FAU, it showed very high disproportionation rates at higher temperatures. This led to high selectivities to MMAc at lower temperatures over MFI, in contrast to the high selectivities to MMAc observed at higher temperatures over FAU. At the chosen temperature of 383 K, the disproportionation rate could still be considered low.

The effect of P_{CO} on the MMAc rate over FAU and MFI is shown in Figure 4.6a, the effect on DME rate is shown in Figure 4.6b, the effect on MMAc selectivity from DMM is shown in Figure 4.6c, and the effect on DMM conversion is shown in Figure 4.6d. The partial pressure of DMM in the feed gas was fixed at 0.02 atm, and the space time was fixed at ~0.27 mmol Al min L^{-1}.

Increasing the partial pressure of CO increased the rate of MMAc formation over both FAU and MFI. Both catalysts showed almost linear increases in the rate of MMAc formation with increasing P_{CO} up to 2 atm, followed by slightly slower increases at higher partial pressures. The rate of disproportionation showed almost no dependence on carbon monoxide pressure over FAU, even at zero carbon monoxide pressure, increasing only slightly with increasing P_{CO}. Over MFI, the disproportionation rate showed a very strong dependence on P_{CO}, decreasing rapidly from a very high rate of DME formation at zero carbon monoxide pressure to a moderate rate at 0.2 atm of CO and then continuing to decrease more gradually. Despite the difference in trends, both FAU and MFI showed similar rates of DME formation for CO partial pressures between 1 and 2.5 atm.

The selectivity to MMAc increased monotonically over both zeolites with increasing P_{CO}. The selectivity over FAU increased due to the increasing rate of MMAc formation. The near-constant disproportionation rate caused the rate of increase in the selectivity to decrease with increasing P_{CO}, leveling out near 75%. Over MFI, the increase in selectivity to MMAc was mainly due to the decrease in the rate of DMM disproportion. While the MMAc formation rate also increased with increasing P_{CO}, this increase was small compared to the decrease in the DME/MF formation rates. The different causes for the observed selectivity increases over FAU and MFI were reflected in the conversion as a function of CO pressure: the overall conversion of DMM increased with P_{CO} over FAU as the MMAc rate increased, whereas the overall conversion of DMM decreased with P_{CO} as the DME formation rate decreased.

The effect of varying DMM partial pressure (P_{DMM}) on the rate of MMAc synthesis (Figure 4.7a) and the rate of DME synthesis (Figure 4.7b) was compared over FAU and MFI. The reaction temperature was fixed at 383 K, the partial pressure of CO in the feed gas was fixed at 0.98 atm, and the space time was fixed at ~0.27 mmol Al min L^{-1}.

The rate of MMAc synthesis was nearly independent of DMM partial pressure for both FAU and MFI over the range of 0.003–0.035 atm. In the case of FAU, the rate of MMAc formation showed a shallow maximum, whereas for MFI the rate of MMAc formation showed very little change with DMM partial pressure above 0.005 atm after an

initial increase between 0.003 and 0.005 atm. The disproportionation rate increased monotonically with P_{DMM}, exhibiting very similar trends for both FAU and MFI.

The space time, τ, of the reaction was varied at a fixed temperature (383 K), P_{CO} (1.98 atm), and P_{DMM} (0.02 atm), over FAU and MFI by varying the amount of catalyst used in the experiment. The effect of τ on MMAc selectivity from DMM is shown in Figure 4.8a, and the effect on DMM conversion is shown in Figure 4.8b.

Both zeolites showed similar selectivity trends with increasing space time, with the selectivity of DMM to MMAc increasing at short space times and then remaining relatively constant for space times above 0.2 mmol Al min L^{-1}. Conversion of DMM increased with increasing space time over both zeolites, albeit much more slowly over MFI. With selectivity nearly constant as a function of space time, higher yields could be achieved by increasing the space time.

4.4. Discussion

4.4.1 Proposed reaction mechanism

The effects of framework type and Si/Al ratio on the activity and selectivity of zeolites to the carbonylation of DMM are best discussed in the context of the proposed reaction mechanism shown in Figure 4.9. The first step (Reaction 1) in this scheme is the reaction of DMM with the Brønsted acidic protons of the zeolite (species HZ), which leads to the formation of methoxymethoxy species (MMZ). The methanol released in this manner either is flushed from the reactor or is dehydrated to form DME and water in a manner consistent with the mechanism for DME carbonylation as reported in [14].

The methoxymethoxy species MMZ can react with CO (Reaction 2) to form methoxyacetyl species (MAZ), which can then undergo methoxylation by DMM (Reaction 3), to release MMAc and regenerate the methoxymethoxy species. DMM disproportionation is envisioned to proceed via the reaction of methoxymethoxy species with DMM to form dimethoxymethoxy species (DMZ) and DME (Reaction 4). These newly formed surface species can then decompose, releasing a second molecule of DME and forming a new surface formate species (MFZ) (Reaction 5), which undergoes methoxylation to release MF and regenerate the methoxymethoxy species (Reaction 6).

It is thought that MMAc synthesis occurs by the Koch mechanism [2,4,16]. The initiation (Reaction 1) and MMAc synthesis (Reactions 2 and 3) mechanisms proposed here are consistent with those proposed for similar Koch carbonylation reactions [14,17-18]. As formaldehyde disproportionation occurs by the Cannizzaro reaction [19-21], the first step (Reaction 4) of the DMM disproportionation mechanism (Reactions 4–6) proposed here is similar to that for the Cannizzaro reaction of formaldehyde in the liquid phase catalyzed by strong acids [21].

The mechanism proposed in Figure 9 shows that at steady state methoxymethoxy species can undergo carbonylation or disproportionation and that the relative partial pressures of CO and DMM will control the selectivity between these competing reactions. Increasing P_{CO} increases the rate of carbonylation as methoxymethoxy species are converted to methoxyacetyl species in Reaction 2. Increasing P_{DMM} increases the disproportionation rate as methoxymethoxy species are converted to dimethoxymethoxy species in Reaction 4.

Surface methyl groups were excluded from the mechanism due to the very high activation barrier to their formation [22], and are thought to be generally absent from the reaction system considered here. The only exception may be on MOR at higher temperatures, where the formation of surface methoxyls may explain the observed formation of methyl acetate [13-15]. MOR may possess a greater ability to stabilize surface methoxyls compared to other zeolites [23], which may in turn promote MF decomposition, which was much more prevalent over MOR than any other zeolite.\

4.4.2 Effect of zeolite framework type

Although the rates of MMAc formation were comparable over FAU, MFI, MOR, and BEA (see Figure 4.2a), varying by roughly a factor of two, the selectivity to MMAc was much greater over FAU than the other three zeolites (Figure 4.2c). This was due to the very low rate of DMM disproportionation observed over FAU.

Of the three proposed steps of the disproportionation mechanism, the hydrogen-transfer step (Reaction 4) is most likely to be the rate-determining step over the P_{DMM} range studied here. The disproportionation rate was observed to depend on P_{DMM}, meaning that the unimolecular decomposition in Reaction 5 cannot be rate-determining, and methoxyl exchanges, such as in Reaction 6, are generally considered to be fast [14].

The hydrogen transfer step probably begins with coordination of the nucleophilic oxygen in gas-phase DMM with the bound methoxymethoxy species (MMZ) as shown in Figure 4.10. Interaction between DMM and surface methoxymethoxy groups is expected to be similar to the interaction between DME and surface methyl groups as described in [23]. After coordination, in order for hydrogen transfer to occur, the methylene hydrogens on the central carbon of DMM must rotate and face the carbon atom of the methoxymethoxy species. If the C–H bond of DMM comes close enough to the adsorbed species, the hydrogen can transfer to the nearby carbon, forming DME from the former species, and replacing it with the new dimethoxymethoxy carbocation (DMZ). The rotated C–H bond of DMM in the hydrogen-transfer step is highlighted as the proposed transition state in Figure 4.10.

Since zeolites with Si/Al ratios >10 are generally considered to possess the same acidity regardless of framework type [24], zeolite acidity cannot explain the observed difference in MMAc selectivity among FAU, MFI, MOR, BEA. As discussed in the following paragraphs, these differences can be ascribed to differences in pore size.

Table 4.1 shows the maximum included sphere diameters in each zeolite framework type, as defined and calculated by Foster et al. [25]. For reference, the T atom counts (Si or Al) in the major channel systems of each zeolite are also shown. The maximum included sphere is considered the largest hard sphere that would fit within the zeolite framework without overlapping framework atoms or distorting the structure [25]. It is usually located inside channel intersections or cage structures and is stationary. The maximum included sphere is nearly uniform for all of the zeolites except FAU, which can fit a sphere at least 68% larger than any of the other zeolites.

Since disproportionation rates were high when the zeolite pore sizes were small, i.e. for MFI, MOR, and BEA (Figure 4.2b), we propose that the small pores of these zeolites helped to promote the transfer of hydrogen in the transition state shown in Figure 4.10. Conversely, the large pores of FAU led to low disproportionation rates by disfavoring the hydrogen-transfer step.

Figure 4.11a shows, using MFI as an example, a molecule of DMM interacting with the methoxymethoxy species MMZ in a zeolite possessing smaller pores. Figure 4.11b shows a similar interaction in the larger pores of FAU. In the former case, it is seen that the steric constraint of the pore walls forces the hydrogen donor into an orientation that is likely to promote hydrogen transfer. By contrast, the large pores of FAU allow the hydrogen donor to remain far from the acceptor, so that the driving force for hydrogen transfer is not as strong.

If CO insertion (Reaction 2) is the rate-determining step in the formation of MMAc, then both carbonylation and disproportionation involve interactions of gas-phase molecules with the methoxymethoxy species MMZ. However, since CO is much smaller than DMM, this interaction is expected to be much less sensitive to spatial constraints than that for the first step in DMM disproportionation (Reaction 4). For this reason, the rate of MMAc formation was almost uniform for FAU, MFI, MOR, and BEA (Figure 4.2a), while the disproportionation rate was strongly dependent on the pore size of the zeolite (Figure 4.2b).

Zeolite dimensionality is believed to play a role in the stability of the different zeolites tested as a function of time on stream. It is generally considered that 1-D and 2-D zeolites are susceptible to deactivation by pore blocking, causing a portion of the catalyst inner surface to become inaccessible [26]. 3-D zeolites are usually much more stable because all pores are interconnected, and hence pore blockage does not lead to as much loss of access to the catalytically active sites. Figure 4.3 shows that FAU and MFI, both 3-D zeolites (Table 4.1), reached steady-state behavior within 150 min of time on stream, whereas MOR, a 1-D zeolite, continued to decline in activity up to at least 350 min. This difference in time-on-stream behavior may have been a consequence of pore blockage in MOR, which was not a problem in the 3-D zeolites. The low reactivity of FER may also be attributable to its 2-D pore dimensionality. Due to the very low rates of carbonylation and disproportionation, time-on-stream data over FER could not be collected to confirm this projection.

4.4.3 Effect of Si/Al ratio

Figure 4.5 shows that increasing the Si/Al ratio increased the carbonylation rate of DMM per Al over FAU as well as over MFI samples from two different suppliers. Looked at another way, increasing the Al content of the zeolites reduced the rate of MMAc formation. The lower activity of zeolites with Si/Al ratios <10 may be due to lower acidity at each Al center; however, for Si/Al ratios >10, zeolites are considered to have constant acidity as the Al centers are spaced far enough apart to have properties of isolated sites [24]. However, DMM carbonylation rates increased up to Si/Al ratios of ≈ 30 over FAU and up to ≈ 40 over MFI.

As mentioned above, CO insertion (Reaction 2 in Figure 4.9) is likely to be the rate-determining step in the carbonylation mechanism. Figure 4.12 illustrates the proposed transition state for this process based on DFT calculations [27]. The methoxymethoxy species (MMZ) dissociates partially from its adsorption site before inserting CO between the methoxymethoxy carbon and the framework oxygen atom to form the methoxyacetyl species (MAZ) [27]. The partial dissociation of the methoxymethoxy species produces a cationic transition state, as expected in a Koch

carbonylation mechanism [14,16,22,23], and localizes positive charge on the dissociating fragment.

For Si/Al ratios >10, spacing between Al centers is sufficient to have no effect on acidity [24], although surface species adsorbed on these centers may be close enough to interact with each other. Figure 4.13 illustrates the distance between two methoxymethoxy species if they were located within the same supercage of FAU. A distance of 1.5 Å is typical for carbon-framework oxygen distances in adsorbed species on zeolite surfaces (e.g. [23]). The location of the two Al atoms was chosen as an intermediate distance – some Al–Al pairs lead to longer distances between adsorbed species, while most pairs lead to shorter distances. In this representative example, the distance between methoxymethoxy species is only 6.2 Å. Upon the dissociation of one of these species to form the transition state shown in Figure 4.12, the distance between species decreases as the positive charge on the dissociating fragment increases. Had the zeolite been drawn with more than two Al atoms in a single supercage, the distances between surface species would have been smaller still.

The distances between dissociated carbocations and neighboring surface species, when less than 6 Å, may be short enough for Coulombic interactions to have an effect. Thus, a carbocation might experience an increase in the activation energy required for dissociation due to these repulsive interactions. This would imply that the activation energy should decrease with increasing distance between active sites within a zeolite. Since decreasing the Al content of a zeolite would increase the distance between Al centers, higher Si/Al ratios would be expected to lead to higher reaction rates due to the lower activation barriers. This effect can be seen in Figure 4.5, and holds for both FAU and MFI.

Figure 4.14 shows the calculated average number of Al atoms in each cage structure of FAU and MFI for each Si/Al ratio shown in Figure 4.5 [28]. The supercages of FAU are the cage structures, and in MFI the channel intersections are the cage structures. In Figure 4.5, the rate of MMAc synthesis over FAU increased with increasing Si/Al ratio up to a Si/Al ratio of ≈ 30, which also corresponded to the Si/Al ratio at which there was no more than one Al atom per supercage. This suggests that in FAU, the size of the supercage is roughly the same as the distance at which surface species no longer interact with each other. In MFI, the rate of MMAc synthesis increased up to a Si/Al ratio of ≈ 40, which corresponded to 0.59 Al atoms per channel intersection. This suggests that one active site for every 1.7 channel intersections is a sufficient distance to avoid interaction between surface species. Note that the largest stationary sphere in FAU, corresponding to the supercage, was 1.8 times larger than the largest sphere in MFI, which corresponds to a channel intersection (see Table 4.1). This gives a similar estimate for the minimum separation for active sites in both FAU and MFI to avoid interactions between surface species.

The differences between the Süd-Chemie and Zeolyst samples may be the location of the Al atoms in the framework as a function of their synthesis techniques – i.e. samples from Zeolyst may have Al atoms clustered closer together, resulting in more interactions between adsorbed species, while samples from Süd-Chemie may have them more evenly spaced.

4.4.4 Effect of reaction conditions

The rate of MMAc formation was observed to go through a maximum with temperature, suggesting that the carbonylation mechanism in Figure 4.9 is not sufficient to describe the observed kinetics. To explain the maximum, either Reaction 2 or Reaction 3 of the mechanism must be reversible. A maximum in the MMAc formation rate was observed over all zeolite samples tested here, including FER, which gave a maximum at a MMAc partial pressure of 2×10^{-4} atm. As the reversibility was observed even for such low MMAc partial pressures, it is unlikely that Reaction 3 was reversible under the reaction conditions tested here. Therefore, it is likely that Reaction 2 is reversible, at least at higher temperature.

Taken together, the observed effects of P_{CO} and P_{DMM} on the rates of DMM carbonylation and disproportionation indicate slightly different mechanisms over FAU and MFI. DMM carbonylation showed roughly first-order dependence on P_{CO} and zero-order dependence on P_{DMM} over both zeolites (Figures 4.6a and 4.7a). Additionally, DME formation over both FAU and MFI showed less than first-order dependence on DMM pressure (Figure 4.7b). However, the two zeolites showed differences in the dependence of DME formation on the partial pressure of CO (Figure 4.6b). Over MFI, DME formation showed negative-order dependence on CO pressure. This suggests that over MFI, carbonylation and disproportionation compete with each other as shown in Figure 4.9, with methoxymethoxy groups undergoing disproportionation if reacting with DMM and undergoing carbonylation if reacting with CO. Over FAU, the rate of DME formation was nearly independent of P_{CO}. This suggests that over FAU, the active sites for disproportionation and carbonylation are somehow distinct, with some methoxymethoxy species primarily undergoing carbonylation and some primarily undergoing disproportionation.

It is known that FAU has four distinct positions for the Brønsted acidic proton, corresponding with the four O atoms surrounding each Al atom in the zeolite framework [29]. Of these, only two are theoretically accessible to gas-phase molecules in the zeolite pores, the so-called O(1) site, whose protons point into the supercages of FAU, and the O(4) site, whose protons point toward the ring openings [29]. When the protons are displaced by reaction with DMM (Reaction 1 of Figure 9), some of the resulting methoxymethoxy species may orient themselves at O(4) sites, while the rest would orient themselves at less sterically hindered O(1) sites. The unhindered O(1) sites may be those responsible for carbonylation, while the O(4) sites may undergo disproportionation. This would be consistent with the conclusion from Section 4.4.2, that more sterically hindered sites promote disproportionation.

4.5 Conclusions

Of the zeolites tested here, FAU was the most effective catalyst toward DMM carbonylation because of its low disproportionation rates and high carbonylation rates. FAU with a Si/Al ratio of ≈ 30 has been shown to achieve 79% selectivity to MMAc from DMM at 3 atm of CO pressure, 0.02 atm of DMM pressure and 383 K [11].

The high selectivity of FAU was shown to derive from its large supercages, which disfavor disproportionation. By contrast, the smaller pores of MFI, MOR, and BEA force

the reactants into an orientation that promote the hydrogen-transfer step critical to disproportionation.

MMAc formation rates over FAU and MFI increased with increasing Si/Al ratio. Low Al zeolites led to higher carbonylation rates because with fewer Al atoms within the zeolite framework, Al centers and the surface species adsorbed on them were spaced farther apart from one another, thereby avoiding repulsive electrostatic interactions between surface species. The closer proximity of surface species in high Al zeolites led to increased activation energies in the cationic transition state of CO insertion step of the carbonylation mechanism.

The effects of P_{CO} and P_{DMM} on the carbonylation rates and the effect of P_{DMM} on the disproportionation rates were similar over both FAU and MFI. By contrast, CO pressure was shown to have a negative effect on disproportionation over MFI, and no effect over FAU. This suggests that while a single active species undergoes both carbonylation and disproportionation over MFI, surface species adsorbed at the O(1) site of FAU are responsible for carbonylation, while those at the O(4) site undergo disproportionation.

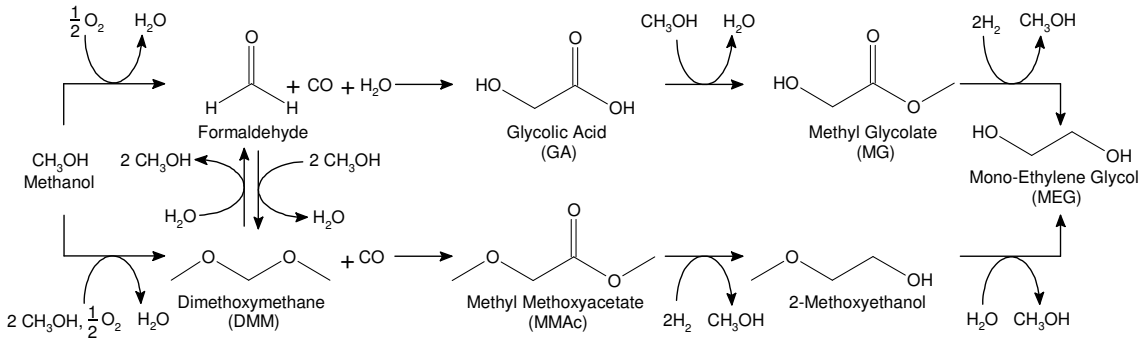

Figure 4.1 Scheme for the production of ethylene glycol from methanol via formaldehyde or dimethoxymethane.

a)

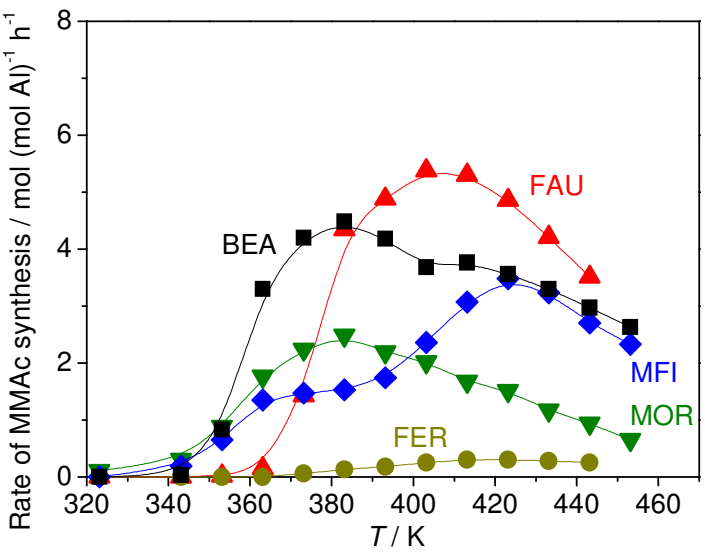
Rate of MMAc synthesis / mol (mol Al)$^{-1}$ h^{-1}
T / K
BEA
FAU
MFI
MOR
FER

b)

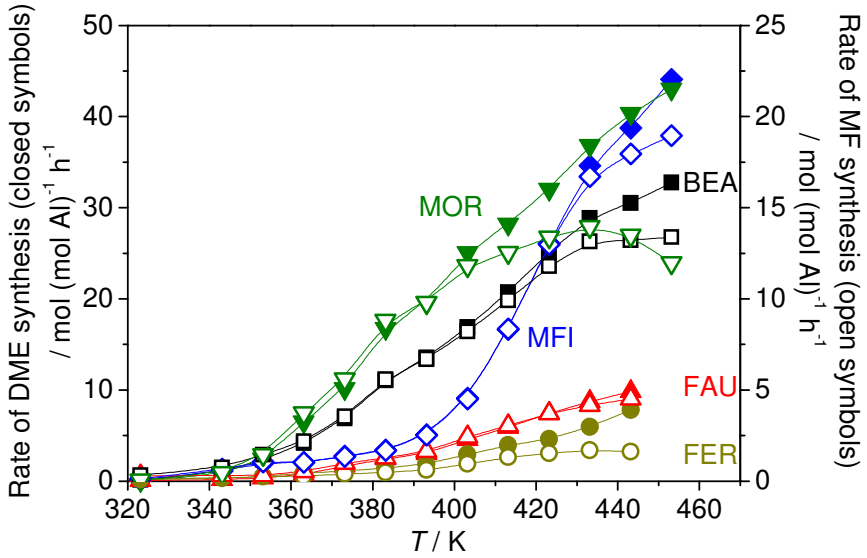
Rate of DME synthesis (closed symbols) / mol (mol Al)$^{-1}$ h^{-1}
Rate of MF synthesis (open symbols) / mol (mol Al)$^{-1}$ h^{-1}
T / K
MOR
BEA
MFI
FAU
FER

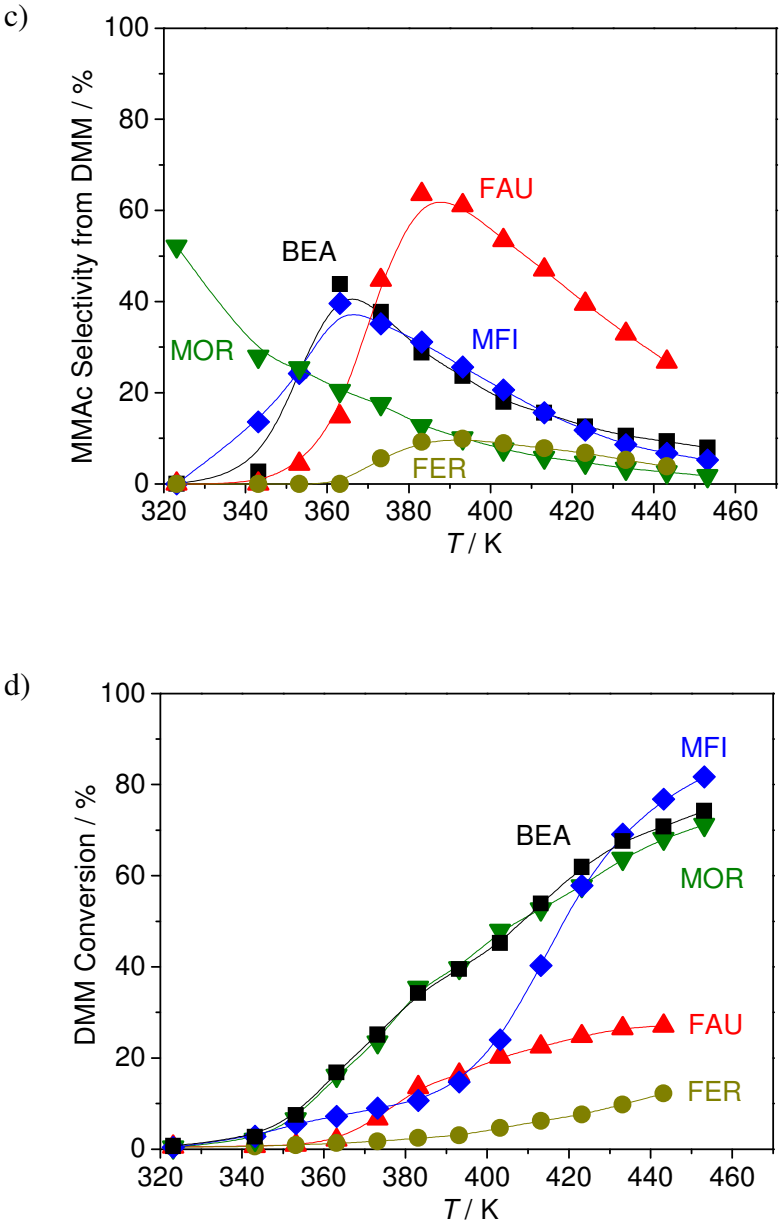

Figure 4.2 The effect of reaction temperature over FAU (Si/Al ≈ 15), MFI (Si/Al ≈ 13.5), MOR (Si/Al ≈ 10), BEA (Si/Al ≈ 12.5), and FER (Si/Al ≈ 10) on the rates of a) MMAc and b) DME and MF formation, c) selectivity of MMAc from DMM, and d) DMM conversion. 0.05-0.08 g catalyst, τ = 0.76-0.86 mmol Al min L^{-1}, P_{CO} = 1.98 atm, P_{DMM} = 0.016-0.019 atm, total gas flow rate = 100 cm^3 min^{-1} at pressure, 200 cm^3 min^{-1} at standard temperature and pressure (STP).

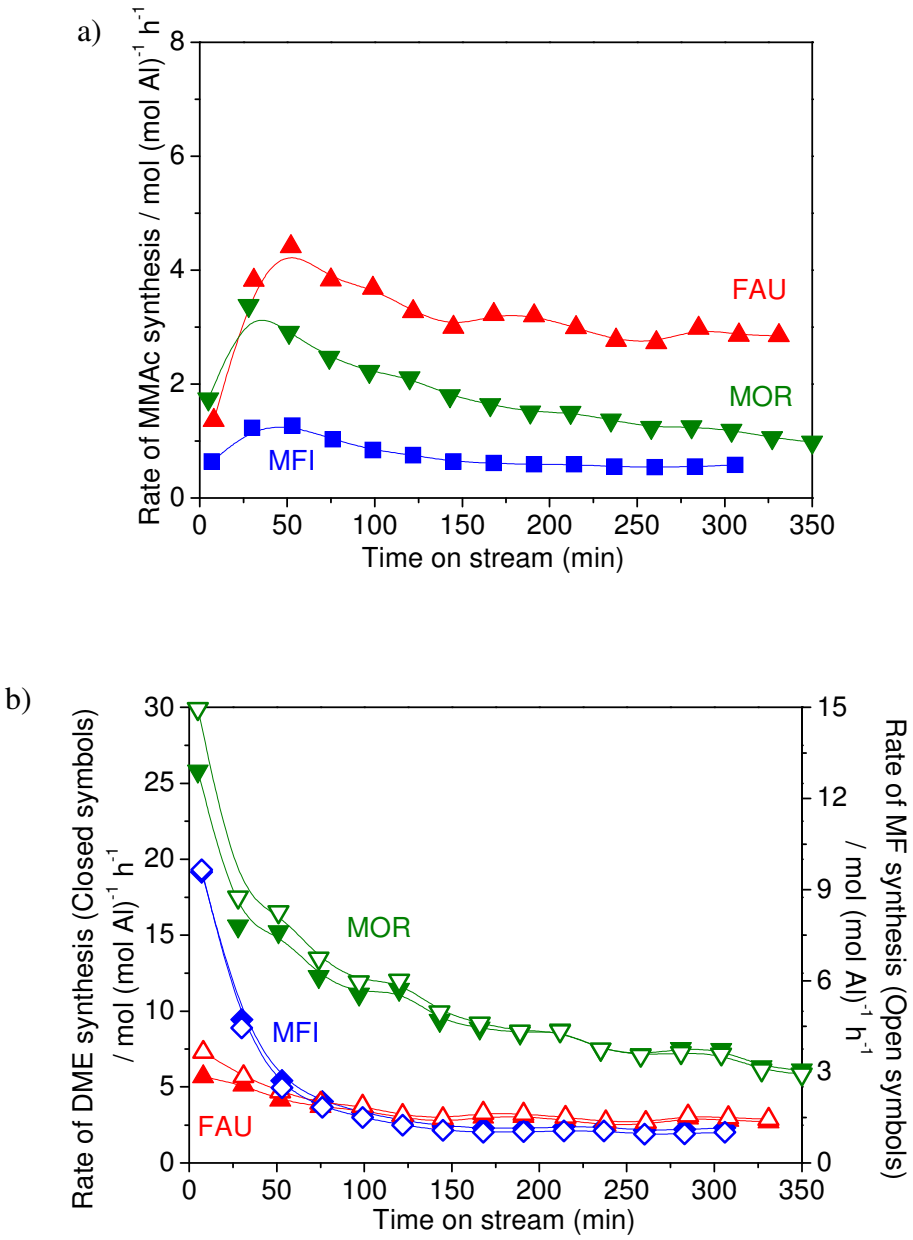

Figure 4.3 The effect of time on stream over FAU (Si/Al ≈ 15), MFI (Si/Al ≈ 13.5), and MOR (Si/Al ≈ 10) on the rates of a) MMAc and b) DME and MF formation. 0.05-0.08 g catalyst, τ = 0.76-0.81 mmol Al min L^{-1}, T = 383 K, P_{CO} = 1.98 atm, P_{DMM} = 0.013-0.017 atm, total gas flow rate = 100 cm^3 min^{-1} at pressure, 200 cm^3 min^{-1} at STP.

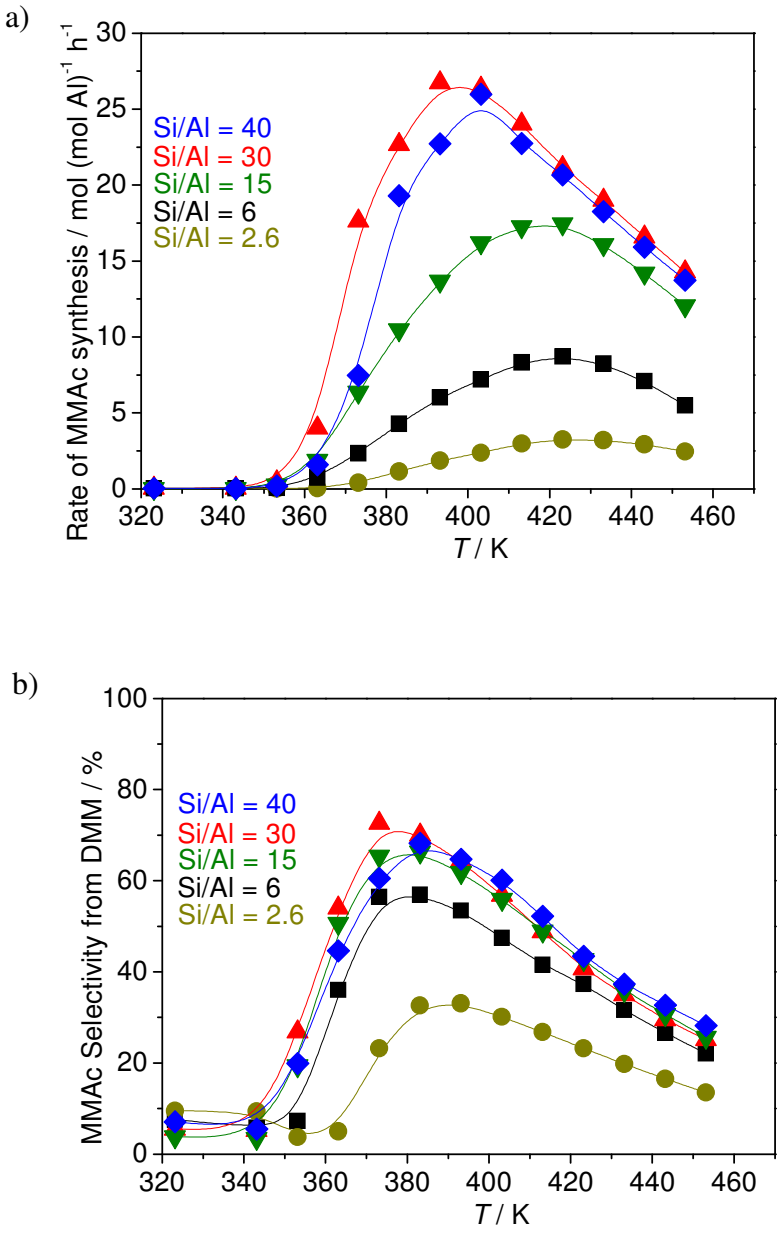

Figure 4.4 The effect of reaction temperature over FAU (Si/Al ≈ 2.6-40) on a) the rate of MMAc formation and b) selectivity of MMAc from DMM. 0.006-0.07 g catalyst, τ = 0.26-0.28 mmol Al min L^{-1}, P_{CO} = 1.98 atm, P_{DMM} = 0.016-0.017 atm, total gas flow rate = 100 cm^3 min^{-1} at pressure, 200 cm^3 min^{-1} at STP.

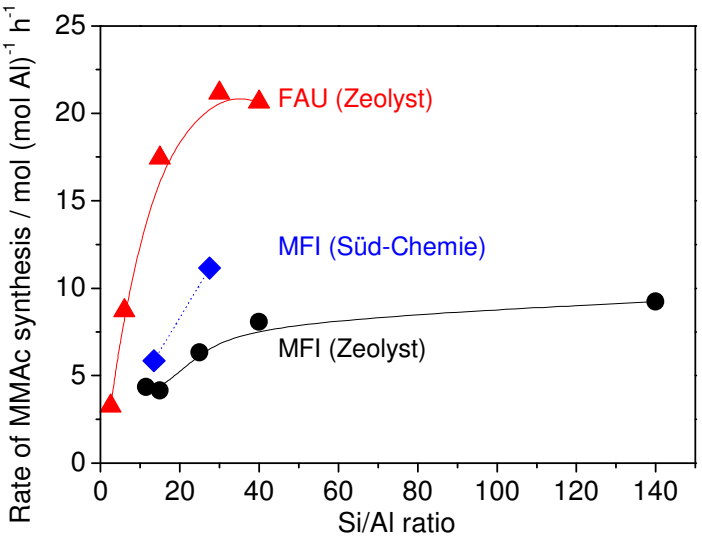

Figure 4.5 The effect of Si/Al ratio over FAU (Si/Al ≈ 2.6-40), and MFI samples from two different commercial suppliers (Süd-Chemie, Si/Al ≈ 13.5, 27.5; Zeolyst Si/Al ≈ 11.5-140) on the rate of MMAc formation. 0.006-0.25 g catalyst, τ = 0.26-0.31 mmol Al min L^{-1}, T = 423 K, P_{CO} = 1.98 atm, P_{DMM} = 0.011-0.019 atm, total gas flow rate = 100 cm^3 min^{-1} at pressure, 200 cm^3 min^{-1} at STP.

a)

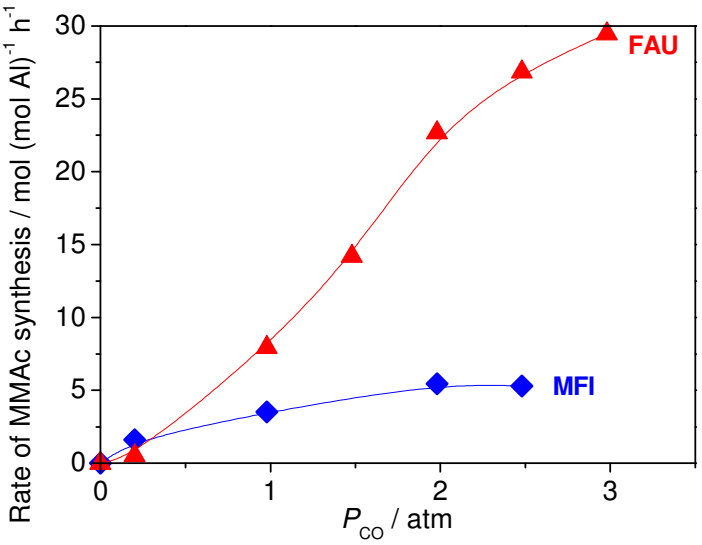
Rate of MMAc synthesis / mol (mol Al)$^{-1}$ h^{-1}
30
25
20
15
10
5
0
0
1
2
3
P_{CO} / atm
FAU
MFI

b)

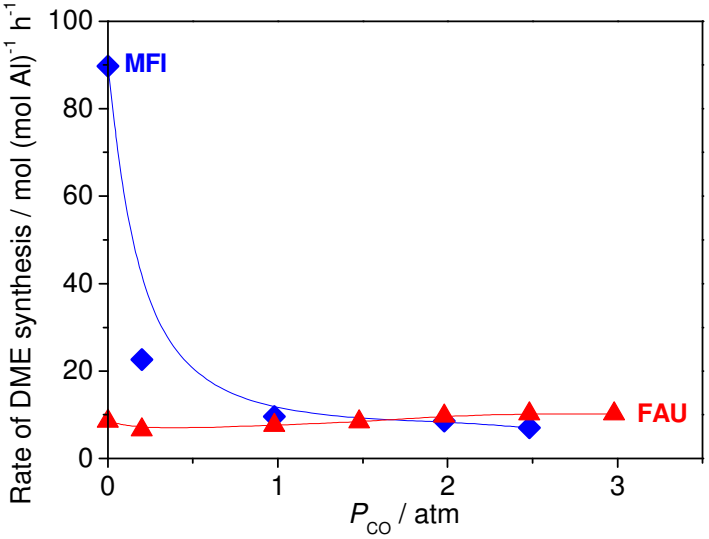
Rate of DME synthesis / mol (mol Al)$^{-1}$ h^{-1}
100
80
60
40
20
0
0
1
2
3
P_{CO} / atm
MFI
FAU

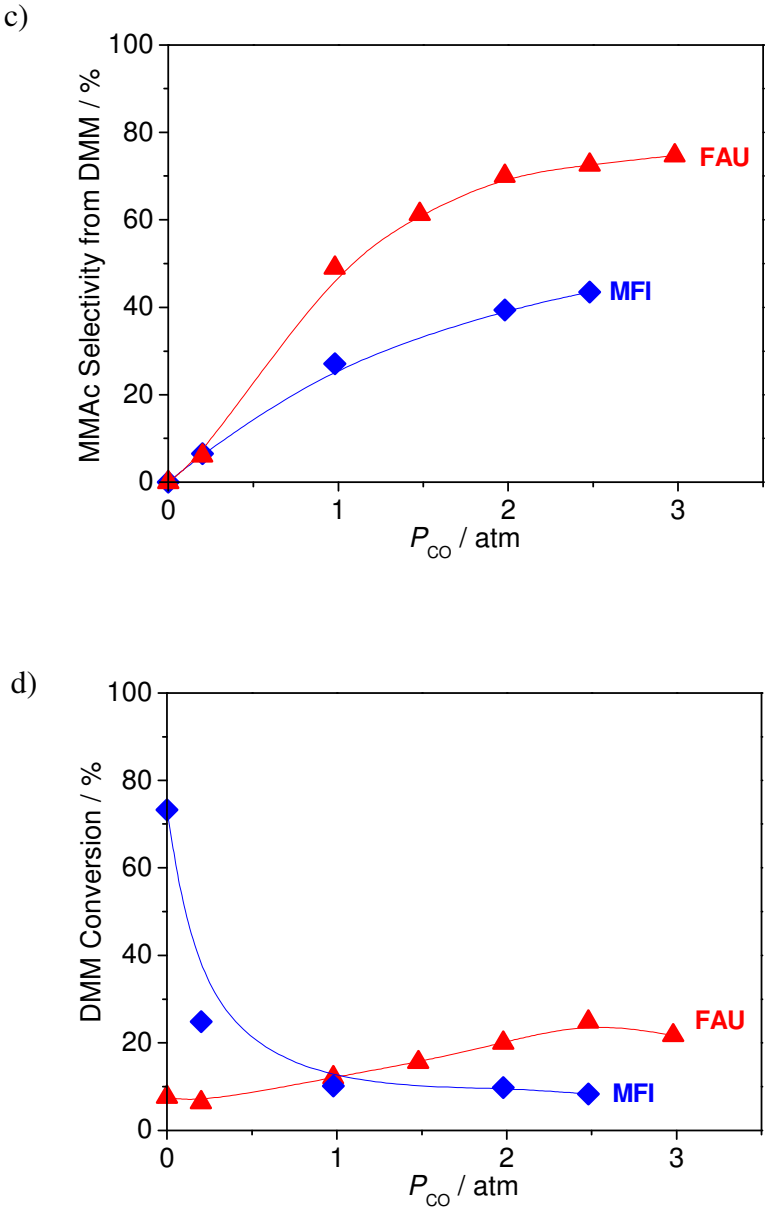

Figure 4.6 The effect of CO partial pressure over FAU (Si/Al ≈ 30) and MFI (Si/Al ≈ 27.5) on the rates of a) MMAc and b) DME and MF formation, c) selectivity of MMAc from DMM, and d) DMM conversion. 0.05 g catalyst, τ = 0.27-0.29 mmol Al min L^{-1}, T = 383 K, P_{DMM} = 0.013-0.019 atm, total gas flow rate = 100 cm^3 min^{-1} at pressure, 100-300 cm^3 min^{-1} at STP.

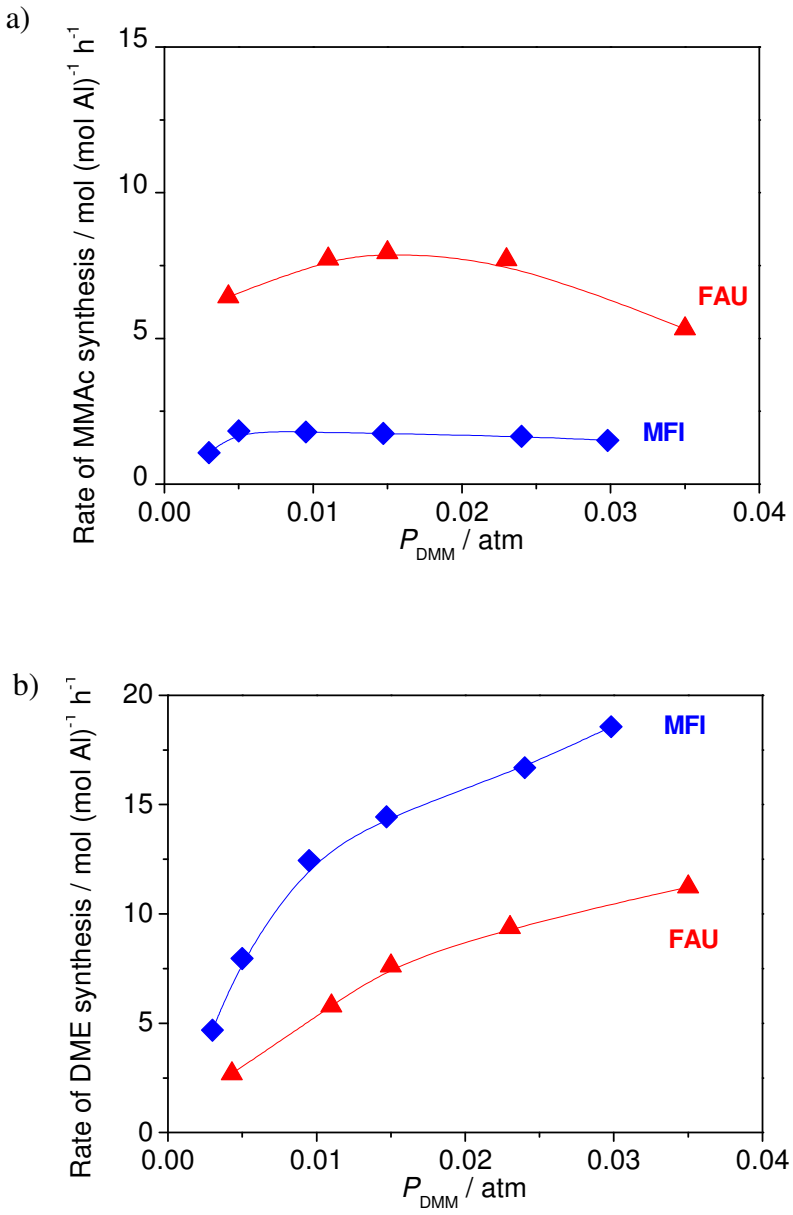

Figure 4.7 The effect of DMM partial pressure over FAU (Si/Al ≈ 30) and MFI (Si/Al ≈ 27.5) on the rates of a) MMAc and b) DME and MF formation. 0.05 g catalyst, τ = 0.27-0.29 mmol Al min L^{-1}, T = 383 K, P_{CO} = 1.0 atm, P_{He} = 0.97-1.0 atm, total gas flow rate = 100 cm^3 min^{-1} at pressure, 200 cm^3 min^{-1} at STP.

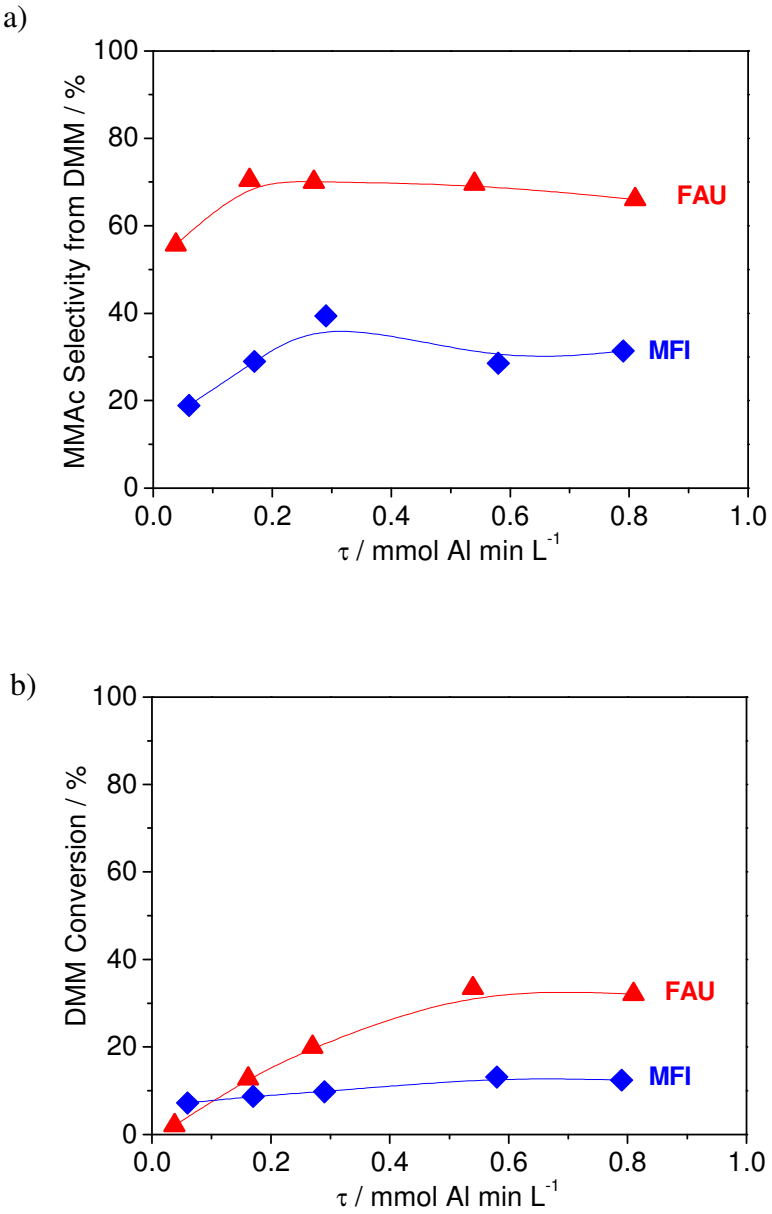

Figure 4.8 The effect of space time over FAU (Si/Al ≈ 30) and MFI (Si/Al ≈ 27.5) on a) selectivity of MMAc from DMM and b) DMM conversion. 0.007-0.15 g catalyst, T = 383 K, P_{CO} = 1.98 atm, P_{DMM} = 0.015-0.019 atm, total gas flow rate = 100 cm^3 min^{-1} at pressure, 200 cm^3 min^{-1} at STP.

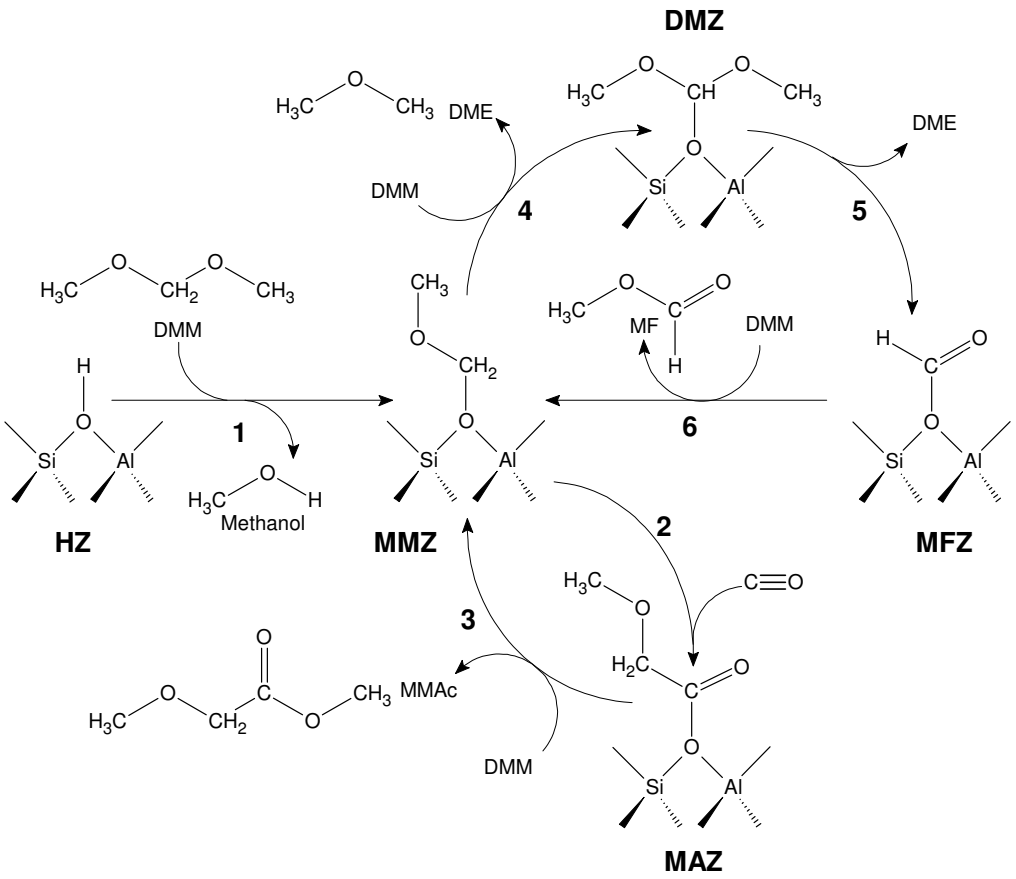

Figure 4.9 Proposed reaction mechanism.

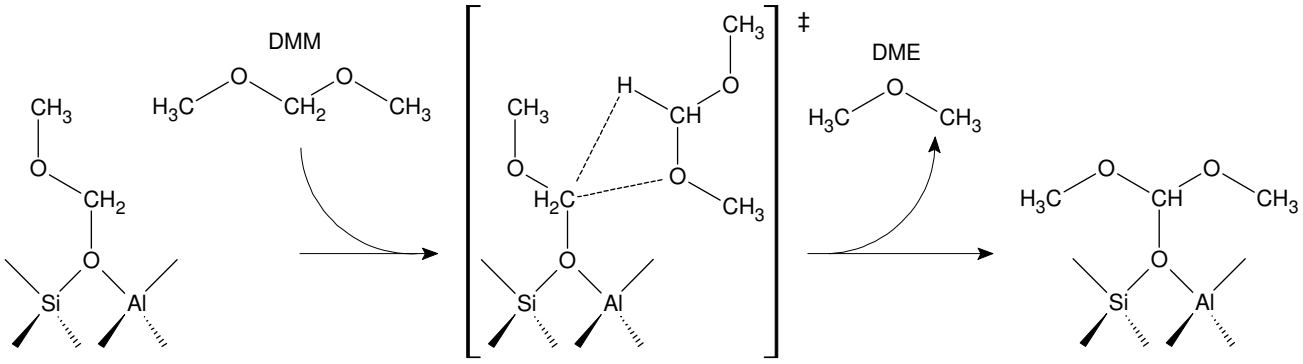

Figure 4.10 Proposed transition state for the rate-determining step of DMM disproportionation, illustrating the hydrogen transfer step.

Table 4.1 Pore size [25] and pore dimensionality of different zeolite framework types.

Framework Type	T-atoms in Pore Rings	Maximum Included Sphere Diameter (Å)	Pore Dimensionality
FER	10 x 8	6.25	2-D
MFI	10 x 10	6.30	3-D
BEA	12 x 12	6.62	3-D
MOR	12 x 8	6.64	1-D
FAU	12	11.18	3-D

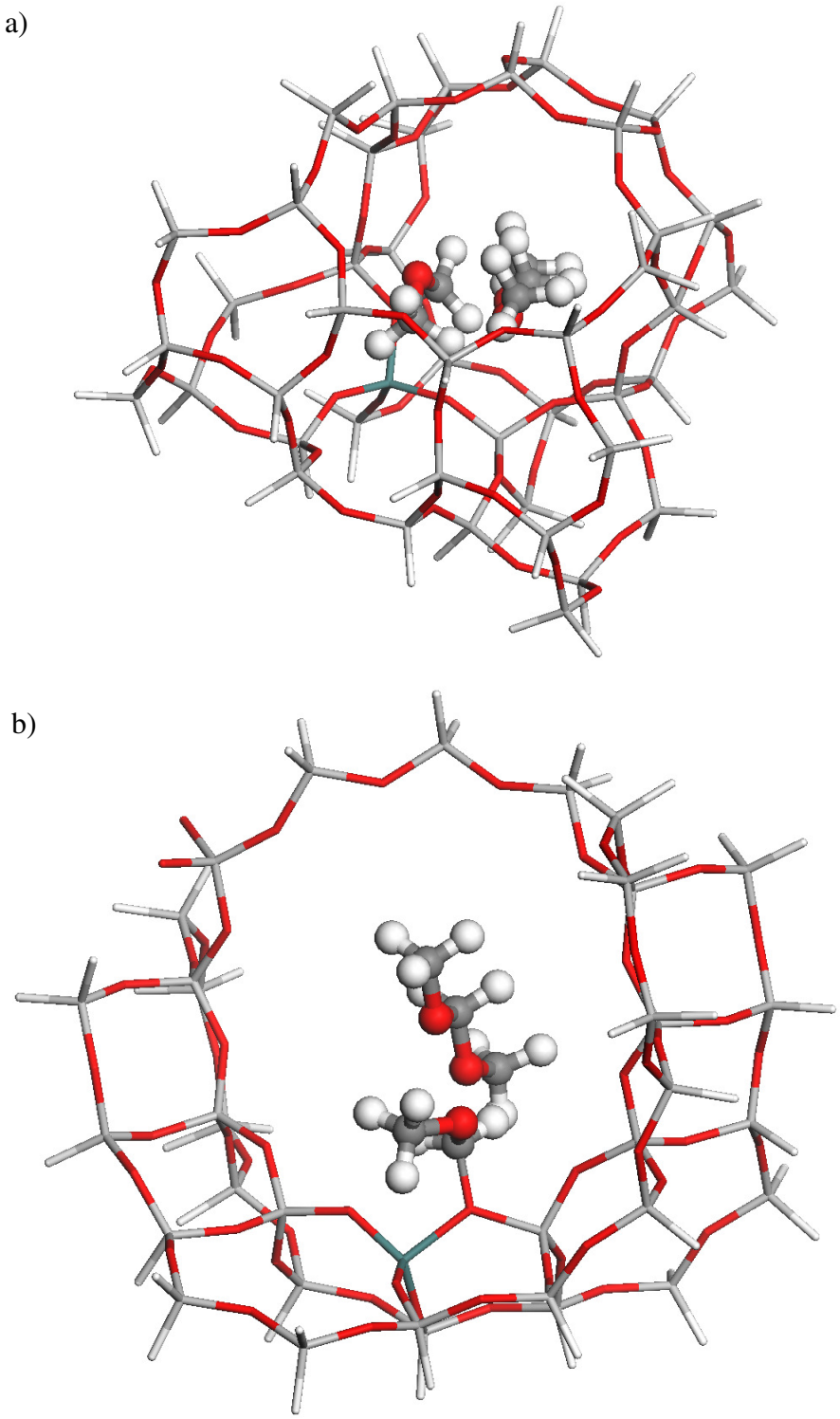

Figure 4.11 Illustration of DMM coordinated with surface methoxymethoxy species on a) MFI and b) FAU.

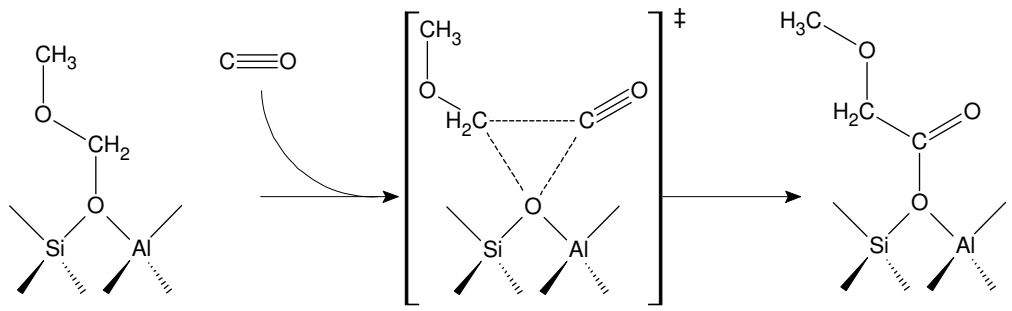

Figure 4.12 Proposed transition state for the rate-determining step of DMM carbonylation, illustrating the CO insertion step.

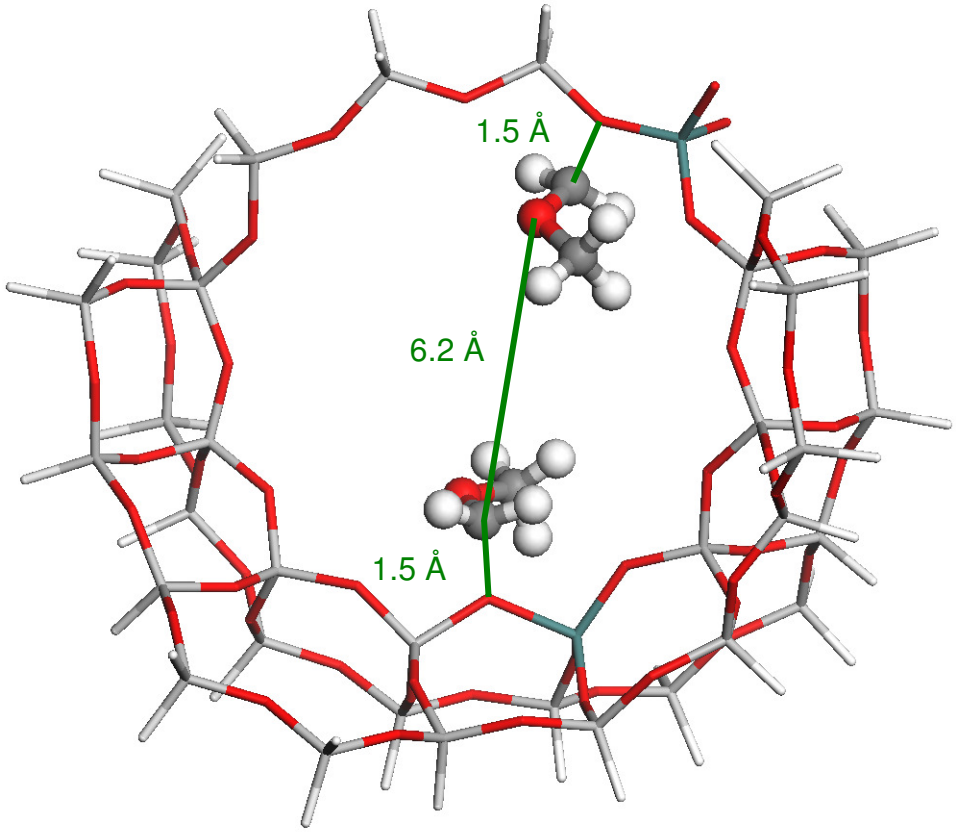

Figure 4.13 Illustration of interspecies distances for two methoxymethoxy species coordinated to Al atoms within the same supercage of FAU.

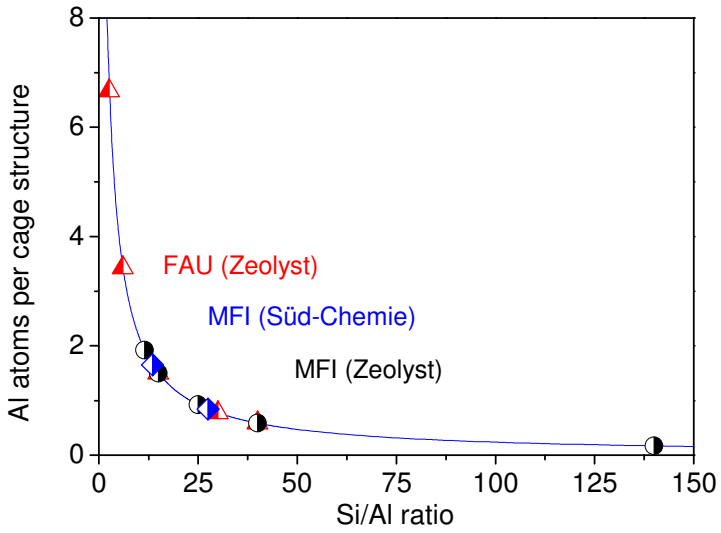

Figure 4.14 Calculated average number of Al atoms per cage structure in FAU and MFI samples from Zeolyst and Süd-Chemie of different Si/Al ratios as reported by the suppliers. A cage structure is a supercage in FAU and a channel intersection in MFI. A curve of $24/(1+R)$, where R is the Si/Al ratio, has been plotted passing through all the points [28].

References

[1] D.J. Loder, US Patent 2 152 852 (1939), to E. I. du Pont de Nemours & Co.
[2] D.E. Hendriksen, Prepr. Pap.—Am. Chem. Soc., Div. Fuel Chem. 28 (1983) 176.
[3] H.J. Schmidt, H.J. Arpe, US Patent 4 501 917 (1985), to Hoechst AG.
[4] S.Y. Lee, J.C. Kim, J.S. Lee, Y.G. Kim, Ind. Eng. Chem. Res. 32 (1993) 253.
[5] E. Drent, W.P. Mul, B.J. Ruisch, US Patent 6 376 723 (2002), to Shell Oil Company.
[6] T. Li, Y. Souma, Q. Xu, Catal. Today 111 (2006) 288.
[7] F.E. Celik, H. Lawrence, A.T. Bell, J. Mol. Catal. A: Chem. 288 (2008) 87.
[8] K. Ivanov, Appl. Catal., A 116 (1994) L1.
[9] J.M. Berty, Ethylene Oxide Synthesis, in: B.L. Leach (Ed.), Applied Industrial Catalysis Vol. 1, Academic Press, New York, 1983, 207.
[10] J.M. Tatibouet, Appl. Catal., A 148 (1997) 213.
[11] F.E. Celik, T. Kim, A.T. Bell, Angew. Chem. Int. Ed. 48 (2009) 4813.
[12] ΔG° values for reactions were estimated from published ΔG_f° or ΔH_f° and S° values where available [Standard Thermodynamic Properties of Chemical Substances, in: D.R. Lide (Ed.), CRC Handbook of Chemistry and Physics, 88th Edition (Internet Version 2008), CRC Press/Taylor and Francis, Boca Raton, FL, 2008; P.J. Linstrom, W.G. Mallard (Eds.), NIST Chemistry WebBook, NIST Standard Reference Database Number 69 National Institute of Standards and Technology, Gaithersburg, MD, http://webbook.nist.gov, (retrieved March 13, 2008)] or from group contribution theory otherwise [Prediction and Correlation of Physical Properties, in: D.W. Green (Ed.), Perry's Chemical Engineers' Handbook, 7th Edition, McGraw Hill, New York, 1997].
[13] P. Cheung, A. Bhan, G. J. Sunley, E. Iglesia, Angew. Chem. Int. Ed. 45 (2006) 1617.
[14] P. Cheung, A. Bhan, G. J. Sunley, D. J. Law, E. Iglesia, J. Catal. 245 (2007) 110.
[15] A. Bhan, A. D. Allian, G. J. Sunley, D. J. Law, E. Iglesia, J. Am. Chem. Soc. 129 (2007) 4919.
[16] H. Bahrmann, Koch Reactions, in: J. Falbe (Ed.), New Syntheses with Carbon Monoxide, Springer, Berlin, 1980, p. 372.
[17] A.G. Stepanov, M.V. Luzgin, V.N. Romannikov, V.N. Sidelnikov, K.I. Zamaraev, J. Catal. 164 (1996) 411.
[18] Q. Xu, S. Inoue, N. Tsumori, H. Mori, M. Kameda, M. Tanaka, M. Fujiwara, Y. Souma, J. Mol. Catal. A: Chem. 170 (2001) 147.
[19] J.F. Walker, Formaldehyde, American Chemical Society Monograph Series, Reinhold, London, 1964, p. 214.
[20] Y. Tsujino, C. Wakai, N. Matubayashi, M. Nakahara, Chem. Lett. (1999) 287.
[21] S. Morooka, N. Matubayasi, M. Nakahara, J. Phys. Chem. A 111 (2007) 2697.
[22] Y.J. Jiang, M. Hunger, W. Wang, J. Am. Chem. Soc. 128 (2006) 11679.
[23] M. Boronat, C. Martinez-Sanchez, D. Law, A. Corma, J. Am. Chem. Soc. 130 (2008) 16316.
[24] H.G. Karge, Concepts and Analysis of Acidity and Basicity, in: G. Ertl, H. Knözinger, F. Schüth, J. Weitkamp (Eds.), Handbook of Heterogeneous Catalysis, Second Edition, Wiley, New York, 2008, p. 1103.
[25] M.D. Foster, I. Rivin, M.M.J. Treacy, O. Delgado Friedrichs, Microporous Mesoporous Mater. 90 (2006) 32.
[26] K. Yoo, E.C. Burckle, P.G. Smirniotis, J. Catal. 211 (2002) 6.

[27] V. Shapovalov, A.T. Bell, manuscript in preparation.
[28] The FAU structure contains 192 T atoms (either Si or Al) per unit cell and 8 supercages per unit cell [G. H. Kühl, Modification of Zeolites, in: J. Weitkamp, L. Puppe (Eds.), Catalysis and Zeolites, Springer, Berlin, 1999, p. 89], giving 24 T atoms per supercage. The average number of Al atoms per supercage is then 24//(1+*R*), where *R* is the Si/Al ratio. The MFI structure contains 96 T atoms and 4 channel intersections per unit cell [B. Millot, A. Méthivier, H. Jobic, H. Moueddeb, J.A. Dalmon, Microporous Mesoporous Mater. 38 (2000) 85], giving 24 T atoms per channel intersection, so that the average number of Al atoms per channel intersection is also 24/(1+*R*).
[29] K. Schröder, J. Sauer, J. Phys. Chem. 100 (1996) 11043.

Chapter 5

An Investigation of the Mechanism and Kinetics of Dimethoxymethane Carbonylation over FAU and MFI Zeolites

Abstract

In situ IR spectroscopy was used to observe the intermediates formed on zeolites FAU and MFI during the synthesis of methyl methoxyacetate (MMAc) via carbonylation of dimethoxymethane (DMM) and the disproportionation of DMM to dimethyl ether (DME) and methyl formate (MF). Both reactions are initiated by the reaction of DMM with the Brønsted acid protons of the zeolite to form methanol and methoxymethoxy groups (MMZ). The latter species then undergoes one of two processes – carbonylation to form methoxyacetyl species, the precursors to MMAc or reaction with DMM, resulting in DMM disproportionation. Surface intermediates for both DMM carbonylation and disproportionation respond to changes in reaction conditions in a manner consistent with observed steady state kinetic. DMM carbonylation occurred more rapidly in the presence than absence of physisorbed DMM, a phenomenon attributed to solvation of the carbocationic transition state involved in the addition of CO to MMZ predicted by DFT calculations. The surface concentration of the methoxyacetyl species at steady state was 10 times smaller on FAU than on MFI, consistent with the higher rate of DMM carbonylation on FAU. Rate expressions for the formation of each product, based on the proposed mechanisms, in combination with a suitable set of rate coefficients, give a good description of the experimentally observed dependences of the rates product formation of on temperature and the feed partial pressures of CO and DMM.

5.1 Introduction

Monoethylene glycol (MEG) is a commodity chemical widely used as antifreeze and as a monomer in the synthesis of polyester fibers. The current production of MEG is by epoxidation of ethylene and subsequent hydration of the resulting ethylene oxide [1]. While this technology is highly developed, the rising cost of ethylene derived from petroleum or natural gas has motivated consideration of alternative routes. The lower cost of carbon derived from synthesis gas (CO and H_2), produced by gasification of coal or other low hydrogen content feed stocks, relative to that derived from ethylene, has led to an interest in identifying routes to MEG from synthesis gas. While the direct production of MEG from synthesis gas has been investigated, such processes suffer from low yields and require very high pressures (1300–7000 atm) [2-3]. An alternate approach to forming MEG from synthesis gas is to begin with methanol, which can then oxidized to obtain formaldehyde or its dimethyl acetal, dimethoxymethane (DMM) [4-5]. Since these are C_1 compounds lacking a C–C bond, they can be converted to C_2 compounds by carbonylation. Several attempts to carry out the acid-catalyzed carbonylation of formaldehyde in the liquid phase have been reported [6-9], with efforts being made to achieve high selectivity at low pressure [10-12]. However, the rate of formaldehyde

carbonylation in all cases has been limited by the low solubility of CO in the solvent used, which results in poor selectivity for reactions carried out at low pressures due to the reactivity of the formaldehyde [12].

We have recently shown that the vapor phase carbonylation of DMM can catalyzed by acidic zeolites [13-14]. The product of DMM carbonylation is methyl methoxyacetate (MMAc), which can then be converted to MEG in two steps. In the first step MMAc is hydrogenated to ethylene glycol monomethyl ether, and in the second step, this intermediate is hydrolyzed to produce MEG. Using FAU, 79% selectivity to MMAc was achieved at 393 K and a total pressure of 3 atm [13]. DMM disproportionation, which produces dimethyl ether (DME) and methyl formate (MF), was the only side-reaction, in contrast to liquid-phase reactions, which produced a large number of byproducts [7,9,12]. The highest selectivity to MMAc was achieved with FAU, whereas smaller pore zeolites such as MFI, BEA, MOR, and FER were significantly less selective. MMAc formation rates increased with increasing CO partial pressure and were nearly independent of DMM partial pressure over both MFI and FAU. Both catalysts exhibited a maximum MMAc formation rate as a function of reaction temperature, whereas DMM disproportionation rates increased monotonically with temperature. DMM disproportionation rates increased with increasing DMM partial pressure, and were independent of CO partial pressure on FAU. The activity of MFI for DMM disproportionation was severely inhibited by the presence of CO [14]. Attainment of high MMAc selectivity required a high ratio of CO/DMM partial pressures and a low DMM partial pressure (~0.01–0.02 atm).

The aim of present study is to confirm the mechanism, proposed in our earlier work [14]. In situ FTIR spectroscopy was used to identify reaction intermediates and to probe key elementary processes involved in the carbonylation of DMM to MMAc. The spectroscopic evidence supports our proposed mechanism and is consistent with steady-state rate data that we reported earlier [14] and with an analysis of the proposed mechanism using density functional theory [15]. Rate expressions derived from the proposed mechanism provide an accurate description of the dependences of the rates of MMAc, DME, and MF formation on temperature and feed partial pressures of CO and DMM observed experimentally.

5.2 Experimental Methods

5.2.1 Catalyst preparation

H-FAU with Si/Al ratio ≈ 30 was obtained from Zeolyst and Na-MFI with Si/Al ≈ 27.5 was obtained from Süd-Chemie. Na-ZSM was converted to the NH_4^+-form by aqueous exchange with 1 M NH_4NO_3 solution. 5 g of Na-MFI were exchanged with 0.1 L of solution for 12 h at 353 K three times, filtering and washing with 0.1 L deionized water each time. After the final exchange, the sample was filtered and rinsed again and dried at 383 K for 36 h. Removal of residual moisture and conversion to the H^+ form was achieved by heating to 773 K for 3 h at the rate of 2 K min^{-1} in 100 cm^3 min^{-1} flow of dry air (zero-grade). Residual moisture was removed from H-FAU by treatment in dry air for 3 h at 773 K as described above.

High surface area SiO_2 (MCM-41) was prepared according to established techniques [16] with a surface area of 1106 m^2 g^{-1} (as determined by N_2 adsorption). Prior to use, the SiO_2 was heated to 773 K at 4 K min^{-1} and held for one hour.

5.2.2 Collection of FTIR spectra

Infrared spectra were acquired using a Thermo Scientific Nicolet 6700 FTIR spectrometer equipped with a liquid nitrogen cooled MCT detector. Each spectrum was obtained by averaging 32 scans taken with 1 cm^{-1} resolution. Catalysts were pressed into 20 mm-diameter pellets (< 1 mm thick) and placed into a custom-built transmission cell equipped with CaF_2 windows, a K-type thermocouple for temperature control, and resistive cartridge heaters similar to that described in [17]. All pressed pellets were heated to 773 K with ramp rates and durations listed above) in the transmission cell prior to the introduction of adsorbate gases. All scans were acquired at 383 K. Experiments at elevated pressure were carried out by throttling a needle valve located downstream from the reactor. Unless otherwise noted, the total gas flow rate through the reactor was maintained at 100 cm^3 min^{-1}, meaning that at elevated pressures, the gas flow rate exceeded 100 cm^3 min^{-1} at STP. Gases used included CO (99.99% pure research grade, Praxair), DMM (9.96% in He, Praxair), MF (9.94% in He, Praxair), DME (99.5% chemically pure, Praxair), He (99.999% ultra-high purity, Praxair), and 3.99% DMM in CO (Praxair). Pure CO was supplied in a stainless steel cylinder, leading to the formation of iron pentacarbonyl [18]. A trap packed with 3.2 mm pellets of 3A molecular sieve was placed in the CO gas line to remove the iron pentacarbonyl.

All absorption spectra were taken relative to the empty transmission cell. In addition, spectra above 3160 cm^{-1} were baseline corrected and spectra below 3060 cm^{-1} were baseline corrected after subtracting the spectrum of the bare support (FAU, MFI, or SiO_2).

2.3 Steady-state and transient-response kinetic data

Rate measurements were carried out in a 6.35 mm OD quartz tube reactor with an expanded section (~12.7 mm OD, ~20 mm length). The reactor was packed with quartz wool above and below the catalyst bed to hold the catalyst powder in place. The reactor was placed inside a resistively heated ceramic furnace with external temperature control and the catalyst bed temperature was measured with a K-type thermocouple sheathed in a quartz capillary placed in direct contact with the bed. Reaction products were analyzed using an Agilent 6890n gas chromatograph equipped with a bonded polystyrene-divinylbenzene (HP-PLOT Q) capillary column connected to a flame ionization detector and an MKS Mini-Lab quadrupole mass spectrometer. Reaction conditions were chosen to reproduce the conditions in the transmission IR cell.

5.3 Results and Discussion

5.3.1 FTIR spectra of DMM and DMM-like adsorbed species

The spectrum of physically adsorbed DMM physisorbed on SiO_2 was acquired in the following manner. High-surface area SiO_2 was saturated under a flow rate of 100 cm^3 min^{-1} of 0.01 atm DMM in He at 383 K. Table 5.1 lists the IR bands observed in this experiment and compares then with those for gas-phase DMM [19]. A one-to-one

correlation of C–H stretching- and bending-vibrations between vapor-phase DMM and DMM adsorbed on SiO_2 at 383 K is seen, indicating that DMM physisorbs on SiO_2 intact. Certain modes for physisorbed DMM (asymmetric CH_2 stretching, symmetric CH_3 stretching, and an unassigned band shifting from 2774 cm^{-1} to 2782 cm^{-1}) appear at higher frequencies than seen in the gas-phase spectrum of DMM, due likely to dispersive interaction of the physisorbed molecule with the SiO_2. Upon switching the gas flow to pure He, all C–H vibrations rapidly disappeared, indicating that only physisorbed species were present. Table 5.1 also shows that the spectrum of DMM interacting with FAU taken at 383 K is very similar to that for SiO_2, indicating that the spectrum is dominated by physisorbed DMM.

The spectrum of H-FAU (Figure 5.1, black curve), taken prior to exposure of the zeolite to DMM, exhibits a peak at 3744 cm^{-1} due to silanol groups associated with external, lattice-terminating defects and internal SiOH nests associated with defect groups generated upon dealumination of the zeolite [20-21]. In FAU samples with high Si/Al ratios, the contribution to the silanol peak from internal nested defects is significant because FAU is synthesized with a Si/Al ratio ≈ 2.6 and then dealuminated to give the desired Si/Al ratio [22]. The large peak at 3744 cm^{-1} observed for H-FAU with Si/Al ≈ 30 is the result of significant zeolite dealumination. The peaks at 3628 and 3564 cm^{-1} are due to Brønsted acidic protons associated with O(1) sites located in the FAU supercages and O(3) sites located in the sodalite cages [20-21,23]. The shoulder at 3550 cm^{-1} is unassigned, but may be due to protons at the O(2) sites that point into the hexagonal prisms of FAU. The peak at 3602 cm^{-1} is assigned to extra-framework aluminum species (EFAL) [20-21]. The low intensity of this peak, coupled with the lack of a peak at ~3695 cm^{-1} indicates the sample has a very low EFAL content.

The interactions of DMM with H-FAU (Si/Al ≈ 30) were characterized in the following manner. The zeolite was first exposed to flow of 100 cm^3 min^{-1} of 0.01 atm DMM in He at 383 K. IR spectra were acquired for about 1000 s , at which point they no longer changed with time. Upon exposure to DMM (Figure 5.1), the O–H stretching vibrations associated with both Brønsted acidic sites as well as non-acidic SiOH groups decreased, while a broad feature around 3430 cm^{-1} grew concurrently with the growth in the C–H stretching (2740–3060 cm^{-1}) and C–H deformation vibrations (1360–1500 cm^{-1}) associated with physisorbed species. The broad peak at 3430 cm^{-1} is attributed hydrogen bonding of DMM with O–H groups on the zeolite surface, which causes a bathochromic shift in the all of the O–H stretching vibrations. After 90 s of DMM exposure, all of the Brønsted acidic O–H groups were covered by either physically or chemically adsorbed DMM molecules, resulting in a disappearance of both the high- and low-frequency bands.

The steady-state spectrum of FAU taken in flowing DMM (Figure 5.1, red and Figure 5.2, black) is similar to that of DMM physisorbed on SiO_2. All of the peaks of physisorbed DMM are observed with only small shifts in frequency. During the approach to steady state, the band assigned primarily to asymmetric CH_2 stretching vibrations (2955 cm^{-1}) grew more slowly but reached a greater intensity than the adjacent band assigned primarily to symmetric CH_3 stretching vibrations (2946 cm^{-1}). Similarly, the symmetric CH_2 stretching band at 2910 cm^{-1} grew more slowly than the symmetric CH_3 stretching band at 2836 cm^{-1}. The slower growth rate of bands associated with CH_2 groups relative to CH_3 groups indicates that the CH_2/CH_3 ratio in the surface species increased with time from an initially low value.

After ~1000 s of DMM exposure, the sample was flushed with He to remove gaseous and physisorbed species (Figure 5.2), leaving only chemisorbed species. The C–H stretching vibration peaks associated with CH_2 groups (2962 cm^{-1} and 2910 cm^{-1}) decreased in intensity less than those associated with CH_3 (2995–3003 cm^{-1}, 2946 cm^{-1}, and 2836 cm^{-1}), such that the relative intensities of peaks for CH_2 groups were larger than those for CH_3 groups. It was also observed that as physisorbed DMM was removed from the IR cell, the intensities of both the silanol groups and Brønsted acidic groups increased.

Figure 5.3 shows the proposed physical and chemical adsorption modes of DMM at a zeolite Brønsted acid site. Hydrogen-bonded physisorbed DMM possesses a CH_2/CH_3 ratio of 0.5, identical to gas-phase DMM. Physisorbed DMM is envisioned to undergo protonation with the loss methanol and formation of methoxymethoxy species (MMZ). Two experimental observations support the occurrence of this process. The first is the observation by mass spectrometry of a burst of methanol when the zeolite is first contacted with DMM, as shown in Figure 5.4. A small amount of water is also observed, which is attributed to the dehydration of methanol to form DME. The total number of protons displaced in 600 s is equivalent to 53% of the Brønsted acidic protons in the sample. The remaining protons were likely associated with physisorbed DMM. Prolonged flushing of physisorbed DMM with He (Figure 5.2) showed the regeneration of roughly half of the original IR peak intensity for Brønsted acidic OH groups, providing further evidence that half the Brønsted acid sited had reacted with DMM to form MMZ and other surface species. Further evidence for the formation of MMZ is the observed change in the CH_2/CH_3 ratio, which increase with time of exposure of the zeolite to DMM. This is exactly what would be expected from Figure 5.3.

Comparison of the bands for DMM chemisorbed on FAU and physisorbed on SiO_2 (Table 5.1) shows the appearance of several new features, some of which were also observed when both chemisorbed and physisorbed species were present during DMM flow. These new bands occur at 2995, 2982, 2802, 1734, 1490, 1458, 1435, 1417, and 1385 cm^{-1}, and may be associated with surface species other than MMZ generated by the disproportionation of DMM (see below). However, all of these new bands were small peaks or shoulders on the bands associated with MMZ, indicating that MMZ was the principal adsorbed species.

5.3.2 FTIR spectra of DME, MF, MMAc, and their derivatives

Table 5.2 lists the IR bands observed when 0.01 atm DME in He (total flow rate = 100 cm^3 min^{-1}) was passed over SiO_2 and FAU. Also listed in Table 5.2 are the bands observed after removal of physisorbed DME from FAU by flushing the infrared cell with He. The assignment of these bands to specific vibrational modes is based on gas phase DME [24] and DME adsorbed on MFI [25]. Similar results are presented in Table 5.3 for MF, and here too the band assignments are based on the results of previous studies [26-27]. Table 5.4 lists the bands reported in the literature for liquid-phase MMAc [28]. Assignments of these bands were made by analogy with DMM, as it has been shown that spectra of species containing CH_3OCH_2- groups, such as DMM and MMAc, tend to show similar C–H stretching and deformation region vibrations [29].

Methoxy species formed by the reaction of DME with Brønsted-acid centers exhibit bands at near 2985 and 2885 cm^{-1} [25,30-31]. The absence of such in the spectra for chemisorbed DME on FAU indicates that methoxy species were formed at 383 K

upon exposure of this zeolite to DME. This finding is consistent with the observation that surface methoxy species are generated from hydrogen-bonded DME at temperatures closer to 473 K [25]. The generation of surface methoxy species at lower temperatures is highly disfavored because of the relatively high activation energy associated with their formation [32].

5.3.3 Mechanisms of DMM carbonylation and disproportionation

Figure 5.5 shows the proposed catalytic cycles for DMM carbonylation (Reactions 2/2' and 3/3') and DMM disproportionation (Reactions 4–6). This scheme is adapted from [14] to incorporate new evidence presented here. DMM carbonylation takes place in two steps. In the first step, Reaction 2, CO reacts with methoxymethoxy species (MMZ) to form a methoxyacetyl species (MAZ). MAZ then undergoes methoxylation by DMM, Reaction 3, to release MMAc and regenerate MMZ. Reactions 2 and 3 are both reversible as suggested by the observation that at higher temperatures the rate of MMAc formation decreases [14]. In the first step of DMM disproportionation, MMZ reacts with another molecule of DMM, resulting in hydrogen-transfer to form a dimethoxymethoxy species (DMZ) and DME (Reaction 4). DMZ then decomposes to release a second molecule of DME and form a formate species (MFZ), Reaction 5, which then undergoes methoxylation by DMM to release MF and regenerate MMZ, Reaction 6. In what follows, we present evidence to support the proposed schemes for MMAc formation and DMM disproportionation. The kinetics of these processes are discussed in Section 3.6.

Both under DMM flow (Figure 5.1) and after flushing with He (Figure 5.2), a small peak at 1734 cm^{-1} was observed superimposed over a broader band located between ~1700 and ~1800 cm^{-1}, that grew in the presence of DMM vapor (Figure 5.1). The peak at 1734 cm^{-1} is similar to that observed when MF was sorbed on FAU (Table 5.3), and, therefore, this band is assigned to a C=O stretching mode in chemisorbed MF.

Surface formate species in zeolites can be either mono- or bidentate coordinated [33]. Monodentate surface formates exhibit a peak for C=O stretching above 1700 cm^{-1} and a peak for C–O stretching below 1350 cm^{-1}, whereas bidentate formates exhibit asymmetric and symmetric O=C–O stretching vibrations around 1610 cm^{-1} and 1385 cm^{-1} [34]. Similar peaks have been reported for MF adsorbed on alumina [35]. The presence of bands near 1385 cm^{-1} for both DMM and MF chemisorbed on FAU (Tables 5.1 and 5.3) could indicate the formation of bidentate formates, whereas the peak at 1734 cm^{-1} could be assigned to C=O stretching vibrations of monodentate formates (MFZ in Figure 5.5). In summary, the presence of the peak at 1734 cm^{-1} in Figure 5.1 indicates the formation of products of DMM disproportionation.

The band between ~1700 and ~1800 cm^{-1} is associated with the interaction of strongly adsorbed species and the zeolite framework [36]. This feature was observed whenever DMM, DME, or MF were present in the gas phase, and diminished in intensity when these gases were flushed from the IR cell with either He or CO.

In addition to the peaks at 1734 cm^{-1} and 1385 cm^{-1}, peaks were observed at 2982, 1458, and 1417 cm^{-1} in the spectra obtained when DMM was contacted with FAU (Figures 5.1 and 5.2), but not SiO_2 (Table 5.1). These features could also be seen upon exposure of FAU to MF (Table 5.2), supporting the assignment of these bands to intermediates involved in the disproportionation of DMM.

Further evidence supporting the relationship between the peak at 1734 cm^{-1} and the production of MF was obtained by collecting a series of spectra in "batch mode" (Figure 5.6). After exposing FAU to 0.01 atm DMM in He flowing at 100 cm^3 min^{-1} (Figure 5.6, black), the inlet and outlet valves of the IR cell were closed, sealing a small volume of the reactant gas in the cell. The IR cell then acted as a batch reactor. Under these conditions, the band at 1734 cm^{-1} grew initially, reached a maximum intensity after 5188 s, and then began to decline. This band was accompanied by a peak at 1722 cm^{-1}, which grew and then decayed somewhat more slowly than the peak at 1734 cm^{-1}. The band at 1722 cm^{-1} can be assigned to physisorbed MF, as observed on SiO_2 (Table 5.3, [27,29]), suggesting that MFZ is the precursor to physisorbed MF. The concentration of physisorbed MF was sufficiently large to form some gas-phase MF as evidenced by the presence of the Q branch observed at 1754 cm^{-1} and the R branch at 1768 cm^{-1} [26-27]. The P branch was obscured by the peaks for MFZ and physisorbed MF. The C–H deformation region of the spectrum taken at the end of the batch mode experiment showed several bands and intensities in common with those generated by adsorbing MF on FAU.

DMZ is proposed as an intermediate in the disproportionation of DMM. As noted Figure 5.5, it is thought that DMZ is formed by the reaction of MMZ with DMM and then to decompose to form MFZ. The structure proposed for DMZ was chosen to satisfy both the stoichiometry of the overall disproportionation reaction and the product of a hydrogen-transfer reaction (Reaction 4) between DMM and MMZ. The presence of DMZ may help account for some of the CH_3 deformation vibrations seen in DMM chemisorbed on FAU (e.g., Figure 5.1) as some of these bands coincide with vibrations of trimethyl orthoformate, which possesses a structure very similar to DMZ [37].

Figure 5.7 shows a series of spectra taken up exposure of DMM chemisorbed on FAU to pure CO flowing at 100 cm^3 min^{-1}. While little change occurred in the O–H and C–H stretching vibration regions, three new bands appeared in the C=O stretching region. The peak at 1734 cm^{-1} became a shoulder on a new peak that appeared at 1744 cm^{-1} together with two smaller peaks at 1765 and 1718 cm^{-1}. The largest of these new peaks, the one at 1744 cm^{-1}, is attributed to the C=O stretching vibration of MAZ. As shown in Figure 5.5, this species is formed by carbonylation of MMZ.

After flushing CO from the IR cell with He, the catalyst was again exposed to 0.01 atm DMM in He flowing at 100 cm^3 min^{-1}. The spectrum recorded at this point is shown in black in Figure 5.8. The feed to the IR cell was then switched to 0.01 atm DMM in CO flowing at 100 cm^3 min^{-1}. The resulting spectra are shown in Figure 5.8. The C=O stretching vibration of MAZ at 1744 cm^{-1} rapidly grew in intensity in the presence of both CO and DMM in the gas phase, and the maximum intensity reached was far greater than that attained in the presence of CO alone. Very little change was observed in the rest of the spectrum, consistent with the fact that both MMZ and MAZ possess the same ratio of CH_2 to CH_3 groups (see Reaction 2 in Figure 5.5).

Comparison of the spectra presented in Figure 5.7 and 5.8 shows that when CO alone was passed over FAU containing MMZ (Figure 5.7), the extent of CO insertion into the framework O–C bond of MMZ to form MAZ was far less than when the same surface was exposed to CO and DMM simultaneously (Figure 5.8). This is clearly evidenced by the changes in intensity of the peak at 1744 cm^{-1} in the two cases. The peak intensity in the presence of DMM was ~4.5 times greater than that reached without DMM,

suggesting that the presence of DMM enhances the rate of CO insertion. As discussed below, this is thought to be due to stabilization of the carbocationic transition state involved in the carbonylation of MMZ (Reaction 2 in Figure 5.5). To support this hypothesis, FAU was exposed to DMM and then flushed with He to generate MMZ species without physisorbed DMM, as in Figure 5.2. The zeolite was then exposed to CO as in Figure 5.8, generating a small peak for the C=O stretch of MAZ at 1744 cm^{-1}. The gas flow was then switched to 0.01 atm DME in CO. The C=O stretch of MAZ increased by a factor of ~4.5 when DME was present in the gas phase relative to when the gas phase was pure CO. Thus, both DME and DMM were found to increase the intensity of the C=O stretching band of MAZ by a similar factor of ~4.5 relative to what was observed in the absence of either gas. This effect is thought to be due to solvation of the carbocationic transition state involved in Reaction 2 by nucleophilic oxygen atoms in DMM and DME, in a manner similar to what is known to occur in liquid-phase systems [38-40].

The effect of CO pressure on the carbonylation of MMZ to form MAZ is shown in Figure 5.9. Increasing the CO pressure from 0 to 3 atm had almost no effect on the C–H stretching and deformation regions of the spectra, but increased the intensity of the C=O stretching frequency of MAZ at 1744 cm^{-1}. The intensities of the C–H vibrations should not change very much because both MMZ and MAZ contain CH_3OCH_2- groups, and hence would be expected to exhibit similar spectra in the C–H stretching and deformation regions [29]. Moreover, if the extent of conversion of MMZ to MAZ via CO insertion were small, any changes in the appearance of the spectrum in the C–H stretching regime would be difficult to detect. The apparent peaks appearing on either side of the band at 1744 cm^{-1} seen at higher pressures result from an interference pattern created by multiple reflections of the IR beam in the gaps between the CaF_2 windows contained in the IR cell.

The intensity of the C=O stretching vibration of MAZ, measured as the peak height normalized by the pellet weight, can be compared to the rate of MMAc formation at steady state. Figure 5.10 shows that both increased nearly linearly with CO pressure from 0 atm up to 3 atm. Since peak intensities of absorbance spectra follow the Beer-Lambert law, the intensity of the C=O stretching vibration of MAZ is directly proportional to the concentration of MAZ on the surface of FAU. Because both the IR peak intensities and steady state MMAc synthesis rates showed the same linear dependence on the CO pressure, the rate of MMAc formation must therefore be proportional to the concentration of MAZ, as suggested by Reaction 3 in Figure 5.5.

5.3.4 DMM carbonylation and disproportionation over MFI

The spectrum of H-MFI (Si/Al ≈ 27.5) is shown in Figure 5.11 (black). The large peak at 3610 cm^{-1} is assigned to the Brønsted acid site of MFI, and the smaller peaks at 3743 and 3722 cm^{-1} are assigned to external and internal silanol groups, respectively [30]. Because MFI can be synthesized directly in high Si/Al ratios, the number of SiOH defect sites is small compared to that in FAU. A shoulder around 3660 cm^{-1} is likely assigned to extra-framework alumina (EFAL) species [30-31]. The small size of this peak indicates that EFAL species were present in small concentrations.

MFI was exposed to 0.01 atm DMM in He flowing at 100 cm^3 min^{-1}. The resulting spectrum is shown in Figure 5.11 (blue). The Brønsted acid peak disappeared upon interaction of DMM with the zeolite. No peak for physisorbed DMM was observed in the O–H stretching region, as compared to the broad peak at 3430 cm^{-1} observed on FAU because of the far smaller concentration of SiOH groups on which to adsorb. The C–H stretching and C–H deformation regions are very similar to those observed when FAU is contacted with DMM, indicating that the species formed in MFI are similar to those formed in FAU, either MMZ or DMM physisorbed on Brønsted-acid sites. By contrast, though, the deformations bands at 1457, 1436, 1381 cm^{-1} were more prominent for MFI than for FAU. These bands were tentatively assigned to surface intermediates associated with the disproportionation of DMM, and were prominent in the spectra recorded upon exposing FAU to MF as well (Table 5.3). The peak at 1734 cm^{-1} was much more intense than the same band assigned to MFZ on FAU, indicating a greater rate of DMM disproportionation over MFI compared to FAU [14].

Upon flushing the IR cell with He, physisorbed and vapor-phase species were removed, leaving behind only chemisorbed species (Figure 5.11, red). In contrast to FAU, the spectrum generated in this manner over MFI differed significantly from the spectrum of gaseous DMM and DMM physisorbed on SiO_2, indicating that a DMM-like molecule was either absent or did not constitute the majority species. The most significant change was in the C–H deformation region, where peaks at 1456, 1437, and 1381 cm^{-1}, and peak shoulders at 1409 cm^{-1}, 1400 cm^{-1}, and 1388 cm^{-1} were observed, while peaks at 1475, 1467, and 1450 cm^{-1}, characteristic of DMM-like molecules (Table 5.1) were absent. The observed C–H deformation vibrations were similar to the spectrum of MF chemisorbed on FAU (Table 5.3), suggesting that the adsorbed species were predominantly disproportionation products. However, the intensity of the C=O stretching mode of MFZ at 1734 cm^{-1} decreased rapidly, and did not persist as it did on FAU. Some of the C–H stretching vibration frequencies observed, 3009, 2970, 2949, 2854, and 2843 cm^{-1} were similar to bands found in the spectra of MF and DMM chemisorbed on FAU.

After flushing the IR cell with He as described above, a flow of 100 cm^3 min^{-1} CO was introduced. In contrast to what was observed for FAU, no evidence was seen for carbonylation. However exposing MFI to CO in this manner did have an irreversible effect on the DMM disproportionation activity. When the gas flow was switched to 100 cm^3 min^{-1} of 0.01 atm of DMM in He, a smaller peak at 1734 cm^{-1} for MFZ was formed compared to that observed before the introduction of CO. This poisoning of disproportionation activity by CO was also observed for MFI in steady-state kinetic experiments, but not for FAU [14], and introduction of CO had little lasting effect on the surface species on FAU as observed by FTIR spectroscopy.

The inhibition of DMM disproportionation over MFI was also observed under reaction conditions when the gas flow was switched from 100 cm^3 min^{-1} of 0.01 atm DMM in He (Figure 5.12 black) to 100 cm^3 min^{-1} of 0.01 atm DMM in CO (Figure 5.12 blue). The MFZ peak at 1734 cm^{-1} disappeared, and the C–H deformation region of the spectrum became similar to that generated under similar conditions on FAU. This indicates that the more species containing CH_3OCH_2- groups, such as MMZ and MAZ, and fewer species associated with disproportionation, such as MFZ, were adsorbed in MFI. At the same time, the C=O stretch of MAZ appeared at 1763 cm^{-1}. Increasing the CO pressure to 2 atm (Figure 5.12 green) and 3 atm (Figure 5.12 red) caused little change

in the rest of the spectrum aside from the increase in the intensity of the C=O stretching band of MAZ.

Figure 5.13 compares the steady state rate of MMAc formation with the intensity of the C=O stretching vibration at 1763 cm^{-1} for MAZ. As with FAU, the steady-state kinetic data and the IR peak intensities showed similar trends with increasing CO partial pressure. Unlike FAU, both increased with less than first order dependence on the CO pressure. Although the rate of MMAc synthesis was ~5x greater on FAU than on MFI, the intensity of the peak for C=O stretching vibrations of MAZ normalized by the catalyst pellet mass was ~10x larger for MFI than for FAU. This indicates that the concentration of MAZ species was higher for MFI than for FAU, and suggests that the rate of removal of MAZ to form MMAc is much higher on FAU than on MFI. This conclusion is supported by analysis of the energetics of DMM carbonylation [15].

The relative concentrations of MAZ observed by IR spectroscopy on FAU and MFI can be rationalized in terms of recent theoretical calculations carried out at the DFT/B3LYP/6-311++G(3df,3pd) level [15]. Figure 5.14 shows the potential energy profile as a function of reaction coordinate for FAU and MFI. The zero on the potential energy diagram is for MMZ and gas-phase CO. MMAc is formed in two steps – carbonylation of MMZ followed by a methoxylation of the resulting MAZ. The calculated barrier for MMZ carbonylation is 58 kJ/mol for MFI and 74 kJ/mol for FAU, whereas the calculated activation barrier for methoxylation of MAZ is 63 kJ/mol for MFI and 32 kJ/mol for FAU. The smaller activation barrier for methoxylation of MAZ on FAU relative to MFI means that MAZ would be expected to react with DMM more readily on FAU than MFI. Because of the larger methoxylation barrier over MFI, MAZ accumulates on this zeolite more than on FAU, leading to the expectation of a higher surface concentration of MAZ on MFI than FAU, consistent with what is observed (see Figures 5.10 and 5.13).

5.3.5 Derivation of the kinetic rate expression and the plug-flow reactor model

The kinetics of DMM disproportionation and carbonylation can be developed from the mechanism presented in Figure 5.5. Since Reaction 1 only occurs for a short time immediately after exposing the catalyst to DMM, it does not affect the steady-state kinetics. In the expressions below, r_i is the rate of formation of gaseous species i, k_j is the rate constant for reaction j, P_k is the partial pressure of gaseous species k, θ_l is the surface coverage of surface species l. By treating each of Reactions 2-6 as elementary, the rates of MMAc, DME, and MF formation can be expressed as:

$$r_{\mathrm{MMAc}} = k_3 P_{\mathrm{DMM}} \theta_{\mathrm{MAZ}} - k_{3'} P_{\mathrm{MMAc}} \theta_{\mathrm{MMZ}}$$
$$r_{\mathrm{DME}} = k_4 P_{\mathrm{DMM}} \theta_{\mathrm{MMZ}} + k_5 \theta_{\mathrm{DMZ}}$$
$$r_{\mathrm{MF}} = k_6 P_{\mathrm{DMM}} \theta_{\mathrm{MFZ}}$$

The rate of accumulation of each surface species (MMZ, MAZ, DMZ, and MFZ) can be written as:

$$\frac{d\theta_{\mathrm{MMZ}}}{dt} = -k_2 P_{\mathrm{CO}} \theta_{\mathrm{MMZ}} + k_{2'} \theta_{\mathrm{MAZ}} + k_3 P_{\mathrm{DMM}} \theta_{\mathrm{MAZ}} - k_{3'} P_{\mathrm{MMAc}} \theta_{\mathrm{MMZ}} - k_4 P_{\mathrm{DMM}} \theta_{\mathrm{MMZ}} + k_6 P_{\mathrm{DMM}} \theta_{\mathrm{MFZ}}$$

$$\frac{d\theta_{\mathrm{MAZ}}}{dt} = k_2 P_{\mathrm{CO}} \theta_{\mathrm{MMZ}} - k_{2'} \theta_{\mathrm{MAZ}} - k_3 P_{\mathrm{DMM}} \theta_{\mathrm{MAZ}} + k_{3'} P_{\mathrm{MMAc}} \theta_{\mathrm{MMZ}}$$

$$\frac{d\theta_{\mathrm{DMZ}}}{dt} = k_4 P_{\mathrm{DMM}} \theta_{\mathrm{MMZ}} - k_5 \theta_{\mathrm{DMZ}}$$

$$\frac{d\theta_{\mathrm{MFZ}}}{dt} = k_5 \theta_{\mathrm{DMZ}} - k_6 P_{\mathrm{DMM}} \theta_{\mathrm{MFZ}}$$

Applying the pseudo-steady-state hypothesis to each surface species and setting each of the above expressions to zero, results in the following expressions for the surface coverages, θ_l:

$$\theta_{\mathrm{MAZ}} = \frac{k_2 P_{\mathrm{CO}} + k_{3'} P_{\mathrm{MMAc}}}{k_{2'} + k_3 P_{\mathrm{DMM}}} \theta_{\mathrm{MMZ}}$$

$$\theta_{\mathrm{DMZ}} = \frac{k_4}{k_5} P_{\mathrm{DMM}} \theta_{\mathrm{MMZ}}$$

$$\theta_{\mathrm{MFZ}} = \frac{k_4}{k_6} \theta_{\mathrm{MMZ}}$$

By combining the above equations, the rates of formation of the products can be written as:

$$r_{\mathrm{MMAc}} = \frac{k_2 P_{\mathrm{CO}} k_3 P_{\mathrm{DMM}} - k_{2'} k_{3'} P_{\mathrm{MMAc}}}{k_{2'} + k_3 P_{\mathrm{DMM}}} \theta_{\mathrm{MMZ}} \qquad (1)$$

$$r_{\mathrm{DME}} = 2k_4 P_{\mathrm{DMM}} \theta_{\mathrm{MMZ}} = 2r_{\mathrm{MF}}$$

$$r_{\mathrm{DMM}} = -r_{\mathrm{MMAc}} - r_{\mathrm{DME}}$$

Applying a site balance to surface species MMZ, MAZ, DMZ, and MFZ gives the following expression for θ_{MMZ}:

$$\theta_{\mathrm{MMZ}} = \left(1 + \frac{k_2 P_{\mathrm{CO}} + k_{3'} P_{\mathrm{MMAc}}}{k_{2'} + k_3 P_{\mathrm{DMM}}} + \frac{k_4}{k_5} P_{\mathrm{DMM}} + \frac{k_4}{k_6} \right)^{-1} \qquad (2)$$

By treating the reactor as an isothermal, plug-flow reactor, the mole balance for any species can be written as a first-order differential equation in species pressure, P_{i}. Equation 3 assumes that the change in the total volumetric flow rate is small (due to the large excess of CO used):

$$\frac{dF_{\mathrm{i}}}{dW} = \frac{Q}{RT} \frac{dP_{\mathrm{i}}}{dW} = r_{\mathrm{i}} \text{ or } W = \frac{Q}{RT} \int_{P_{i0}}^{P_i} \frac{dP_{\mathrm{i}}}{r_{\mathrm{i}}} \qquad (3)$$

Here F_i is the molar flow rate of species i in the gas phase, W is the moles of active sites or Al atoms in the sample, Q is the total gas volumetric flow rate, R is the molar gas constant, T is the reaction temperature, and P_{i0} is the initial partial pressure of species i at the reactor inlet. Substituting for r_{DMM} and assuming that P_{CO} was constant (again due to large excess of CO used), the following expression is obtained:

$$W = -\frac{Q}{RT}\int_{P_{DMM\,0}}^{P_{DMM}} \frac{\left(k_{2'} + \frac{k_{2'}k_4}{k_6} + k_2 P_{CO}\right) + \left(k_3 + \frac{k_{2'}k_4}{k_5} + \frac{k_3 k_4}{k_6}\right)P_{DMM} + \frac{k_3 k_4}{k_5} P_{DMM}^{\ 2} + k_{3'} P_{MMAc}}{(k_2 k_3 P_{CO} + 2k_{2'}k_4)P_{DMM} + 2k_3 k_4 P_{DMM}^{\ 2} - k_{2'}k_{3'}P_{MMAc}} dP_{DMM} \quad (4)$$

Assuming that $k_{3'}P_{MMAc}$ was small and eliminating this product from Equation 4, the analytical solution is:

$$W = -\frac{Q}{RT}\left[\begin{array}{l} \frac{1}{2k_5}\left(P_{DMM} - P_{DMM,0}\right) + \frac{k_{2'} + \frac{k_{2'}k_4}{k_6} + k_2 P_{CO}}{k_2 k_3 P_{CO} + 2k_{2'}k_4} \ln\frac{P_{DMM}}{P_{DMM,0}} + \\ \frac{\left(\frac{k_2 k_3 P_{CO}}{2k_4} + \frac{k_2 k_3 P_{CO}}{2k_6} - \frac{k_2^{\ 2} k_3 P_{CO}^{\ 2}}{4k_4 k_5}\right)}{\left(k_2 k_3 P_{CO} + 2k_{2'}k_4\right)} \ln\frac{\left(k_2 k_3 P_{CO} + 2k_{2'}k_4 + 2k_3 k_4 P_{DMM}\right)}{\left(k_2 k_3 P_{CO} + 2k_{2'}k_4 + 2k_3 k_4 P_{DMM,0}\right)} \end{array}\right] \quad (5)$$

from which P_{DMM} at the reactor exit can be solved for iteratively. By substituting Equations 1 and 2 into Equation 3, P_{MMAc} and P_{DME} can be determined from:

$$\int_0^{P_{MMAc}} dP_{MMAc} = -\int_{P_{DMM0}}^{P_{DMM}} \frac{k_2 P_{CO} k_3}{k_2 P_{CO} k_3 + 2k_{2'}k_4 + 2k_3 k_4 P_{DMM}} dP_{DMM}$$

$$P_{MMAc} = -\frac{k_2 P_{CO}}{2k_4} \ln\frac{\left(k_2 P_{CO} k_3 + 2k_{2'}k_4 + 2k_3 k_4 P_{DMM}\right)}{\left(k_2 P_{CO} k_3 + 2k_{2'}k_4 + 2k_3 k_4 P_{DMM,0}\right)} \quad (6)$$

and $P_{DME} = P_{DMM,0} - P_{DMM} - P_{MMAc}$ (7)

5.3.6 Determination of kinetic rate parameters and reactor model results

To evaluate the effectiveness of Equations 5-7 for describing the kinetics of MMAc, DME, and MF requires estimates for the values of the pre-exponential factor (A) and activation energy (E_a) for each of the rate coefficients appearing in these equations. All pre-exponential factors were constrained to lie within the range of values expected for unimolecular and bimolecular reactions involving a gas-phase reactant and an adsorbed reactant [41-42]. Estimates for E_a for Reactions 2, 2', and 3 were obtained by adjusting the values obtained from DFT calculations [15] (see Figure 5.14) in order to obtain a good fit to the experimental data for FAU (see Figures 5.15a-c below). The values of E_a and A for Reactions 3 and 6 were set equal to each other because of the similarity of the

methoxylation reactions. The values of E_a for Reactions 4 and 5 were chosen to be reasonable. Since Reactions 4-6 are irreversible, the fit of theory to experiment was much more sensitive to the value of activation energy chosen for Reaction 4 than Reaction 5.

The value of W in Equation 5 was taken to be one half of that used experimentally, to account for the observation that only half of the Brønsted acid protons react upon exposure to DMM (see Figures 5.4 and 5.7). The acid sites that did not react with DMM are assumed to be catalytically inactive.

Figure 5.15 compares the results of the plug-flow reactor model with the steady state rates of product formation reported previously as functions of reaction temperature (Figure 15a), feed CO partial pressure (Figure 5.15b), and feed DMM partial pressure (Figure 5.15c) [14]. It is evident that the experimentally observed trends in the carbonylation and disproportionation rates for FAU are well described by Equations 5-7 together with rate parameters listed in Table 5.5. In particular, the model correctly reproduces the maximum in the rate of MMAc formation and predicts the dependence of the MMAc formation rate on the feed partial pressure of CO and DMM. The model also predicts the correct dependences of the rates of DME and MF formation as functions of temperature and feed CO and DMM partial pressures.

The following experiment was carried out in order to assess the validity of the choice of rate parameters listed in Table 5.5. FAU was exposed to 100 cm^3 min^{-1} of 0.01 atm DMM in He. The gas flow was then switched to 100 cm^3 min^{-1} of 0.01 atm DMM in CO and spectra were recorded every 45 s. The peak height of the C=O stretching vibration of MAZ at 1744 cm^{-1} reached a steady-state value after 1800 s. The gas flow was then switched back to 100 cm^3 min^{-1} of 0.01 atm DMM in He, and spectra were recorded every 45 s. The resulting normalized peak height of the C=O stretching vibration for MAZ is plotted as a function of time in Figure 5.16.

The concentration of MAZ on the surface is proportional to the absorbance of the C=O stretching vibration observed. The initial rates of change of the C=O stretching peak following a change in the gas phase composition are therefore directly proportional to the rate of change of the surface concentration of MAZ, $\frac{d\theta_{\mathrm{MAZ}}}{dt}$. The proportionality constant includes the unknown extinction coefficient for the C=O stretching vibration of MAZ, preventing quantitation of the surface coverage directly from the FTIR data. From the proposed mechanism,

$$\frac{d\theta_{\mathrm{MAZ}}}{dt} = k_2 P_{\mathrm{CO}} \theta_{\mathrm{MMZ}} - k_{2'} \theta_{\mathrm{MAZ}} - k_3 P_{\mathrm{DMM}} \theta_{\mathrm{MAZ}} + k_{3'} P_{\mathrm{MMAc}} \theta_{\mathrm{MMZ}} . \qquad (8)$$

The term $k_{3'} P_{\mathrm{MMAc}}$ Equation 8 is small relative to the other terms in the sum and eliminated. At t = 0 when the gas was initially switched from DMM/He to DMM/CO, the surface coverage of MAZ was zero, so the rate of change of the surface coverage of MAZ can be approximated by $\frac{d\theta_{\mathrm{MAZ}}}{dt} = k_2 P_{\mathrm{CO}} \theta_{\mathrm{MMZ}}$. The initial slope at t = 0 was measured from Figure 5.16 as 1.02 x 10^{-3} absorbance units g^{-1} s^{-1}. When the gas flow was switched from DMM/CO back to DMM/He at t = 6498 s, the slope of the peak

height of the C=O stretch as a function of time was measured as -9.91 x 10^{-4} absorbance units g^{-1} s^{-1}. This slope was once again proportional to $\frac{d\theta_{MAZ}}{dt}$. However, this time with no CO in the gas phase and a non-zero MAZ coverage, $\frac{d\theta_{MAZ}}{dt} = -(k_{2'} + k_3 P_{DMM})\theta_{MAZ}$. By taking the ratio of the slopes at t = 0 s and t = 6498 s obtained from the FTIR measurements, the proportionality constant including the extinction coefficient is eliminated, leading to the expression:

$$\frac{\left.\frac{d\theta_{MAZ}}{dt}\right|_{t=0s}}{\left.\frac{d\theta_{MAZ}}{dt}\right|_{t=6498s}} = -\frac{k_2 P_{CO}\theta_{MMZ}|_{t=0s}}{(k_{2'} + k_3 P_{DMM})\theta_{MAZ}|_{t=6498s}}. \quad (9)$$

The value of the left hand side of Equation 9 determined from the experimentally measured slopes is -1.03. The value of the right-hand side of this equation was determined using the plug-flow reactor model to evaluate the average values of θ_{MMZ}, θ_{MAZ}, and P_{DMM}. Using these average values together with the rate constants in Table 5.5, the value of the right-hand side of Equation 9 is -0.97, which is in excellent agreement with the experimentally determined value of -1.03. The agreement between experimental kinetic measurements and the plug-flow reactor model indicates that the parameters chosen are reasonable.

A question then remains concerning the differences between the activation energies for Reactions 2, 2', and 3 determined theoretically (see Figure 14 and Ref. [15]) and those determined by fitting the observed rates of product formation on FAU as a function of temperature. The values of E_a determined for Reactions 2, 2', and 3 by DFT calculations are 74, 92, and 32 kJ/mol, respectively, whereas the corresponding values reported in Table 5 obtained from the fit of the rate data shown in Figure 15a are 58, 108, and 17 kJ/mol, respectively. A part of the difference between theory and experiment could be due to the neglect of dispersion forces in the theoretical calculations. Recent investigations of reactions occurring in zeolites have shown that when such forces are taken into account, the activation barriers for elementary processes can altered by as much as ±10-30 kJ/mol [43-47]. Nevertheless, both sets of activation energies suggest that the formation of MMAc is rate-limited by the carbonylation of MMZ.

5.4 Conclusions

In situ IR spectra taken during the exposure of FAU and MFI to DMM or DMM and CO show evidence for methoxymethoxy (MMZ), formate (MFZ) and methoxyacetyl (MAZ) groups, species that are proposed as intermediates in the carbonylation and disproportionation of DMM. The response of these species to changes in gas composition is consistent with that anticipated on the bases of steady-state rate data. For example, the intensity of the carbonyl stretch for MAZ, the precursor to MMAc, and the rate of MMAc formation increase in parallel with increasing CO partial pressure for both

FAU and MFI. Likewise, the intensity of the MAZ peak observed for MFI is considerably greater than that for FAU, consistent with the lower activity of MFI for MMAc formation. This suggests that the rate of methoxylation of MAZ on MFI is slower than on FAU, consistent with the results of recent DFT calculations. IR observations also reveal that the rate of DMM carbonylation on both FAU and MFI is more rapid in the presence of physisorbed DMM or DME. This effect is attributable to the enhanced stabilization of the carbocationic transition state due to solvation by the physisorbed species. It is also found that the concentration of MFZ, the final precursor to MF, decreases with increasing CO partial pressure for MFI but not for FAU, consistent with the observed effects of CO partial pressure on the rates of DMM disproportionation on both zeolites. Rate expressions for the formation of all reaction products, derived on the basis of the proposed mechanism of DMM carbonylation and disproportionation, give an accurate description of the dependences of the experimentally observed rates on temperature and the feed partial pressures of CO and DMM.

Table 5.1 Comparison of vibrational frequencies in DMM and DMM-like species at 383 K (cm^{-1}).

DMM vapor	DMM/SiO_2 flowing 0.01 atm DMM in He	DMM/FAU flowing 0.01 atm DMM in He	DMM/FAU flowing He	Band assignments [a]
3004 m	3006 m	3005* w	3003* w	a-ν CH_3
		2995* m	2995* w	a-ν CH_3
			2982* w	
2942 m	2960* m	2955* m	2962 s	a-ν CH_2, ν CH_3, 2δ CH_3
2936 s	2946 s	2946 s	2946* w	s-ν CH_3, a-ν CH_2, 2δ CH_3
2901* m	2898 m	2910 s	2912 s	s-ν CH_2
2853 w	2850* w	2855* w	2858 s	unassigned
2838 m	2838 m	2836 s	2839 m	s-ν CH_3
		2802 w	2802 m	
2774 w	2782 w	2780 w		unassigned
1755				
		1734	1734	
		1490* w	1490 m	
1472 w	1477 w	1475* w	1475* w	δ CH_2 scissoring
1467* w	1467 w	1467 m	1467* w	s-δ CH_3
			1458 s	
1456 s	1453 s	1450 s	1450 m	a-δ CH_3
		1435 w	1435* w	
			1417 m	
1398 s	1403 s	1400 s	1400 m	δ CH_2 wagging
		1385* w	1385* w	

ν stretching vibration, δ deformation vibration, s symmetric, a asymmetric

* Frequency estimated from a peak shoulder

s strong, m moderate, w weak relative to bands within same region of spectrum

[a] Band assignments based on DMM vapor [19]

Table 5.2 Comparison of vibrational frequencies in DME and DME-like species at 383 K (cm^{-1}).

DME vapor	DME/SiO_2 flowing 0.01 atm DME in He	DME/FAU flowing 0.01 atm DME in He	DME/FAU flowing He	Band assignments
2997 m	2999 m	2998* w	3002* w	a-ν CH_3 [a b]
2937* w	2941 s	2947 s	2967 s	a-ν CH_3 [a b]
	2898 w	2907* w	2914 w	a-ν CH_3 [b]
2878* w	2879 w	2877* w		combination [b]
		2856* w	2858 m	s-ν CH_3 [b]
2815 s	2831 s	2833 m	2843 w	s-ν CH_3 [a b]
		2804* w	2806 w	
1462 w	1476 w			δ CH_3 [a b]
1453 s	1459 s	1459 s		δ CH_3 [a b]
		1448 w	1448 s	
		1417 w	1416 w	
			1390 m	
		1384 w	1384 m	

[a] Band assignments based on DME vapor [24]
[b] Band assignments based DME adsorbed on MFI [25]

Table 5.3 Comparison of vibrational frequencies in MF and MF-like species at 383 K (cm^{-1}).

MF vapor	MF/SiO_2 flowing 0.01 atm MF in He	MF/FAU flowing 0.01 atm MF in He	MF/FAU flowing He	Band assignments
3041 m	3043 m	3045* w		a-ν CH_3 [a b]
3007 m	3011 m	3020* w	3010* w	a-ν CH_3 [a b]
		2980* w	2980 m	
2965 s	2963 s	2965 s	2960 s	s-ν CH_3 [a b]
2939 s	2949 m	2945* w	2945* w	s-ν CH [a b]
	2900* w	2895* w		unassigned [b]
2847 w	2862 m	2856 m	2857 s	unassigned [b]
	2790* w			
1754 s				ν C=O [a]
		1734* w	1734 m	ν C=O [c]
	1722 s	1722* s		ν C=O [b]
1464 m	1465* w		1472* w	a-δ CH_3 [a]
1452 s	1453 s	1456 m	1459 m	a-δ CH_3 [a b]
1437 m	1437 s	1436 s	1438 m	s-δ CH_3 [a b]
		1416 w	1415 w	
	1406 w	1406 w	1406 m	
		1395 w	1396 m	
		1390 w	1390 w	
1371 w	1380 m	1379 m	1382 w	δ CH [a b]

[a] Band assignments based on MF vapor [26]
[b] Band assignments based on MF physisorbed on SiO_2 [27]
[c] Band assignment for surface formates from this work

Table 5.4 Vibrational frequencies in liquid MMAc [28] (cm^{-1}).

MMAc liquid	Band assignments [a]
2996 m	a-ν CH_3
2956 s	a-ν CH_2
2932* w	s-ν CH_3
2904* m	s-ν CH_2
2831 m	s-ν CH_3
1761 s	ν C=O
1742* w	
1468* w	s-δ CH_3
1442 s	a-δ CH_3
1381 m	δ CH_2 wagging

[a] Band assignments based on assignments for similar groups in DMM [19]

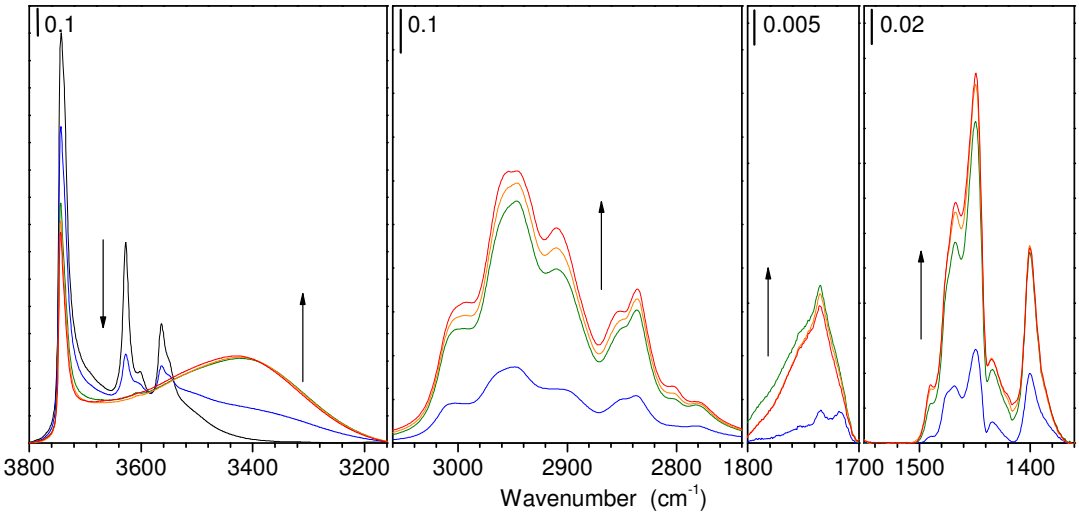

Figure 5.1 IR spectra recorded during transient-response experiments of H-FAU exposed to 0.01 atm DMM. Black: 0 s, blue 45 s, green 90 s, orange 271 s, red 996 s. 0.0479 g catalyst, 383 K, 100 cm^3 min^{-1} at 1 atm.

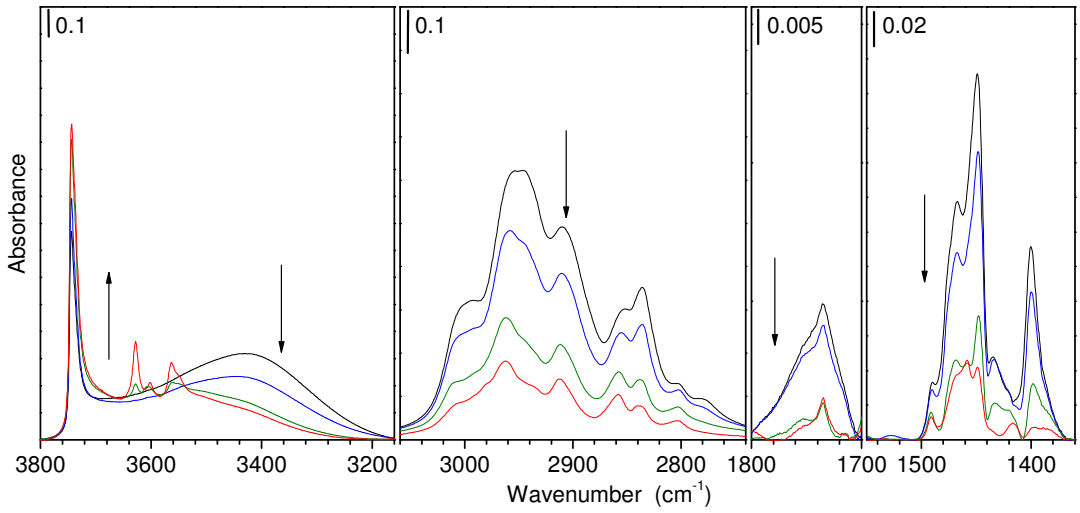

Figure 5.2 IR spectra recorded during transient-response experiments of FAU under He flow following exposure to 0.01 atm DMM/He. Black 0 s, blue 46 s, green 765 s, red 4508 s. 0.0479 g catalyst, 383 K, 100 cm^3 min^{-1} at 1 atm.

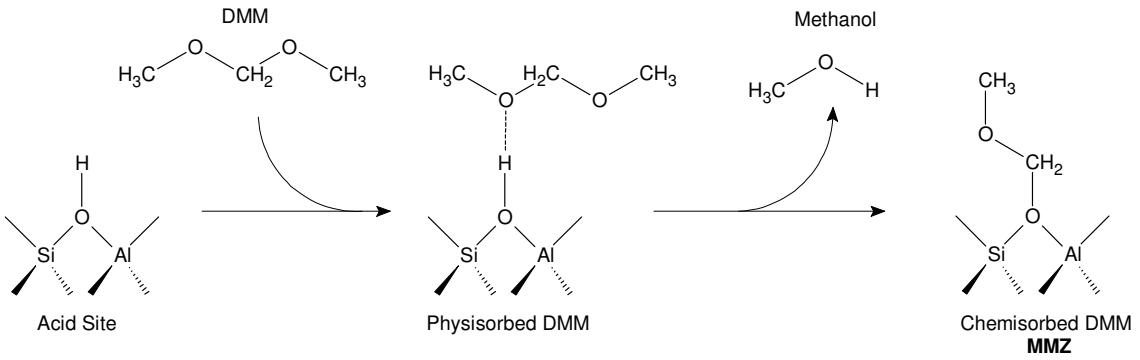

Figure 5.3 Physical and chemical modes of DMM adsorption at Brønsted acid site of a zeolite.

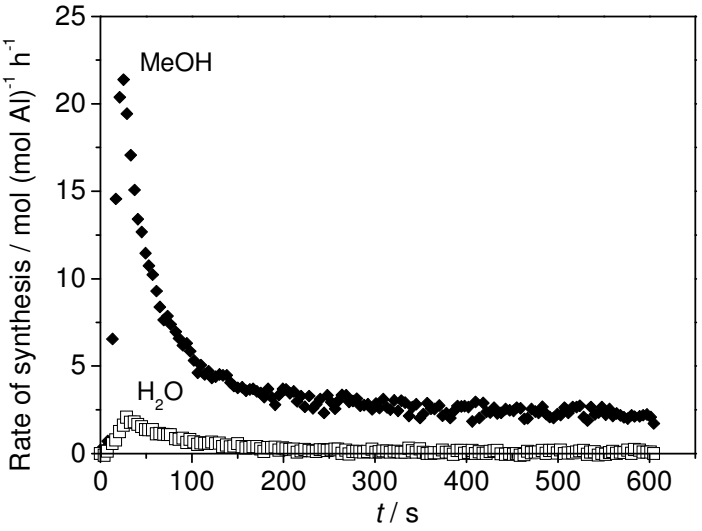

Figure 5.4 Rates of methanol and H_2O synthesis over H-FAU at very short times after initial exposure to 0.017 atm DMM/He. 0.03 g catalyst, 383 K, 100 cm^3 min^{-1} at 1 atm.

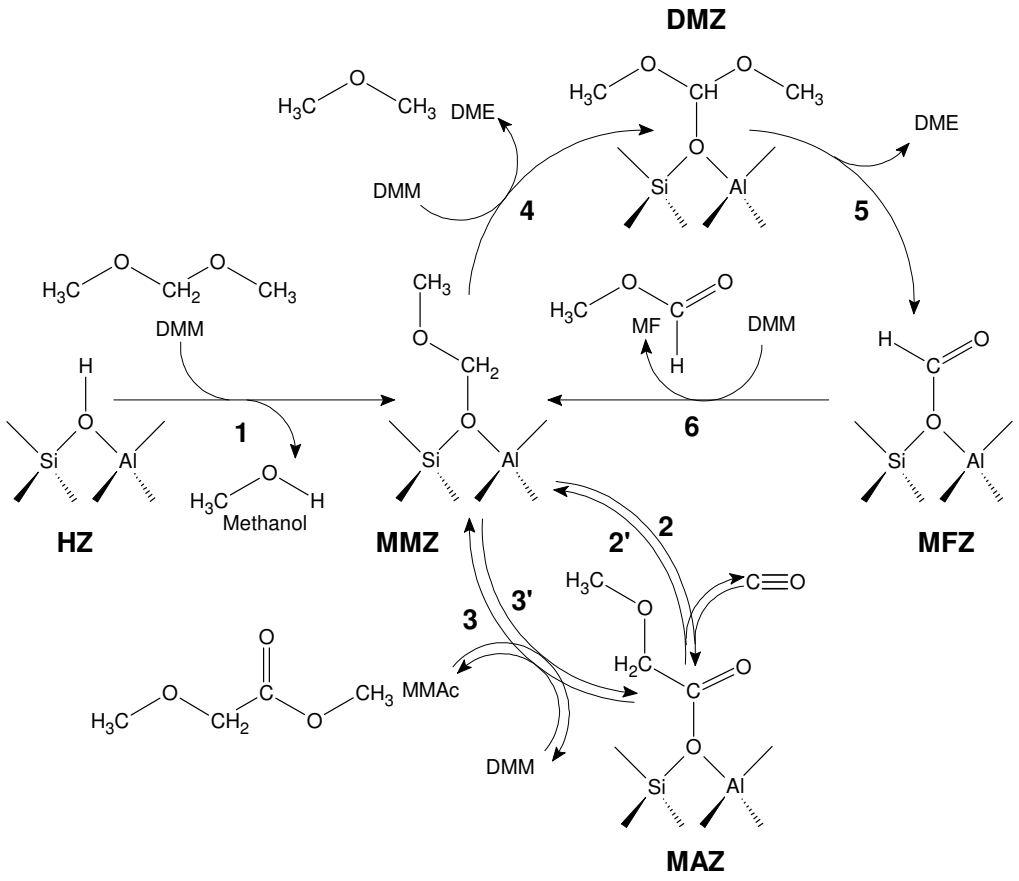

Figure 5.5 Proposed reaction mechanism for DMM adsorption (1), DMM carbonylation (2-3), and DMM disproportionation (4-6).

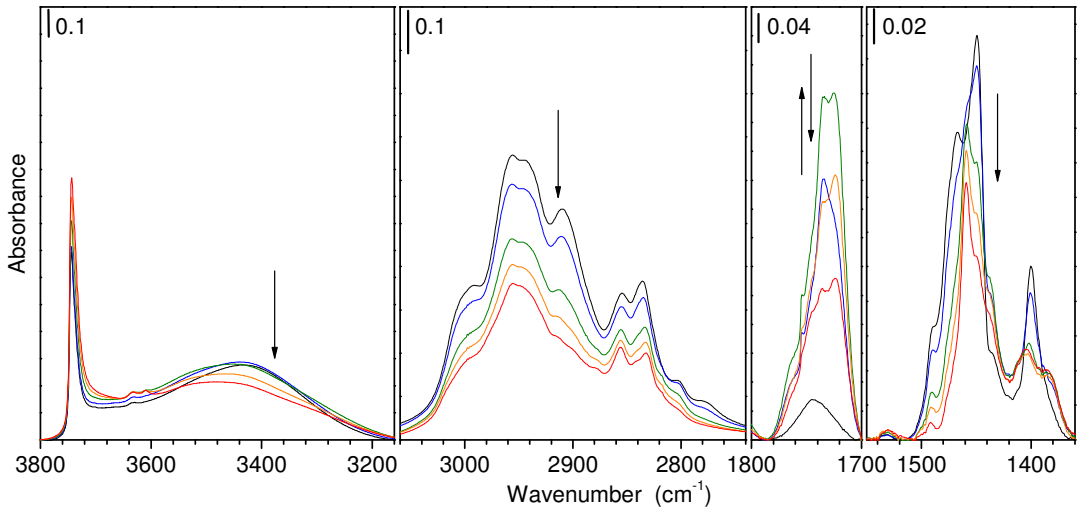

Figure 5.6 IR spectra recorded during transient-response experiments of FAU under a stagnant atmosphere initially composed of 0.01 atm DMM/ He. Black 0 s, blue 857 s, green 5188 s, orange 11181 s, red 21968 s. 0.0479 g catalyst, 383 K, initially at 1 atm.

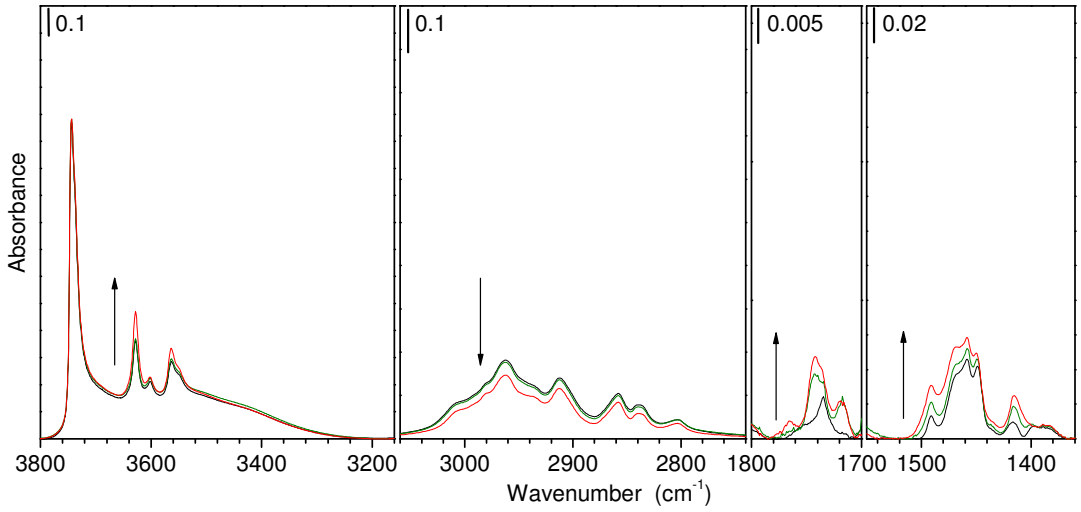

Figure 5.7 IR spectra recorded during transient-response experiments of FAU under 1 atm CO following He flush after exposure to 0.01 atm DMM/He. Black 0 s, blue 271 s, green 1398 s, red 5476 s. 0.0479 g catalyst, 383 K, 100 cm^3 min^{-1} at 1 atm.

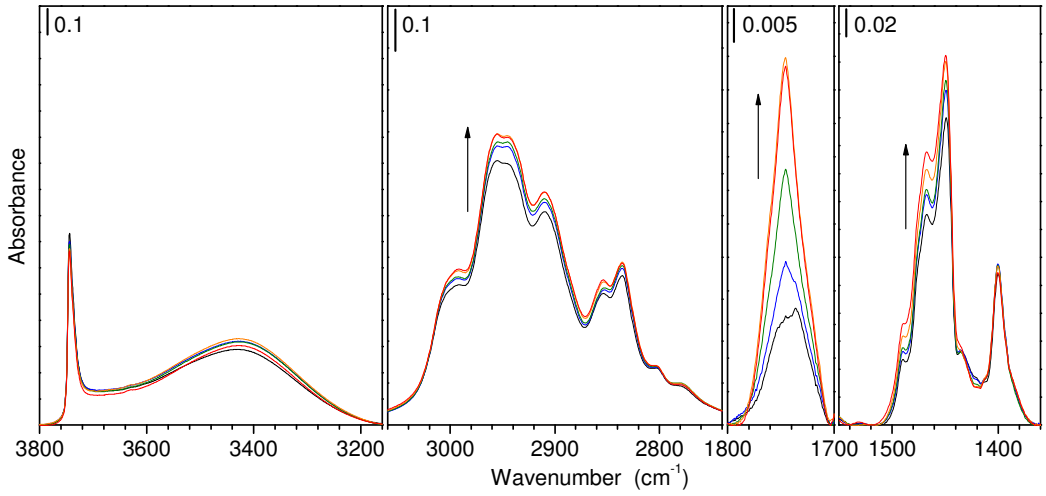

Figure 5.8 IR spectra recorded during transient-response experiments of FAU under 0.01 atm DMM/CO following exposure to 0.01 atm DMM/He. Black 0 s, blue 182 s, green 547 s, orange 4463 s, red 7764 s. 0.0479 g catalyst, 383 K, 100 cm^3 min^{-1} at 1 atm.

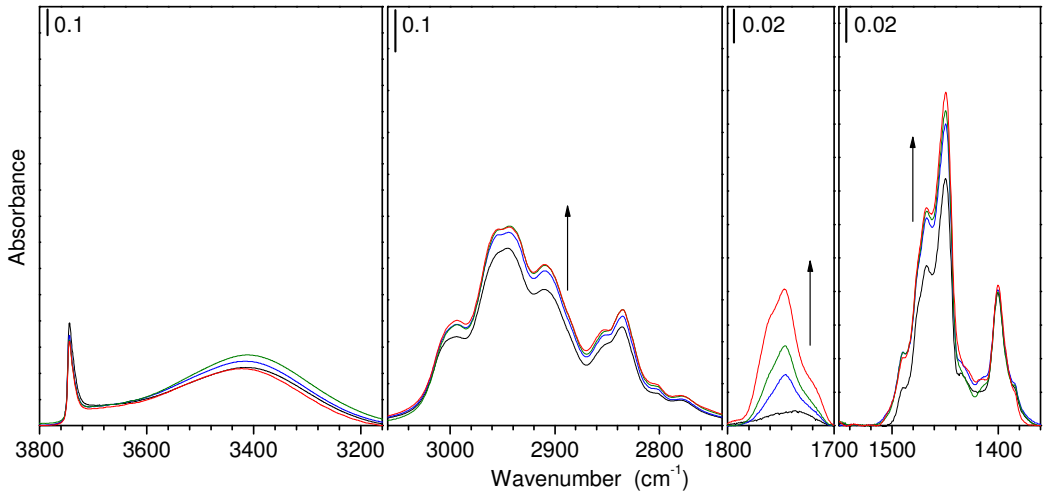

Figure 5.9 Spectra of FAU under 0.01 atm of DMM and different CO partial pressures. Black P_{CO} = 0 atm (balance He), blue P_{CO} = 1.0 atm, green P_{CO} = 2.0 atm, P_{CO} = 3.0 atm. 0.0272 g catalyst, 383 K, 100 cm^3 min^{-1} at reaction pressure, 100-300 cm^3 min^{-1} at STP.

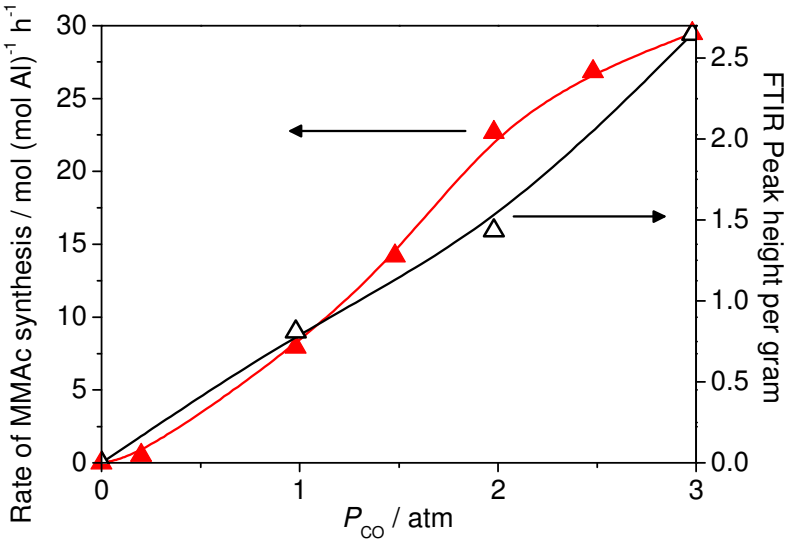

Figure 5.10 Comparison of the effect of CO partial pressure on steady-state MMAc formation rate over FAU (left axis) and normalized peak height of peak at 1744 cm^{-1} (right axis). Steady state data, 0.05 g catalyst, 383 K, P_{DMM} = 0.013-0.019 atm, 100 cm^3 min^{-1} at reaction pressure, 100-300 cm^3 min^{-1} at STP. FTIR peak height, 0.0272 g catalyst, 383 K, P_{DMM} = 0.01 atm, 100 cm^3 min^{-1} at reaction pressure, 100-300 cm^3 min^{-1} at STP.

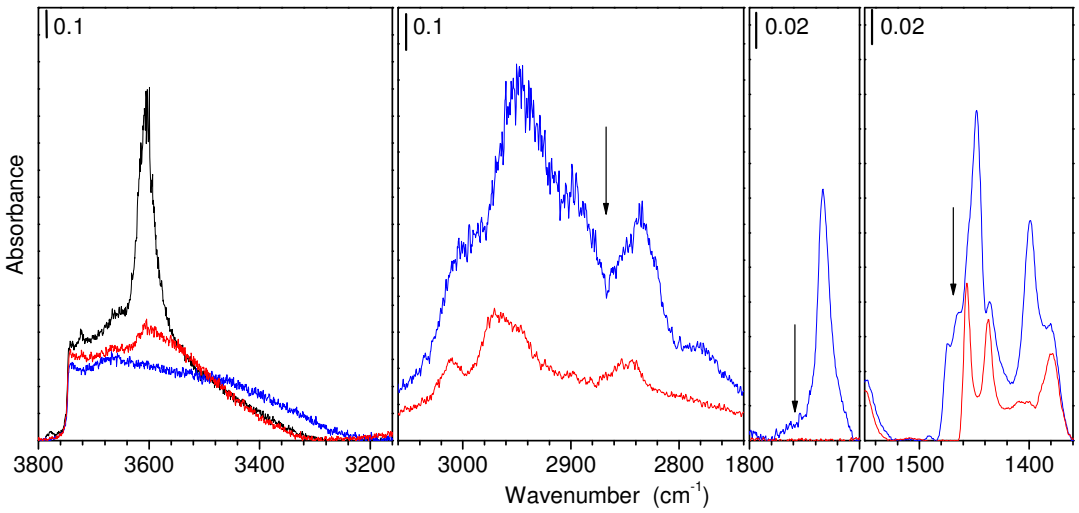

Figure 5.11 Spectra of H-MFI under He (black), after 990 s of exposure to 0.01 atm DMM/He (blue), and under He flow for 3214 s after exposure to DMM/He (red). 0.0510 g catalyst, 383 K, 100 cm^3 min^{-1} at 1 atm.

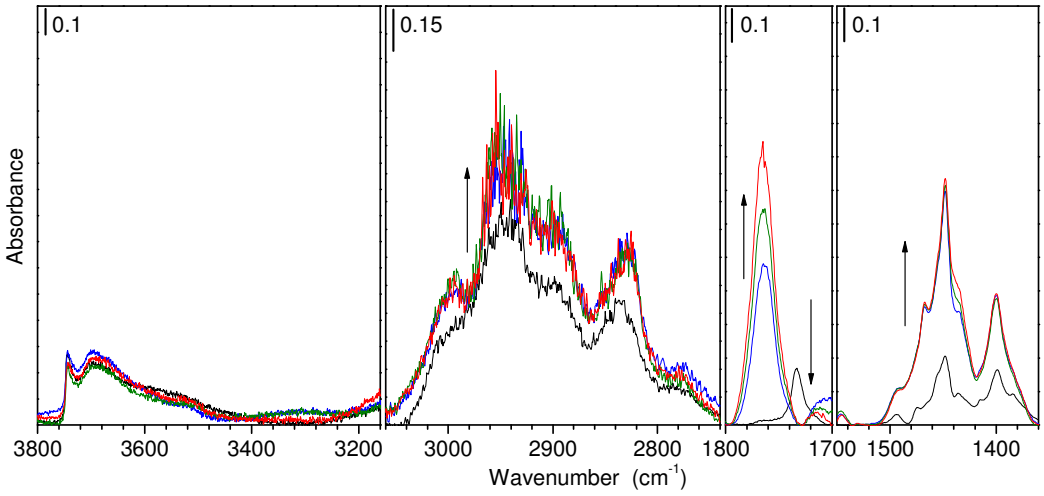

Figure 5.12 Spectra of MFI under 0.01 atm of DMM and different CO partial pressures. Black P_{CO} = 0 atm (balance He), blue P_{CO} = 1.0 atm, green P_{CO} = 2.0 atm, P_{CO} = 3.0 atm. 0.0442 g catalyst, 383 K, 100 cm^3 min^{-1} at reaction pressure, 100-300 cm^3 min^{-1} at STP.

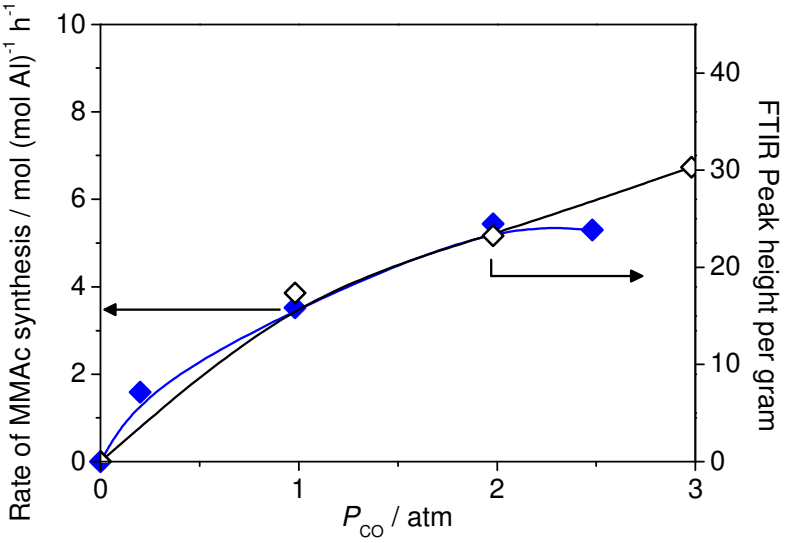

Figure 5.13 Comparison of the effect of CO partial pressure on steady-state MMAc formation rate over MFI (left axis) and normalized peak height of peak at 1763 cm^{-1} (right axis). Steady state data, 0.05 g catalyst, 383 K, P_{DMM} = 0.013-0.019 atm, 100 cm^3 min^{-1} at reaction pressure, 100-300 cm^3 min^{-1} at STP. FTIR peak height, 0.0442 g catalyst, 383 K, P_{DMM} = 0.01 atm, 100 cm^3 min^{-1} at reaction pressure, 100-300 cm^3 min^{-1} at STP.

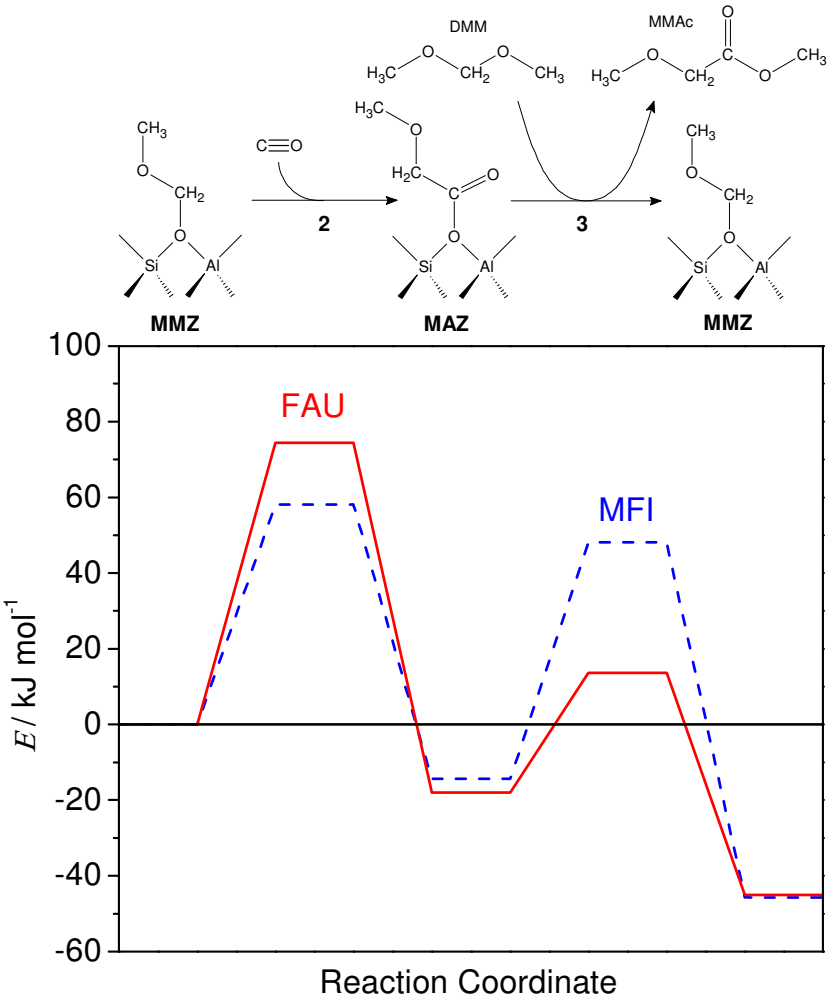

Figure 5.14 Theoretically projected energy profile for MMAc formation calculated at the B3LYP/6-311++G(3df,3pd) level of theory with zero-point energy calculated at the B3LYP/6-31G* level of theory [15]. Calculations performed on 36 T atom cluster for FAU and 44 T atom cluster.

Table 5.5 Activation energies E_a and pre-exponential factors A for FAU (Si/Al ratio ≈ 30) used in plug-flow reactor model.

Reaction	A [a]	E_a **kJ mol^{-1}**	k [a]	$[A]=[k]$
2	1.6 x 10^{6}	58	2.0 x 10^{-2}	atm^{-1} s^{-1} mol Al^{-1}
2'	1.0 x 10^{17}	108	2.0 x 10^{2}	s^{-1} mol Al^{-1}
3	3.1 x 10^{6}	17	1.5 x 10^{4}	atm^{-1} s^{-1} mol Al^{-1}
3' [b]	-	-	-	
4	3.7 x 10^{2}	22	3.7 x 10^{-1}	atm^{-1} s^{-1} mol Al^{-1}
5	8.0 x 10^{12}	112	4.3 x 10^{-3}	s^{-1} mol Al^{-1}
6	3.1 x 10^{6}	17	1.5 x 10^{4}	atm^{-1} s^{-1} mol Al^{-1}

[a] $k = Ae^{-E_a/RT}$, evaluated at 383 K

[b] All terms containing $k_{3'}$ were eliminated from Equation 5, so no values were used in the model

a)

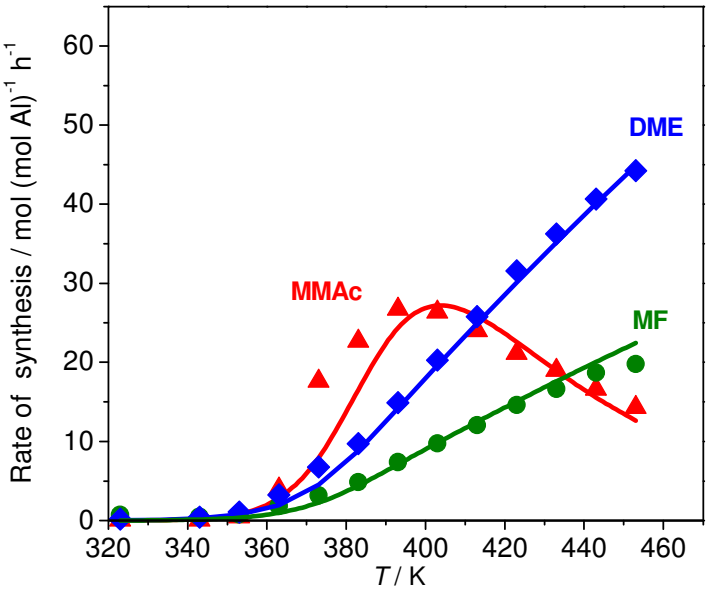
Rate of synthesis / mol (mol Al)$^{-1}$ h^{-1}
60
50
40
30
20
10
0
320
340
360
380
400
420
440
460
T / K
DME
MMAc
MF

b)

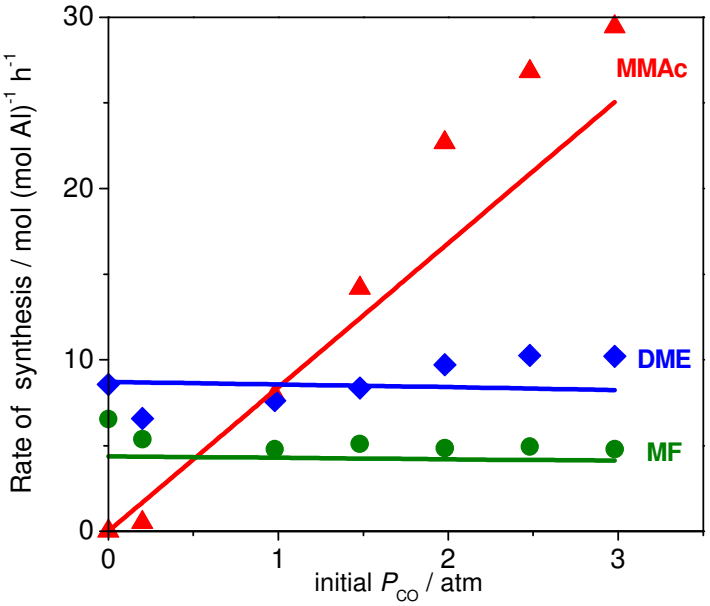
Rate of synthesis / mol (mol Al)$^{-1}$ h^{-1}
30
20
10
0
0
1
2
3
initial P_{CO} / atm
MMAc
DME
MF

c)

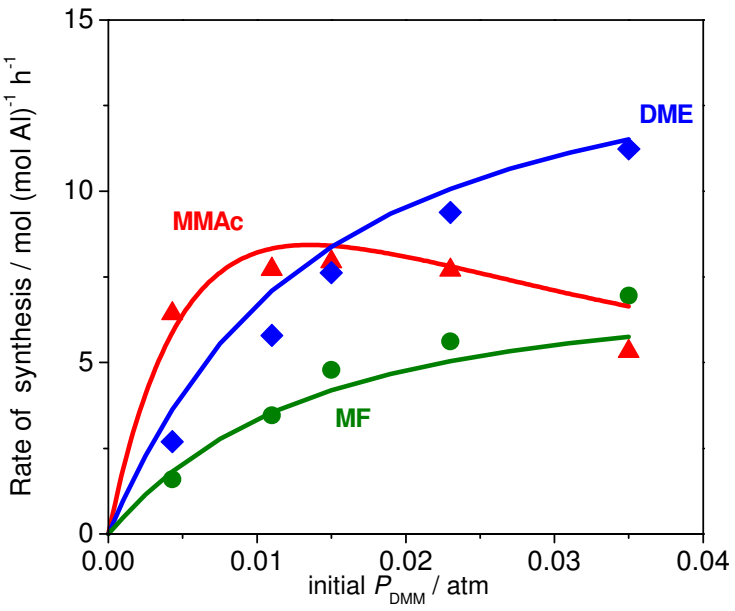

Figure 5.15 Comparison of steady state reaction rate data (symbols) and plug-flow reactor model results (curves) of MMAc, DME, and MF formation rates as a function of a) reaction temperature, b) inlet CO partial pressure, and c) inlet DMM partial pressure. a) Steady state data, 0.05 g catalyst, P_{CO} = 1.98 atm, P_{DMM} = 0.017 atm, 100 cm^3 min^{-1} at reaction pressure, 200 cm^3 min^{-1} at STP. Plug-flow reactor model, 0.05 g catalyst, P_{CO} = 1.98 atm, initial P_{DMM} = 0.017 atm, 100 cm^3 min^{-1} at reaction pressure. b) Steady state data, 0.05 g catalyst, 383 K, P_{DMM} = 0.013-0.019 atm, 100 cm^3 min^{-1} at reaction pressure, 100-300 cm^3 min^{-1} at STP. Plug-flow reactor model, 0.05 g catalyst, initial P_{DMM} = 0.016 atm, 100 cm^3 min^{-1} at reaction pressure.

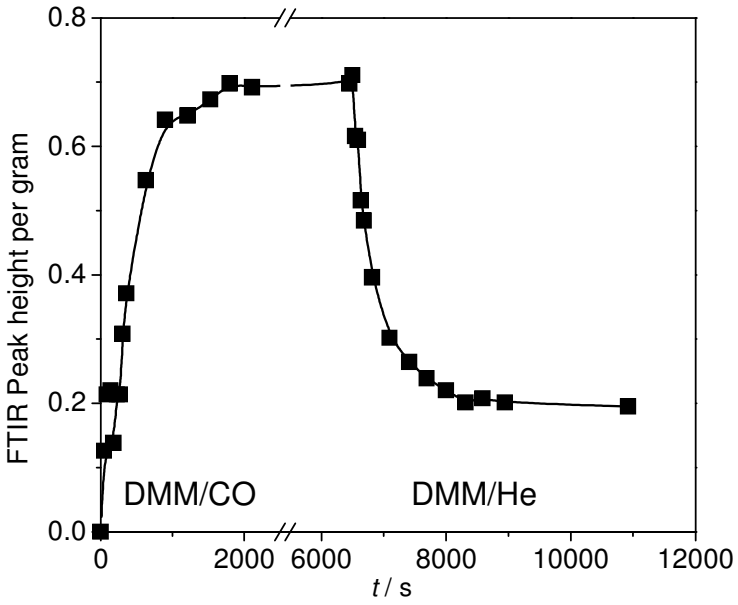

Figure 5.16 Growth of MAZ peak as a function of time after switching to DMM/CO flow over FAU saturated with DMM and decline of MAZ peak after switching back to DMM/He. 0.0159 g catalyst, 383 K, 100 cm^3 min^{-1} at 1 atm.

References

[1] J.M. Berty, Ethylene Oxide Synthesis, in: B.L. Leach (Ed.), Applied Industrial Catalysis Vol. 1, Academic Press, New York, 1983, 207.
[2] R.L. Pruett, W.E. Walker, U.S. Patent 3 957 857 (1976), to Union Carbide Corporation.
[3] D.R. Fahey, J. Am. Chem. Soc. 103 (1981) 136.
[4] K. Ivanov, Appl. Catal., A 116 (1994) L1.
[5] J.M. Tatibouet, Appl. Catal., A 148 (1997) 213.
[6] D.J. Loder, US Patent 2 152 852 (1939), to E. I. du Pont de Nemours & Co.
[7] D.E. Hendriksen, Prepr. Pap.—Am. Chem. Soc., Div. Fuel Chem. 28 (1983) 176.
[8] H.J. Schmidt, H.J. Arpe, US Patent 4 501 917 (1985), to Hoechst AG.
[9] S.Y. Lee, J.C. Kim, J.S. Lee, Y.G. Kim, Ind. Eng. Chem. Res. 32 (1993) 253.
[10] D. He, W. Huang, J. Liu and Q. Zhu, Catal. Today 51 (1999) 127.
[11] T. Li, Y. Souma, Q. Xu, Catal. Today 111 (2006) 288.
[12] F.E. Celik, H. Lawrence, A.T. Bell, J. Mol. Catal. A: Chem. 288 (2008) 87.
[13] F.E. Celik, T. Kim, A.T. Bell, Angew. Chem. Int. Ed. 48 (2009) 4813.
[14] F.E. Celik, T. Kim, A.T. Bell, J. Catal. 270 (2010) 185.
[15] V. Shapovalov, A.T. Bell, manuscript in preparation
[16] K.A. Koyano, T. Tatsumi. Microporous Mater. 10 (1997) 259.
[17] J.F. Joly, N. Zanier-Szydlowski, S. Colin, F. Raatz, J. Saussey, J.C. Lavalley, Catal. Today 9 (1991) 31.
[18] L.Q. Xu, V.L. Zholobenko, L.M. Kustov, W.M.H. Sachtler, J. Mol. Catal. 83 (1993) 391.
[19] K. Nukada, Spectrochim. Acta 18 (1962) 745.
[20] M. Makarova, J. Dwyer, J. Phys. Chem. 97 (1993) 6337.
[21] S. C. L. Dias, J. L. de Macedo, J. A. Dias, Phys. Chem. Chem. Phys. 5 (2003) 5574.
[22] W. Lutz, C.H. Rüscher, D. Heidemann, Microporous Mesoporous Mater. 55 (2002) 193.
[23] K. Schröder, J. Sauer, J. Phys. Chem. 100 (1996) 11043.
[24] Y. Kanazawa, K. Nukada, Bull. Chem. Soc. Jpn. 35 (1962) 612.
[25] T.R. Forester, R.F. Howe, J. Am. Chem. Soc. 109 (1987) 5076.
[26] H. Susi, T. Zell, Spectrochim. Acta 19 (1963) 1933.
[27] G.J. Millar, C.H. Rochester, K.C. Waugh J. Chem. Soc. Faraday Trans. 87 (1991) 2785.
[28] ChemExper chemical directory, Methyl methoxyacetate, http://www.chemexper.com/search/cas/6290499.html, accessed March 5, 2010.
[29] C. Chuang, W. Wu, M. Huang, I. Huang, J. Lin, J. Catal. 185 (1999) 423.
[30] S.M. Campbell, X. Jiang, R.F. Howe, Microporous Mesoporous Mater. 29 (1999) 91.
[31] L. Kubelková, J. Nováková, K. Nedomová, J. Catal. 124 (1990) 441.
[32] Y.J. Jiang, M. Hunger, W. Wang, J. Am. Chem. Soc. 128 (2006) 11679.
[33] T.M. Duncan, R.W. Vaughan, J. Catal. 67 (1981) 49.
[34] T.M. Duncan, R.W. Vaughan, J. Catal. 67 (1981) 469.
[35] K. Hirota, K. Fueki, K. Shindo, Y. Nakai, Bull. Chem. Soc. Japan 32 (1959) 1261.
[36] B. Su, V. Norberg, C. Hansenne, Langmuir 16 (2000) 1132.

[37] NIST Chemistry WebBook, NIST Standard Reference Database Number 69 National Institute of Standards and Technology, Gaithersburg, MD, http://webbook.nist.gov, (retrieved April 18, 2010).
[38] P.S Kalsi, Stereochemistry Conformation and Mechanism, New Age International, New Delhi, 2005, 264.
[39] M. Jones Jr., Organic Chemistry, W.W. Norton & Company, New York, 1997, 270.
[40] T.W.G. Solomons, Organic Chemistry, 6th edition, John Wiley & Sons, New York, 1996, 247.
[41] S.J. Lombardo, A.T. Bell, Surf. Sci. Rep. 13 (1991) 1.
[42] V.P. Zhdanov, J. Pavlicek, Z. Knot, Catal. Rev. - Sci. Eng. 30 (1988) 501.
[43] Y. Zhao, D.G. Truhlar, Org. Lett. 8 (2006) 5753.
[44] Y. Zhao, D.G. Truhlar, J. Phys. Chem. C 112 (2008) 6860.
[45] Y. Zhao, N.E. Schultz, D.G. Truhlar, J. Chem. Theory Comput. 2 (2006) 364.
[46] Y. Zhao, D.G. Truhlar, Acc. Chem. Res. 41 (2008) 157.
[47] N. Hansen, T. Kerber, J. Sauer, A.T. Bell, F.J. Keil, J. Am. Chem. Soc. submitted.